Electronic Supplementary Information

For

Impact of structure and connectivity of thiophene-based bicycles stacking with fluoroarenes in conjugated materials

Elisa Guzman, Gabrielle Buell, Sashen Ruhunage, Peter Müller, Chad Risko, and Samuel W. Thomas III*

General Experimental Information

Experimental

Unless otherwise specified, all reactants and solvents were purchased from commercial sources. Reactions were performed under air-free conditions. Purification by flash column chromatography used silica gel (230-400 mesh) as the stationary phase, with the mobile phases listed in each procedure

Nuclear Magnetic Resonance (NMR)

NMR spectra were acquired using a Bruker Advance III 500 MHz or Bruker Ascend 400 MHz spectrometer in deuterated chloroform, unless otherwise specified in the experimental procedure. TopSpin 3.6 was used to analyze and integrate spectra.

High Resolution Mass Spectrometry (HRMS)

For the compounds that do not have associated crystal structures, high resolution mass spectrometry data is provided. The HRMS data was acquired using a Waters Synapt G2-Si#UGA354 electrospray ionization time of flight spectrometer. The tolerance of this analysis is 5.0 ppm with DBE minimum of -1.5 and maximum of 100.0. This data was collected in collaboration with Furong Sun and the Mass Spectrometry Lab at The University of Illinois, Urbana-Champaign.

Optical Properties: Absorbance, Emission, and Excitation

Solution samples for optical data were prepared in quartz cuvettes and spectroscopy grade chloroform. Thin films used microscope slides and were deposited using spin-cast deposition and annealed in a 100 °C oven for 10 minutes. Powder analysis was performed by either placing the powders in a Teflon holder or pressing onto glass plates. UV/Vis Absorption spectra were collected using a Varian Cary-Flexible spectrometer. Emission and excitation spectra were collected using PTI Quantum Master 4 with a 90° angle detector and a 75 W Xe lamp irradiation source. Quantum yield measurements for solution were collected using dilute chloroform solutions with coumarin 6 as the reference standard for **2TT**, **2BT**, and **6BT** samples, and 9,10 diphenylanthracene as the standard for **5BT** samples. Fluorescence lifetimes in solution were determined using a 403 nm pulsed LED light source for time correlated single photon counting (TCSPC). Ludox (2 drops in 100 mL deionized water) was used as the standard to determine the instrument response function. These results were analyzed using FelixGX with a 1 to 4 exponential lifetime analysis.

Differential Scanning Calorimetry (DSC)

DSC spectra were obtained using a TA Discover DSC 250 with a finned-air cooling system (FACS). 1-2 mg of each powder was placed into a TZero pan with lid. Each sample used a heating rate of 10 °C/min and cooling rate of 5 °C/min.

Single Crystal X-Ray Diffraction (SC-XRD)

Crystals were grown in a 1.0- or 1.5-dram vial by slow vapor diffusion of hexanes into chloroform or dichloromethane. The samples used a low temperature single crystal XRD collected on a Bruker D8 quest diffractometer coupled with a Photon CMOS detector with Mo Kα radiation (λ = 0.71073 Å) from a fine-focused sealed tube source. All structures were analyzed using φ and ω scans, and by using ShelXL and ShelXS to solve and refine the structure solutions.[1]

Quantum-chemical calculations

Density functional theory (DFT) calculations were carried out with the Gaussian 16 Revision A.03 software suite[1] using the ωB97XD[2] functional and the 6-31G(d')[3] basis set. Two conformers (open and closed) for each molecule (Figure 1) were optimized for the ground state (S_0), and normal mode analyses were performed on all optimized structures to confirm that the structures were minima on the potential energy surface. The conformer structures were extracted from experimental crystal structures when available or manually created when no crystal structure was available.

To understand why some molecules prefer either the open or closed conformation, symmetry-adapted perturbation theory (SAPT) calculations[4-7] using the Psi4 software suite[8] were carried out on select fragments from the DFT-optimized closed S_0 conformations. These SAPT results provide information pertaining to the nature and strengths of the noncovalent interactions (i.e., dispersion, electrostatics, induction, and exchange repulsion). We used the SAPT0 approximation[4, 5] with the truncated aug-cc-pVDZ[9] basis set that neglects diffuse functions on H atoms and diffuse *d* functions on other atoms (i.e., the so-called jun-cc-pVDZ basis set)[10] to reduce the computational cost; note that we refer to this method as SAPT0 throughout the manuscript for simplicity. The SAPT0 calculations were carried out for the benzothiophene, thienothiophene, and phenyl (ARF and ARH) molecular scaffolds as shown in Figure S1.[11, 12] In addition to the fragments from the optimized structures, we also derived two sets of idealized fragment structures, one in which the π planes of the rings are cofacial and one in which the conformers are T-shaped.

Time-dependent (TDDFT) calculations at the ωB97XD/6-31G(d') level of theory were carried out to evaluate the vertical excited state transitions for absorption from the conformer S_0 states. TDDFT was then used to optimize the first excited state (S_1),[13, 14] and subsequent single-point TDDFT calculations using the S_1 geometry were used to evaluate vertical transitions corresponding to emission. Normal mode analyses were carried out for all optimized S_1 states to confirm that the geometries were minima on the potential energy surface; note that these analyses for 2BT F3 (closed), 2BT H5 (closed), 2TT F3 (open and closed), 2TT F5 (open and closed), 2TT H5 (closed), and 5BT H5 (open and closed) contained negative frequencies, and so data on these structures are reported here solely for completeness.[15] Energies and oscillator strengths were evaluated for the 15 lowest excited states. An artificial broadening of σ = 0.3 eV was applied to each peak to establish the optical absorption spectra.

Experimental Procedures

Bis((perfluorophenyl)methyl) 2,5 dibromoterephthalate (1)
2,5 dibromoterephthalic acid (0.98 g, 3 mmol), dimethylaminopyridine (DMAP, 150 mg, 1.2 mmol), and dicyclohexylcarbodiimide (DCC, 1.42 g, 6.9 mmol) were added to a flame dried round bottom flask. A solution of pentafluorobenzyl alcohol (0.98 g, 3 mmol) in 50 mL anhydrous dichloromethane was then added. The white solid suspension mixture was stirred at room temperature overnight, followed by filtration over Celite. The filtrate was washed with water and brine, dried over magnesium sulfate, and concentrated by rotary evaporation. The crude product was then purified by flash column chromatography on silica, using pure dichloromethane as the eluent. The resulting solid was recrystallized in chloroform and hexanes, to yield 0.80 g of **1** as a white solid (1.2 mmol, 40% yield).
^{1}H NMR: (500 MHz, $CDCl_3$): δ 8.03 (s, 1H), 5.49 (s, 2H).
These resonances are consistent with those reported in the literature.[8]

Bis(2,4,6-trifluorobenzyl) 2,5-dibromoterephthalate (2)
Following the same procedure as compound **1**, using 2,4,6 trifluorobenzyl alcohol (0.36 g, 2.2 mmol) in place of pentafluorobenzyl alcohol. The reaction afforded 0.12 g of **3** as an off white solid (0.4 mmol, 20% yield).
^{1}H NMR: (400 MHz, $CDCl_3$): δ 8.04 (s, 1H), 6.75 (t, 2H), 5.43 (s, 2H).
These resonances are consistent with those reported in the literature.[8]

Dibenzyl 2,5 dibromoterephthalate (3)
Following an identical procedure as **1**, using benzyl alcohol (0.70 g, 6.5 mmol) in place of pentafluorobenzyl alcohol. The reaction afforded 0.65 g of **3** as a white solid (1.3 mmol, 43% yield).
^{1}H NMR: (400 MHz, $CDCl_3$): δ 8.04 (s, 1H), 7.46 (d, 2H), 7.43-7.34 (m, 3H) 5.38 (s, 2H).
These resonances are consistent with those reported in the literature.[8]

Bis((perfluorophenyl)methyl) 2,5 bis((trimethylsilyl)ethynyl)terephthalate (4)
Compound **1** (1 g, 1.5 mmol) was dissolved in 22 mL of degassed THF/NEt_3 mixture (1:1, v:v). Bis(triphenylphosphine)palladium(II) dichloride (20 mg, 0.03 mmol), and copper(I) iodide (8 mg, 0.04 mmol) were added to a different flame dried round bottom flask under argon. The degassed solvent was cannulated into the flask containing the solids to produce an orange/yellow solution. Trimethylsilyl acetylene (TMSA, 0.35 g, 3.5 mmol, 0.5 mL) was added slowly over 30 second, and the solution lightened to a pale yellow. The reaction was heated to 80 °C and darked to light brown. After stirring overnight under argon, the solution became an opaque black solution. After filtering over Celite, the solvent was removed by rotatory evaporation. The crude product was purified by flash column chromatography on silica, using 40% dichloromethane in hexanes by volume as an eluent. This resulted in 0.87 g of compound **4** as a white solid (1.2 mmol, 80% yield).
^{1}H NMR (500 MHz, $CDCl_3$): δ 8.04 (s, 1H), 5.48 (s, 2H), 0.27 (s, 9H).
The peaks are consistent with those reported in the literature.[9]

Dibenzyl 2,5-bis((trimethylsilyl)ethynyl)terephthalate (5)
Compound **3** (0.5 g, 1 mmol), bis(triphenylphosphine)palladium(II) dichloride (20 mg, 0.03 mmol), and copper(I) iodide (9.5 mg, 0.05 mmol) were added to an oven dried, argon atmosphere round bottom flask. Trimethylsilyl acetylene (TMSA, 0.22 mg, 2.2 mmol, 0.31 mL) was added to a THF/NEt_3 mixture (4:1, v:v) and deoxygenated by sparging with argon. The solvent mixture was transferred into the flask containing the solids by cannula, to produce an orange/yellow solution, which then lighted slightly, and darkened again to a brown solution over several minutes. The reaction was heated to 70 °C and stirred overnight and darkened to an opaque black liquid. 20 mL of CH_2Cl_2 was added, then filtered over Celite, and solvent removed by rotatory evaporation. The crude product was purified by flash column chromatography on silica, using 20% dichloromethane in hexanes by volume as an eluent, for 400 mL, then 40% DCM in hexanes to elute the product. This resulted in 580 mg of compound **5** as a pale-yellow solid (0.56 mmol, 56% yield).
^{1}H NMR: (400 MHz, $CDCl_3$): δ 8.11 (s, 1H), 7.48 (d, 2H), 7.43-7.35 (m, 3H) 5.41 (s, 2H), 0.24 (s, 9H).
The peaks are consistent with those reported in the literature.[9]

Bis((perfluorophenyl)methyl) 2,5-diethynylterephthalate (6)
Compound **4** (870 mg, 1.2 mmol) was dissolved in 10 mL of tetrahydrofuran and cooled to 0°C. Tetra-*n*-butylammonium fluoride (TBAF) was added as a 1.0 M THF solution (2.6 mL, 2.6 mmol) producing a deep purple solution. The mixture was stirred for 15 minutes at 0°C, then quenched by adding cold water. The product was extracted three times diethyl ether, washed with brine, dried over $MgSO_4$, and concentrated by rotary evaporation. The crude product was purified by flash chromatography on silica using 3:2 dichloromethane:hexanes as eluent to afford 670 mg of **6** as an off white solid (1.17 mmol, 98% yield).
^{1}H NMR (400 MHz, $CDCl_3$): δ 8.12 (s, 1H), 5.48 (s, 2H), 3.51 (s, 1H).
The peaks are consistent with those reported in the literature.[9]

Dibenzyl 2,5-diethynylterephthalate (7)
Following the procedure for compound **6**, using compound **5** (300 mg, 0.58 mmol) instead. This produced 165 mg of **7** as an off-white solid (0.42 mmol, 73% yield).
^{1}H NMR (500 MHz, $CDCl_3$): δ 8.19 (s, 1H), 7.49 (d, 2H), 7.44-7.37 (m, 3H), 5.41 (s, 2H), 3.49 (s, 1H).
The peaks are consistent with those reported in the literature.[9]

2-Bromothieno[3,2-b]thiophene (8)
N-Bromosuccinimide (0.651 g, 3.6 mmol) was dissolved in 8.5 mL of *N*,*N*-dimethylformamide. Thienothiophene (0.5 g, 3.5 mmol) was added to a round bottom flask in an inert atmosphere, dissolved in 5 mL of DMF, and cooled to 0°C for 10 min. The NBS solution was added to the flask and stirred at 0°C for 3 hours. The reaction was then quenched with 25 mL of cold water to produce a white solid precipitate. The reaction was then extracted three times with 60 mL of dichloromethane and dried over magnesium sulfate. Using flash chromatography, the resulting solid was purified on silica eluting with hexanes. The resulting solid was recrystallized using ethanol to produce compound **8** as a

white solid (0.31 g, 1.4 mmol, 41% yield).
^{1}H NMR (500 MHz, $CDCl_3$): δ 7.43 (d, 1H), 7.30 (s, 1H), 7.20 (d, 1H).
The peaks are consistent with those reported in the literature.[10]

(Benzo[*b*]thiophene-2-ylethynyl)trimethylsilane (9)
2-bromobenzo[*b*]thiophene (0.32 g 1.5 mmol), copper iodide (17 mg, 0.09 mmol), and bis(triphenyl phosphine)palladium(II) dichloride (32 mg, 0.005 mmol) were added to a flame-dried round bottom flask. Trimethylsilyl acetylene (TMSA, 0.22 g, 2.3 mmol, 0.32 mL) was added to a flask containing 10 mL of a 2:1 toluene:triethylamine (v/v) solvent mixture and sparged for 10 min. The sparged solvent was then added to the flask containing the solids and heated to 80°C and stirred overnight. The reaction mixture was filtered over Celite, reduced *in vacuo*, and purified by flash chromatography on silica eluting with hexanes. This resulted in compound **9** as a pale yellow solid (148 mg, 0.64 mmol, 43% yield).
^{1}H NMR (500 MHz, $CDCl_3$): δ 7.81-7.76 (m, 2H), 7.51 (s, 1H), 7.41-7.38 (m, 2H), 0.35 (s, 9H)
The peaks are consistent with those reported in the literature. [9]

2-ethynylbenzo[*b*]thiophene (10)
Compound **9** (148 mg, 0.64 mmol) was dissolved in 1.0 mL of dichloromethane. Potassium hydroxide (91 mg, 1.63 mmol) was dissolved in 1.6 mL of methanol and added to the reaction flask to stir at room temperature for 3 hours. Solvents were then removed *in vacuo*, and the resulting solid was purified by flash chromatography on silica eluting with hexanes. Compound **10** was solated as 87 mg of light tan solid (0.54 mmol, 86% yield).
^{1}H NMR (500 MHz, $CDCl_3$): δ 7.82-7.78 (m, 2H), 7.56 (s, 1H), 7.44-7.39 (m, 2H), 3.49 (s, 1H)
The peaks are consistent with those reported in the literature. [9]

2-ethynylthieno[3,2-*b*]thiophene (11)
Compound **8** (0.5 g, 2.3 mmol), bis(triphenylphosphine)palladium(II) dichloride (20 mg, 0.03 mmol), and copper(I) iodide (6 mg, 0.03 mmol) were added to an oven dried, argon atmosphere round bottom flask. A degassed solvent mixture of diisopropylamine:tetrahydrofuran (1:1, v:v) was added to the flask. Trimethylsilyl acetylene (TMSA, 270 mg, 2.7 mmol, 0.38 mL) was added to the flask, and the mixture was stirred overnight at 75°C. The resulting dark brown liquid was filtered over Celite, concentrated *in vacuo*, purified by flash chromatography on silica using hexanes as the eluent. This resulted in 400 mg of trimethyl(thieno[3,2-b]thiophen-2-ylethynyl)silane as a white solid (1.7 mmol). This was then dissolved in 6 mL of tetrahydrofuran and 1.5 mL methanol. Potassium hydroxide (55 mg, 1 mmol) was dissolved in 0.3 mL of methanol and added to THF/MeOH solution. After stirring at room temperature for 3 hours, solvents were removed *in vacuo*, and the resulting solid was purified by flash column chromatography on silica eluting with hexanes to yield compound **11** as a yellow oil (0.29 mg, 1.7 mmol, 99%).
^{1}H NMR (500 MHz, $CDCl_3$): δ 7.52 (d, 1H), 7.47 (s, 1H), 7.23 (d, 1H), 3.46 (s, 1H).
The peaks are consistent with those reported in the literature.[11]

(Benzo[*b*]thiophen-5-ylethynyl)trimethylsilane (12)
5-bromobenzo[*b*]thiophene (1.28 g, 6.0 mmol) bis(triphenylphosphine)palladium(II) dichloride (126 mg, 0.18 mmol), and copper(I) iodide (69 mg, 0.36 mmol) was added to a flame dried round bottom flask under argon. Trimethylsilylacetylene (0.8 g, 8.6 mmol, 1.2 mL) was added to 30 mL of 2:1 (v:v) toluene:triethylamine and degassed for 20 minutes transferred to the reaction flask by cannula and stirred at 80 °C overnight. After filtering the reaction mixture through Celite, the filtrate was concentrated *in vacuo* and then purified by flash chromatography eluting with hexanes.This yielded **12** as a yellow solid (0.90 g, 65% yield)
^{1}H NMR (500 MHz, $CDCl_3$): δ 7.98 (s, 1H), 7.81 (d, 1H), 7.48 (d, 1H), 7.44 (d, 1H), 7.32 (d,1H), 0.30 (s, 9H)
The peaks are consistent with those reported in the literature.[12]

5-ethynylbenzo[*b*]thiophene (13)
Following the same procedure for Compound **11**, using compound **12** (0.90 g, 4 mmol) instead. This produced 0.43 g of **13** as a white solid (0.48 mmol, 70% yield).
^{1}H NMR (500 MHz, $CDCl_3$): δ 8.01 (s, 1H), 7.85 (d, 1H), 7.50 (d, 1H), 7.47 (d, 1H), 7.34 (d, 1H) 3.12 (s, 1H).
The peaks are consistent with those reported in the literature.[12]

(Benzo[*b*]thiophen-6-ylethynyl)trimethylsilane (14)
Following the same procedure for Compound **11**, using 6-bromobenzo[*b*]thiophene (0.25 g, 1.15 mmol) instead. This produced 0.22 g of **14** as an off white solid (0.97 mmol, 85% yield).
^{1}H NMR (500 MHz, $CDCl_3$): δ 8.04 (s, 1H), 7.70 (d, 1H), 7.50 (d, 1H), 7.44 (d, 1H), 7.32 (d, 1H) 0.23 (s, 9H).
The peaks are consistent with those reported in the literature. [13]

6-ethynylbenzo[*b*]thiophene (15)
Following the same procedure for Compound **11**, using compound **14** (0.22 g, 0.97 mmol) instead. This produced 0.125 g of **15** as a white solid (0.80 mmol, 82% yield).
^{1}H NMR (500 MHz, $CDCl_3$): δ 8.08 (s, 1H), 7.79 (d, 1H), 7.54 (d, 1H), 7.51 (d, 1H), 7.36 (d, 1H) 3.17 (s, 1H).
The peaks are consistent with those reported in the literature. [13]

Bis((perfluorophenyl)methyl) 2,5 bis(thieno[3,2-*b*]thiophen-2-ylethynyl)terephthalate (2TT-F5)

Compound **11** (100 mg, 0.61 mmol) was added to a flame dried round bottom flask and dissolved in 10 mL of an argon-sparged solvent mixture of 3:2 (v:v) triethylamine and tetrahydrofuran. Once dissolved, copper (I) iodide (2 mg, 0.009 mmol), tetrakis(triphenylphosphine)palladium(0) (17 mg, 0.015 mmol), and compound **1** (200 mg, 0.29 mmol) were added to the flask. This was stirred overnight under argon at 65 °C. After filtering through Celite and rinsing the flask and collected solids with diethyl ether, reduce the filtrate *in vacuo*. The solid was then purified via flash column chromatography on silica eluting with 1:1 hexanes:ether (v:v). The resulting crude product was recrystallized from chloroform, slowly adding hexanes to promote crystallization. This resulted in 0.24 g of an orange solid (0.27 mmol, 94% yield).

^{1}H NMR (500 MHz, $(CD_3)_2CO$): δ 8.22 (s, 1H), 7.92 (s, 1H), 7.76 (s, 1H), 7.63 (s, 1H), 7.41 (s, 1H) 5.61 (s, 2H).

^{13}C NMR (125 MHz, $CDCl_3$): δ 163.8, 141.1, 138.7, 136.2, 133.0, 130.2, 125.1, 123.6, 122.9, 119.4, 108.9, 91.8, 91.7, 54.5.

HRMS m/z: $[M + H]^+$ Calc for $C_{38}H_{12}F_{10}O_4S_4$ 850.9537; Found 850.9525.

Bis(2,4,6-trifluorobenzyl) 2,5-bis(thieno[3,2-*b*]thiophen-2-ylethynyl)terephthalate (2TT-F3)

Compound **2** (61 mg, 0.1 mmol) was added to a flame dried round bottom flask containing compound **11** (40 mg, 0.24 mmol), copper iodide (4 mg, 0.02 mmol), and tetrakis(triphenylphosphine)palladium(0) (12 mg, 0.01 mmol). The solids were then dissolved in argon sparged 1:1 THF:NEt_3. The reaction was heated to 60°C and stirred overnight under an argon atmosphere. After filtering through Celite, and rinsing with dichloromethane, the filtrate was reduced *in vacuo* and purified via flash chromatography on silica eluting with 3:1 CH_2Cl_2:hexanes. The resulting orange solid was recrystallized from dichloromethane resulting in 9 mg of **2TT-F3** (0.012 mmol, 12% yield).

^{1}H NMR (500 MHz, $CDCl_3$): δ 8.21 (s, 1H), 7.56 (d, 1H), 7.42 (s, 1H), 7.26 (d, 1H), 6.69 (t, 2H) 5.48 (s, 2H).

^{13}C NMR (125 MHz, $CDCl_3$): δ 164.4, 141.1, 138.7, 136.0, 133.4, 129.9, 125.1, 124.0, 122.7, 119.4, 107.9, 100.7, 100.5, 100.3, 92.0, 91.3, 54.9.

HRMS m/z: $[M + H]^+$ Calc for $C_{38}H_{16}F_6O_4S_4$ 778.9914; Found 778.9924.

Bis(2,4,6-trifluorobenzyl) 2,5 bis(benzo[*b*]thiophen-2-ylethynyl)terephthalate (2BT-F3)

Following the same procedure for **2TT-F3**, using compound **11** (61 mg, 0.1 mmol) instead. This produced 18 mg of **2BT-F3** as an orange solid (0.046 mmol, 46% yield).

^{1}H NMR (400 MHz, $CDCl_3$): δ 8.24 (s, 1H), 7.83-7.78 (m, 2H), 7.47 (s, 1H), 7.43-7.40 (m, 2H), 6.66 (t, 2H) 5.50 (s, 2H).

^{13}C NMR (125 MHz, $CDCl_3$): δ 164.1, 140.8, 139.0, 136.3, 133.6, 129.8, 125.8, 124.9, 124.0, 122.8, 122.4, 122.1,107.8, 100.5, 92.4, 90.9, 55.0

Dibenzyl 2,5 bis(thieno[3,2-*b*]thiophen-2-ylethynyl)terephthalate (2TT-H5)
Following the same procedure for **2TT-F5**, using compound **3** (146 mg, 0.29 mmol) instead. This produced 42 mg of **2TT-H5** as a yellow solid (0.063 mmol, 22% yield).
^{1}H NMR (500 MHz, $CDCl_3$): δ 8.27 (s, 1H), 7.54-7.52 (m, 3H), 7.42-7.36(m, 3H), 7.25 (d,1H), 7.23 (s, 1H), 5.48 (s, 1H)
^{13}C NMR (125 MHz, $CDCl_3$): δ 164.7, 141.0, 138.7, 136.0, 135.4, 133.7, 129.9, 128.7, 128.6, 128.5, 125.3, 124.0, 122.6, 119.5, 92.4, 91.3, 67.7

Bis((perfluorophenyl)methyl) 2,5 bis(benzo[*b*]thiophen-5-ylethynyl)terephthalate (5BT-F5)
5-Iodo-benzo[*b*]-thiophene (109 mg, 0.42 mmol) was added to a flame dried round bottom flask containing copper iodide (15 mg, 0.08 mmol), and tetrakis(triphenylphosphine)-palladium(0) (23 mg, 0.02 mmol). 16 mL of 1:1 (v:v) triethylamine:tetrahydrofuran was degassed in a separate round bottom flask using the freeze-pump-thaw method, then added to the round bottom flask containing the solids. This mixture was stirred overnight at 65°C under argon. After filtering through Celite and rinsing the flask and collected solids with diethyl ether, the crude product purified by flash chromatography twice, eluting with 2:3 (v:v) dichloromethane:hexane. The resulting solid was recrystallized by chloroform/hexanes multiple times until a pure white solid was obtained (3 mg, 2% yield).
^{1}H NMR (400 MHz, $CDCl_3$): δ 8.22 (s, 1H), 7.94 (s, 1H) 7.87 (d, 1H), 7.52 (d, 1H), 7.43 (d, 1H), 7.41 (d, 1H), 7.35 (d, 1H) 5.51 (s, 2H).
Not soluble enough for ^{13}C NMR

Bis(2,4,6-trifluorobenzyl) 2,5 bis(benzo[*b*]thiophen-5-ylethynyl)terephthalate (5BT-F3)
Following the same procedure for **2BT-F3**, using compound **13** (68.4 mg, 0.432 mmol) instead. This produced 77 mg of **5BT-F3** as a bright yellow solid (0.10 mmol, 56% yield).
^{1}H NMR (500 MHz, $CDCl_3$): δ 8.24 (s, 1H), 7.96 (s, 1H) 7.87 (d, 1H), 7.54 (d, 1H), 7.44 (d, 1H), 7.37 (d, 1H), 6.63 (t, 2H), 5.49 (s, 2H).
^{13}C NMR (125 MHz, $CDCl_3$): δ 164.5, 140.3, 139.5, 136.3, 133.6, 127.6, 127.2, 127.1, 123.7, 123.1, 122.5, 118.6, 100.7, 100.5, 100.2, 97.5, 86.7, 54.8

Dibenzyl 2,5 bis(benzo[*b*]thiophen-5-ylethynyl)terephthalate (5BT-H5)
Compound **13** (48 mg, 0.3 mmol) was added to a purged round bottom flask with tetrakis(triphenylphosphine)palladium(0) (20 mg, 0.02 mmol) and copper iodide (10 mg, 0.065 mmol). 16 mL of sparged 1:1 tetrahydrofuran:triethylamine (v:v) was added to the flask, along with 71 mg of compound **3** (0.14 mmol). This was allowed to stir overnight at 65°C under argon. After filtering through celite, the reaction mixture was purified by flash column chromatography on silica eluting with 1:2 DCM:Hexanes (v:v). This afforded a bright yellow solid that was recrystallized from chloroform and hexanes to give 58 mg of **5BT-H5** (0.08 mmol, 63% yield)
^{1}H NMR (400 MHz, $CDCl_3$): δ 8.30 (s, 1H), 7.89 (s, 1H) 7.83 (d, 1H), 7.53-7.50 (m, 3H), 7.40-7.32 (m, 5H), 5.48 (s, 2H).
^{13}C NMR (125 MHz, $CDCl_3$): δ 165.0, 140.3, 139.5, 136.3, 135.5, 134.0, 128.7, 128.5, 128.4,

127.4, 127.4, 127.3, 123.8, 123.0, 122.5, 118.6, 97.5, 87.1, 67.6

Bis((perfluorophenyl)methyl) 2,5 bis(benzo[*b*]thiophen-6-ylethynyl)terephthalate (6BT-F5)

Compound **15** (50 mg, 0.32 mmol) was added to a flame dried round bottom flask with tetrakis(triphenylphosphine)palladium(0) (17 mg, 0.015 mmol), and compound **1** (103 mg, 0.15 mmol). 24 mL of 2:1 (v:v) tetrahydrofuran: triethylamine was sparged with argon for 20 minutes then added to the flask containing the solids. Once all of the solids were dissolved, add copper (I) iodide (4 mg, 0.02 mmol), and stir overnight under argon at the refluxing temperature of 96 °C. Once cooled to room temperature the next day, filter the reaction mixture over silica, and rinse the flask, and collected solids with 1:2 dichloromethan:hexanes until no more product is being removed from the silica plug, check my thin-layer chromatography. The filtrate was concentrated *in vacuo* and recrystallized twice by dissolving the solid in minimal warm chloroform, and adding hexanes until precipitate appears Let cool to room temperature, and filter by Hirsch funnel to collect 103 mg of **6BT-F5** as an off-white, slightly green solid. (0.12 mmol 82% yield)

^{1}H NMR (500 MHz, $CDCl_3$): δ 8.24 (s, 1H), 8.04 (s, 1H) 7.83 (d, 1H), 7.59 (d, 1H), 7.47 (d, 1H), 7.39 (d, 1H), 5.54 (s, 2H).

^{13}C NMR (125 MHz, $CDCl_3$): δ 164.1, 139.9, 139.7, 136.3, 133.3, 128.6, 127.3, 125.9, 123.9, 123.5, 123.3, 118.2, 97.9, 87.1, 54.4.

HRMS m/z: $[M + H]^+$ Calc for $C_{42}H_{16}F_{10}O_4S_2$ 839.0409; Found 839.0387.

Bis(2,4,6-trifluorobenzyl) 2,5 bis(benzo[*b*]thiophen-6-ylethynyl)terephthalate (6BT-F3)

Following the same procedure for **2TT-F3**, using compound **15** (46 mg, 0.29 mmol) instead. This produced 16.2 mg of **6BT-F3** as a bright yellow solid (0.038 mmol, 17% yield).

^{1}H NMR (500 MHz, $CDCl_3$): δ 8.24 (s, 1H), 8.00 (s, 1H) 7.80 (d, 1H), 7.58 (d, 1H), 7.46 (d, 1H), 7.38 (d, 1H), 6.65 (t, 2H) 5.49 (s, 2H).

^{13}C NMR (125 MHz, $CDCl_3$): δ 164.5, 139.8, 139.6, 136.3, 133.6, 128.4, 127.5, 126.0, 123.9, 123.4, 123.1, 118.5, 100.5, 97.5, 87.3, 54.8.

HRMS m/z: $[M + H]^+$ Calc for $C_{42}H_{20}F_6O_4S_2$ 767.0785; Found 767.0797.

Dibenzyl 2,5 bis(benzo[*b*]thiophen-6-ylethynyl)terephthalate (6BT-H5)

Following the same procedure for **6BT-F5**, using compound **15** (26 mg, 0.17 mmol), and compound **3** (48 mg, 0.08 mmol). Purification of this compound produced 50 mg of **6BT-H5** as a yellow solid (0.75 mmol, 94% yield).

^{1}H NMR (400 MHz, $CDCl_3$): δ 8.30 (s, 1H), 7.84 (s, 1H) 7.78 (d, 1H), 7.56 (d, 1H), 7.53 (d, 1H), 7.43 (d, 1H),7.41-7.36 (m, 4H) 5.49 (s, 2H).

^{13}C NMR (125 MHz, $CDCl_3$): δ 165.0, 139.8, 139.6, 136.3, 135.4, 134.0, 128.7, 128.6, 128.5, 128.4, 127.7, 126.2, 123.8, 123.4, 123.0, 118.5, 97.5, 87.7, 67.6.

HRMS m/z: $[M + H]^+$ Calc for $C_{42}H_{26}O_4S_2$ 659.1351; Found 659.1356.

References

1. G. M. Sheldrick, *Journal*, 2015, **C71**, 3-8 (Open Access).
2. M. J. Frisch, G. W. Trucks, H. B. Schlegel, G. E. Scuseria, M. A. Robb, J. R. Cheeseman, G. Scalmani, V. Barone, G. A. Petersson, H. Nakatsuji, X. Li, M. Caricato, A. V. Marenich, J. Bloino, B. G. Janesko, R. Gomperts, B. Mennucci, H. P. Hratchian, J. V. Ortiz, A. F. Izmaylov, J. L. Sonnenberg, Williams, F. Ding, F. Lipparini, F. Egidi, J. Goings, B. Peng, A. Petrone, T. Henderson, D. Ranasinghe, V. G. Zakrzewski, J. Gao, N. Rega, G. Zheng, W. Liang, M. Hada, M. Ehara, K. Toyota, R. Fukuda, J. Hasegawa, M. Ishida, T. Nakajima, Y. Honda, O. Kitao, H. Nakai, T. Vreven, K. Throssell, J. A. Montgomery Jr., J. E. Peralta, F. Ogliaro, M. J. Bearpark, J. J. Heyd, E. N. Brothers, K. N. Kudin, V. N. Staroverov, T. A. Keith, R. Kobayashi, J. Normand, K. Raghavachari, A. P. Rendell, J. C. Burant, S. S. Iyengar, J. Tomasi, M. Cossi, J. M. Millam, M. Klene, C. Adamo, R. Cammi, J. W. Ochterski, R. L. Martin, K. Morokuma, O. Farkas, J. B. Foresman and D. J. Fox, *Journal*, 2016.
3. S. Grimme, *J Comput Chem*, 2006, **27**, 1787-1799.
4. P. C. Hariharan and J. A. Pople, *Theoretica Chimica Acta*, 1973, **28**, 213-222.
5. T. M. Parker, L. A. Burns, R. M. Parrish, A. G. Ryno and C. D. Sherrill, *The Journal of Chemical Physics*, 2014, **140**.
6. X.-K. Chen, B. W. Bakr, M. Auffray, Y. Tsuchiya, C. D. Sherrill, C. Adachi and J.-L. Bredas, *The Journal of Physical Chemistry Letters*, 2019, **10**, 3260-3268.
7. Q. Zhu, X. Guo and J. Zhang, *J Comput Chem*, 2019, **40**, 1578-1585.
8. W. J. Mullin, R. H. Pawle, S. A. Sharber, P. Müller and S. W. Thomas, *Journal of Materials Chemistry C*, 2019, **7**, 1198-1207.
9. W. J. Mullin, P. Müller, A. J. Schaefer, E. Guzman, S. E. Wheeler and S. Thomas, *J. Mater. Chem. C*, 2022, **10**, 11199-11210.
10. P. Xie, T. Liu, J. Sun and J. Yang, *Adv. Funct. Mater.*, 2022, **32**, 2200843.
11. P.-Y. Huang, C. Kim and M.-C. Chen, *Synlett*, 2011, **2011**, 2151-2156.
12. P. Boehm, N. Kehl and B. Morandi, *Angew. Chem., Int. Ed.*, 2023, **62**, e202214071.
13. B. C. Baciu, P. J. Bronk, T. de Ara, R. Rodriguez, P. Morgante, N. Vanthuyne, C. Sabater, C. Untiedt, J. Autschbach, J. Crassous and A. Guijarro, *J. Mater. Chem. C*, 2022, **10**, 14306-14318.

Nuclear Magnetic Resonance Spectra

Figure S1: ^{1}H NMR spectrum of **2BT-F3**

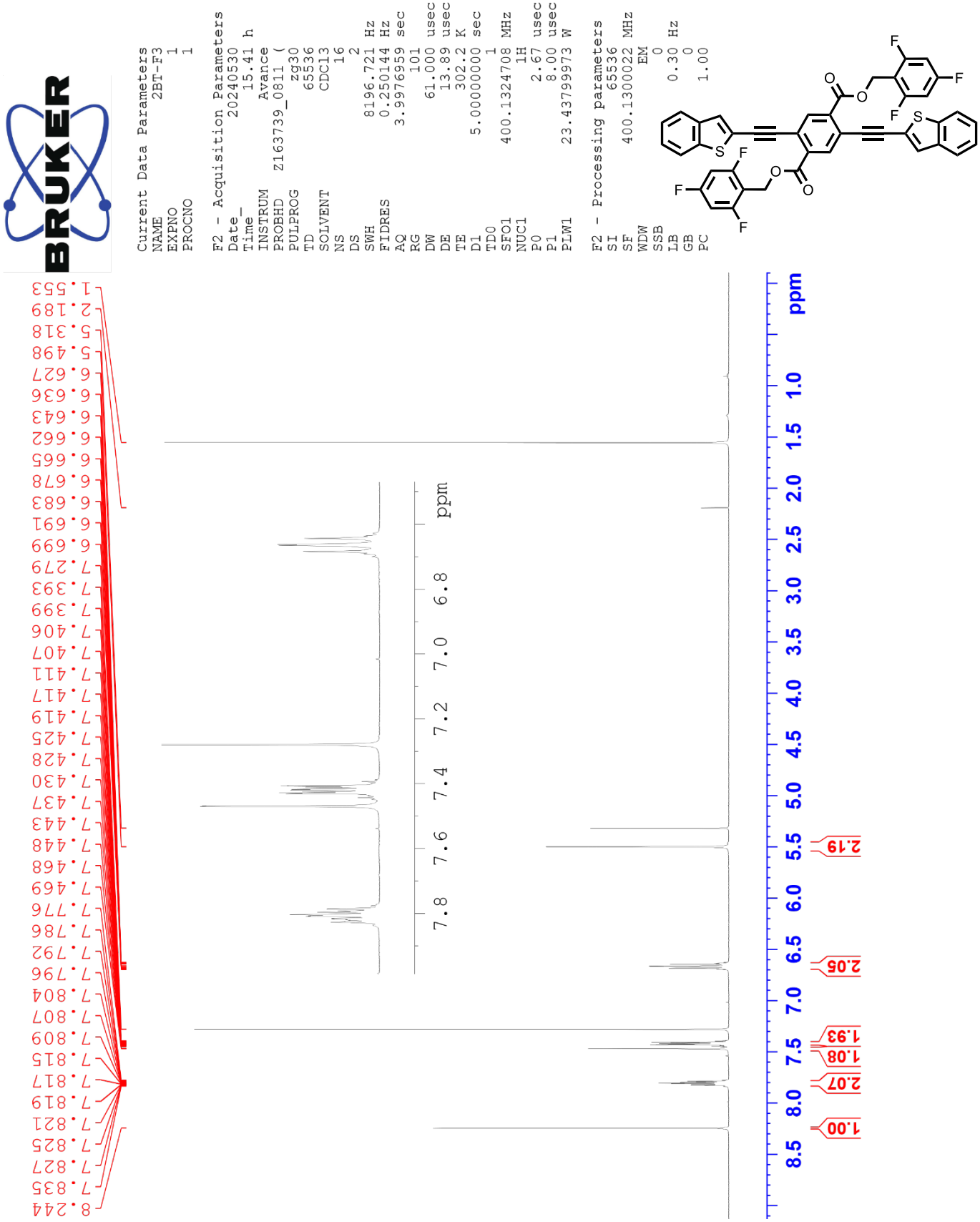

Figure S2: ^{13}C NMR spectrum of **2BT-F3**

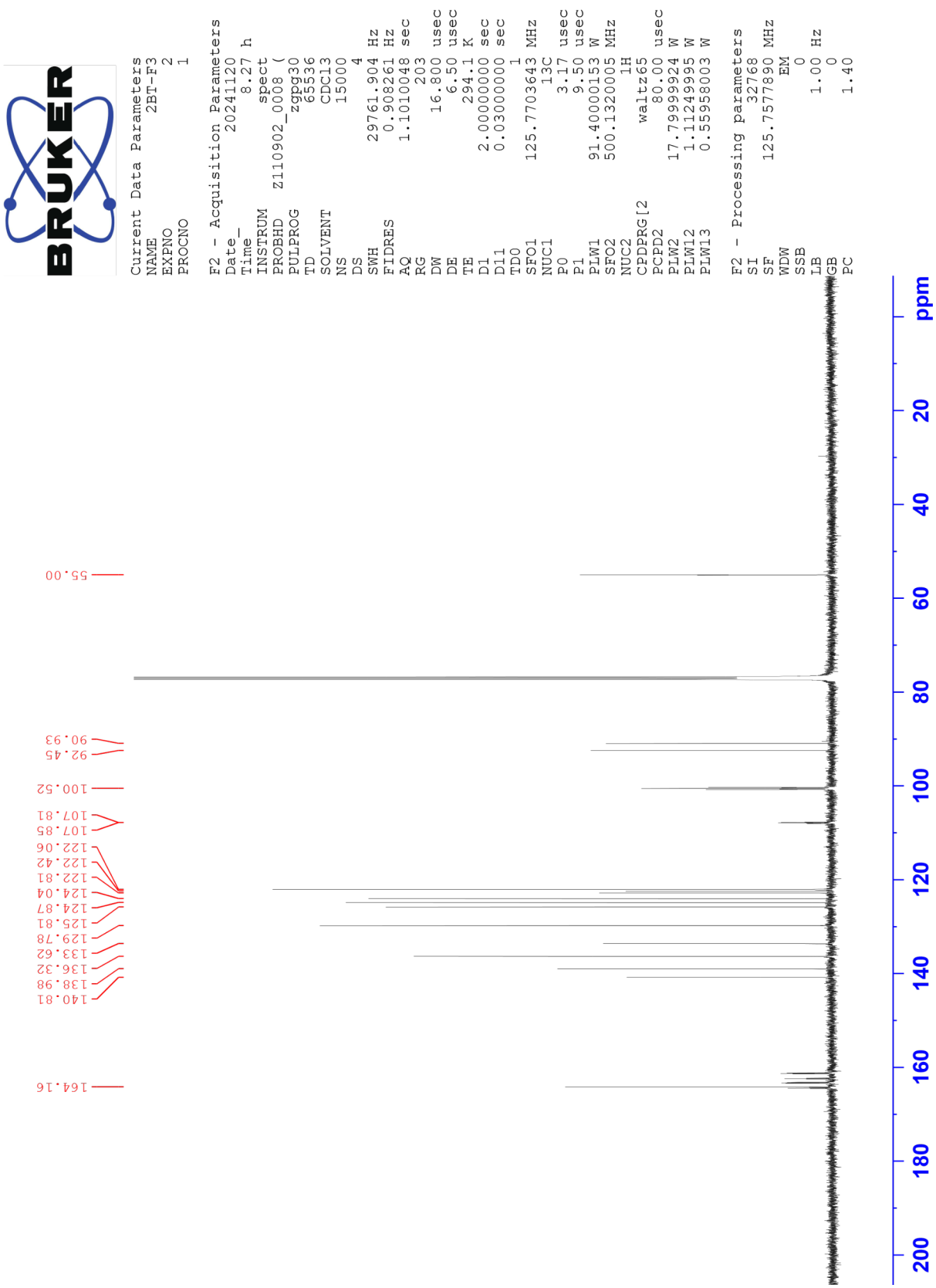

Figure S3: ^{1}H NMR spectrum of **2TT-F5**

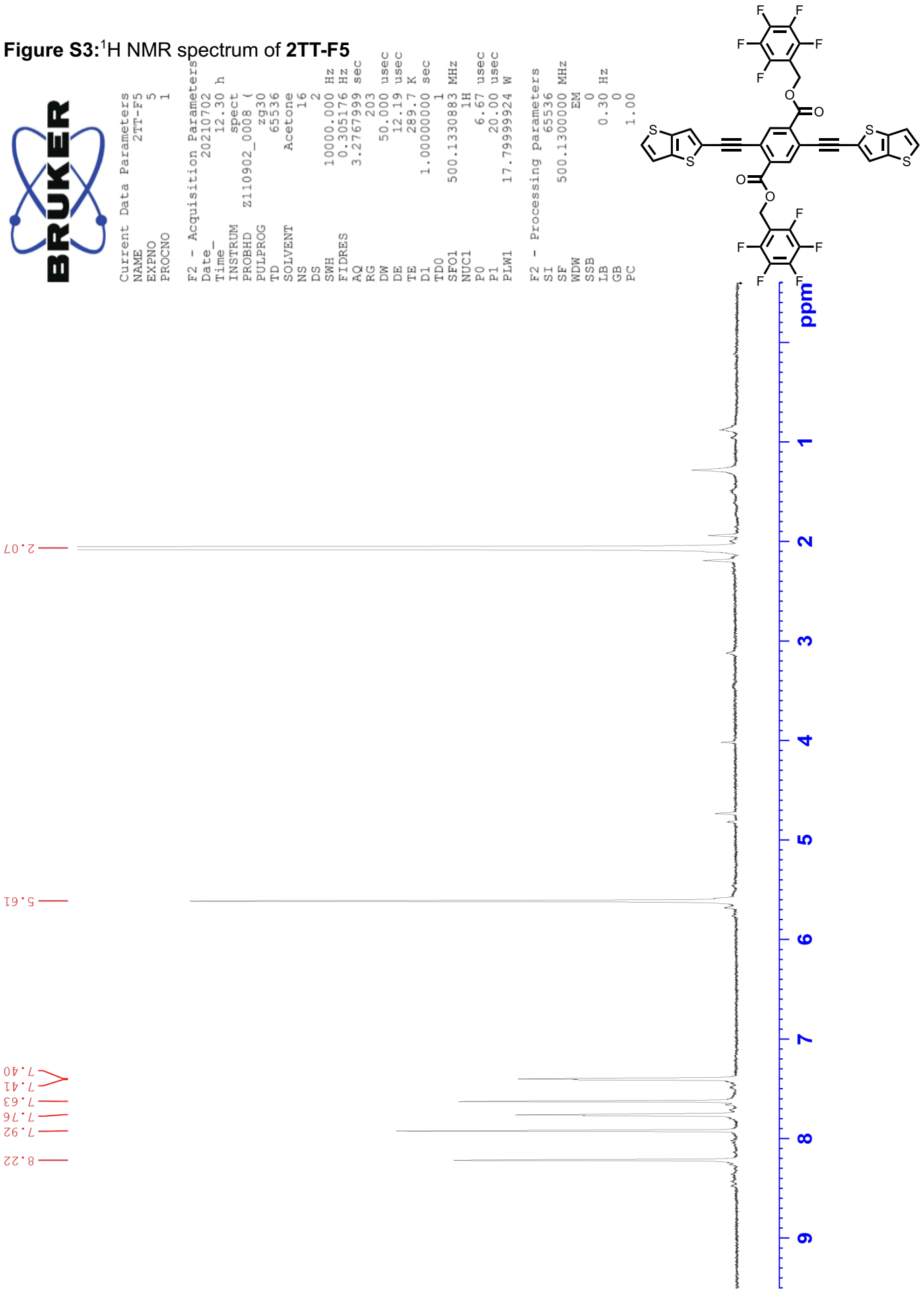

Figure S4: ^{13}C NMR spectrum of **2TT-F5**

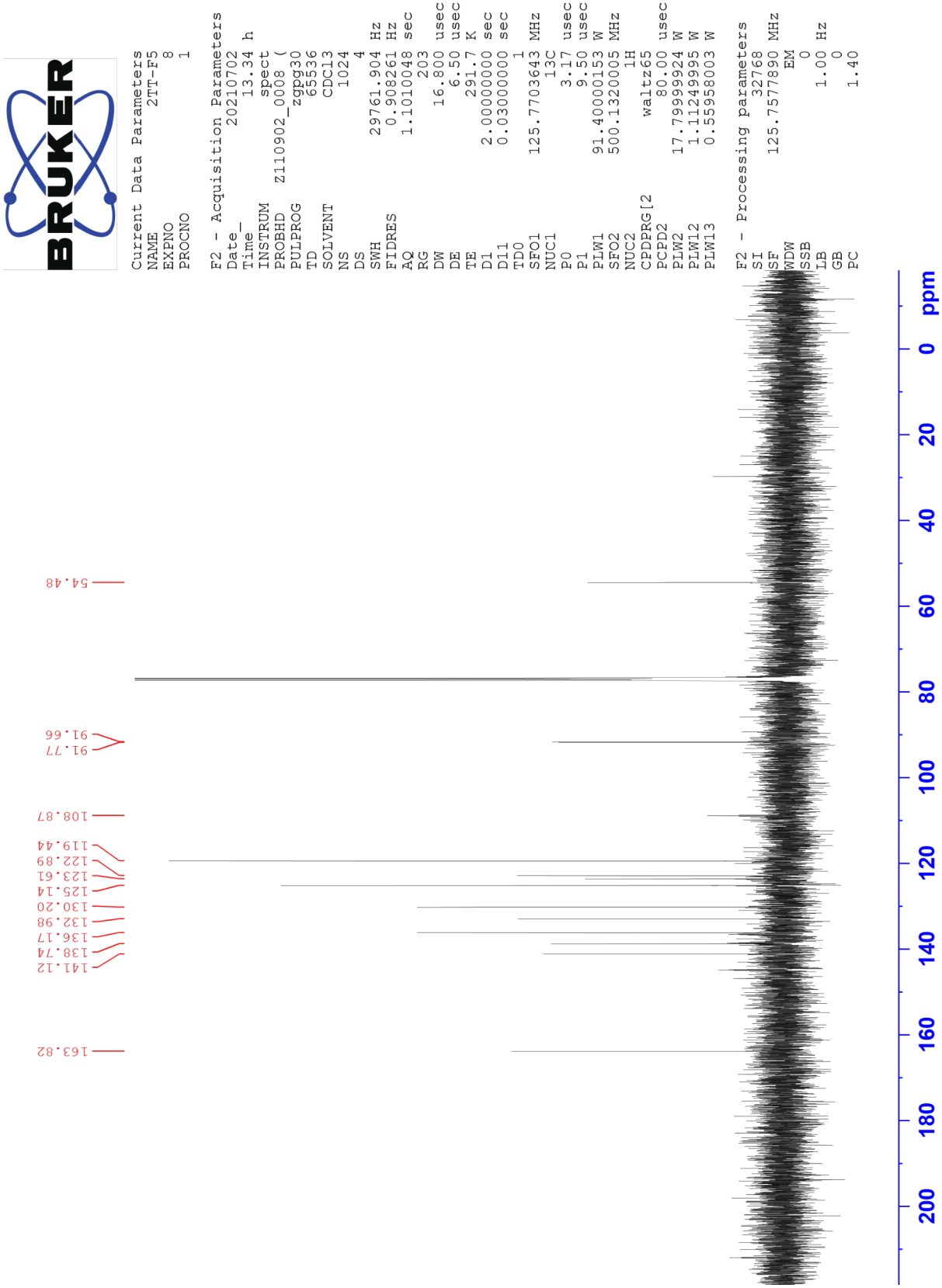

Figure S5: ^{1}H NMR spectrum of **2TT-F3**

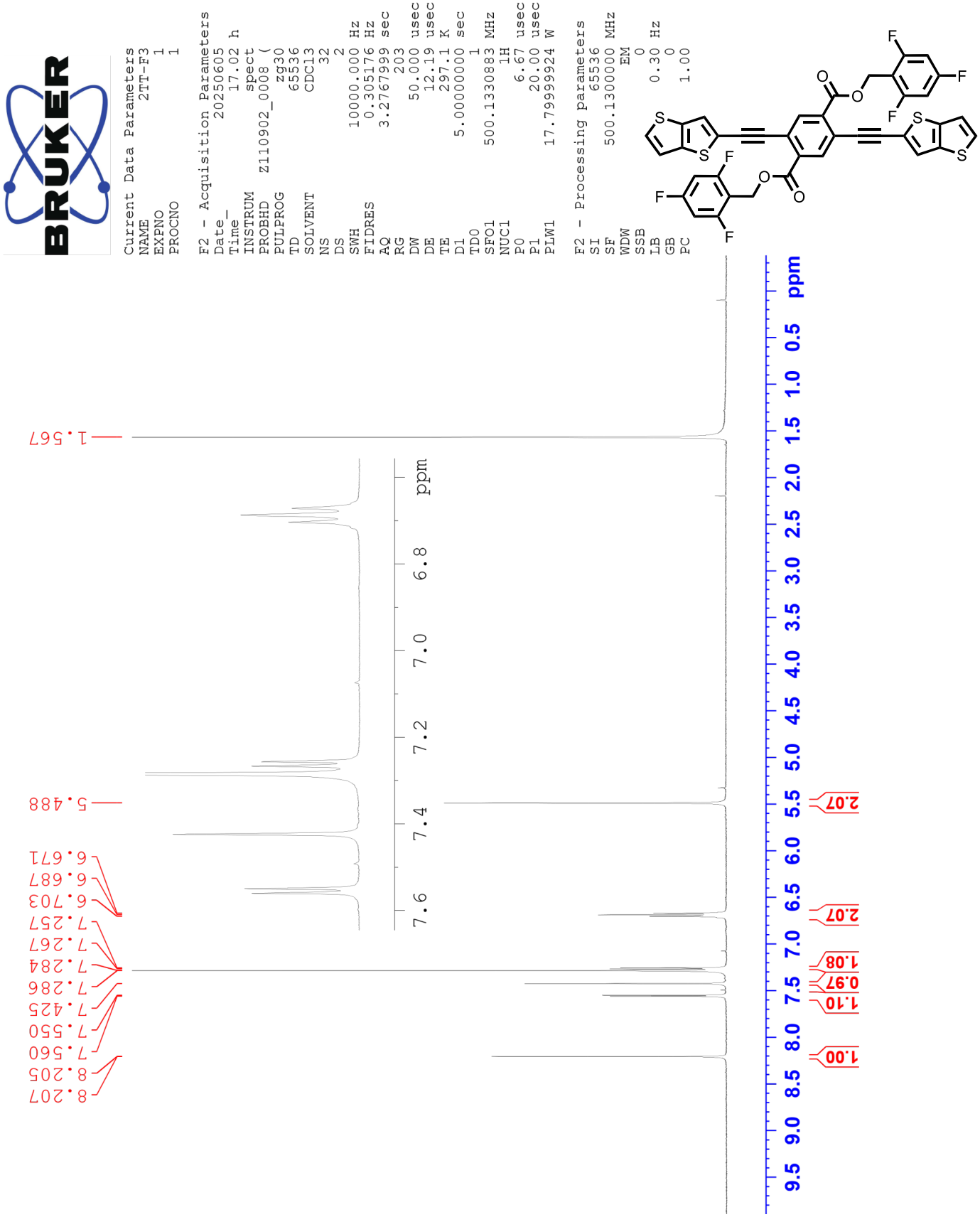

Figure S6: ^{13}C NMR spectrum of **2TT-F3**

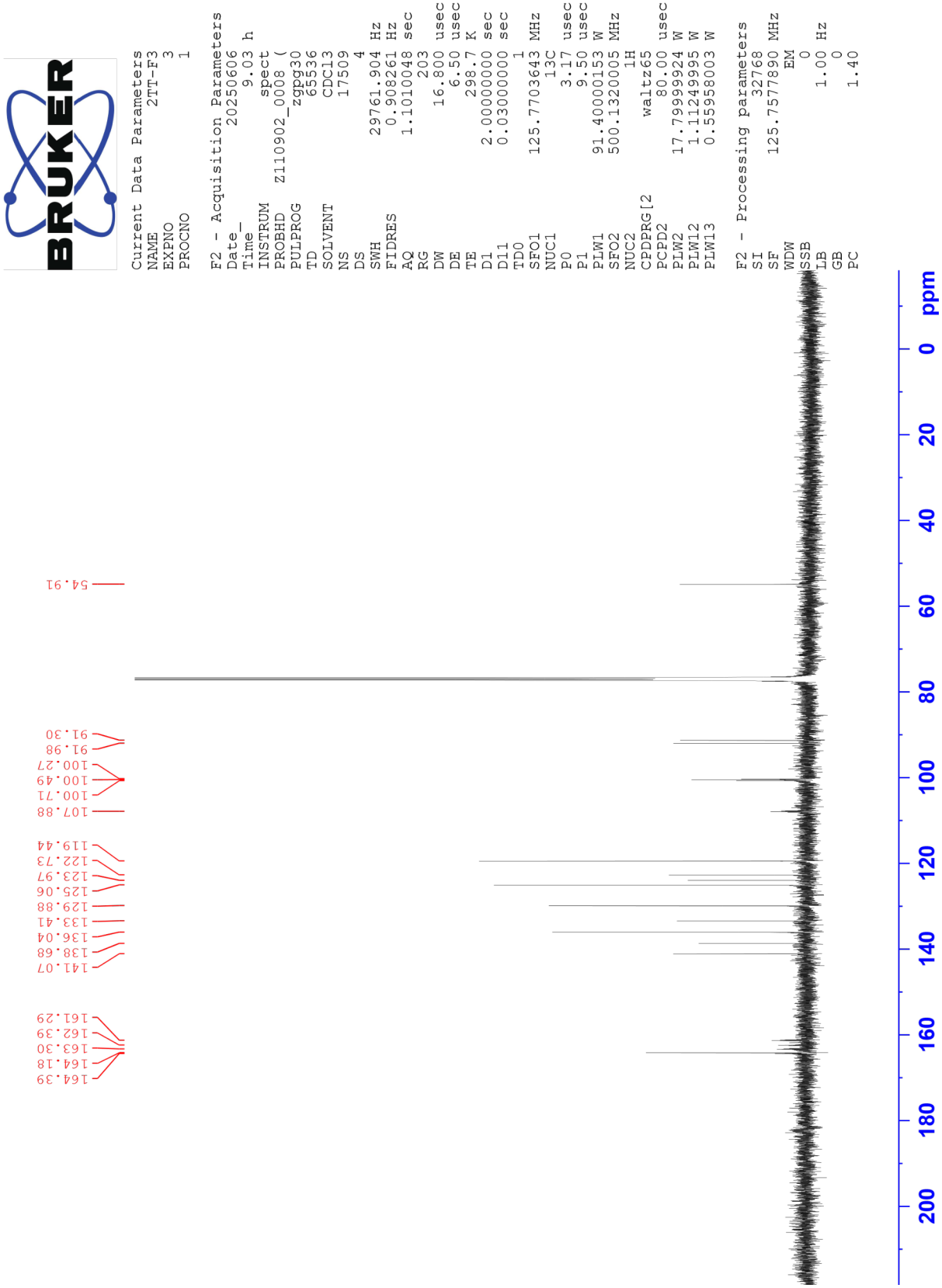

Figure S7: ^{1}H NMR spectrum of **2TT-H5**

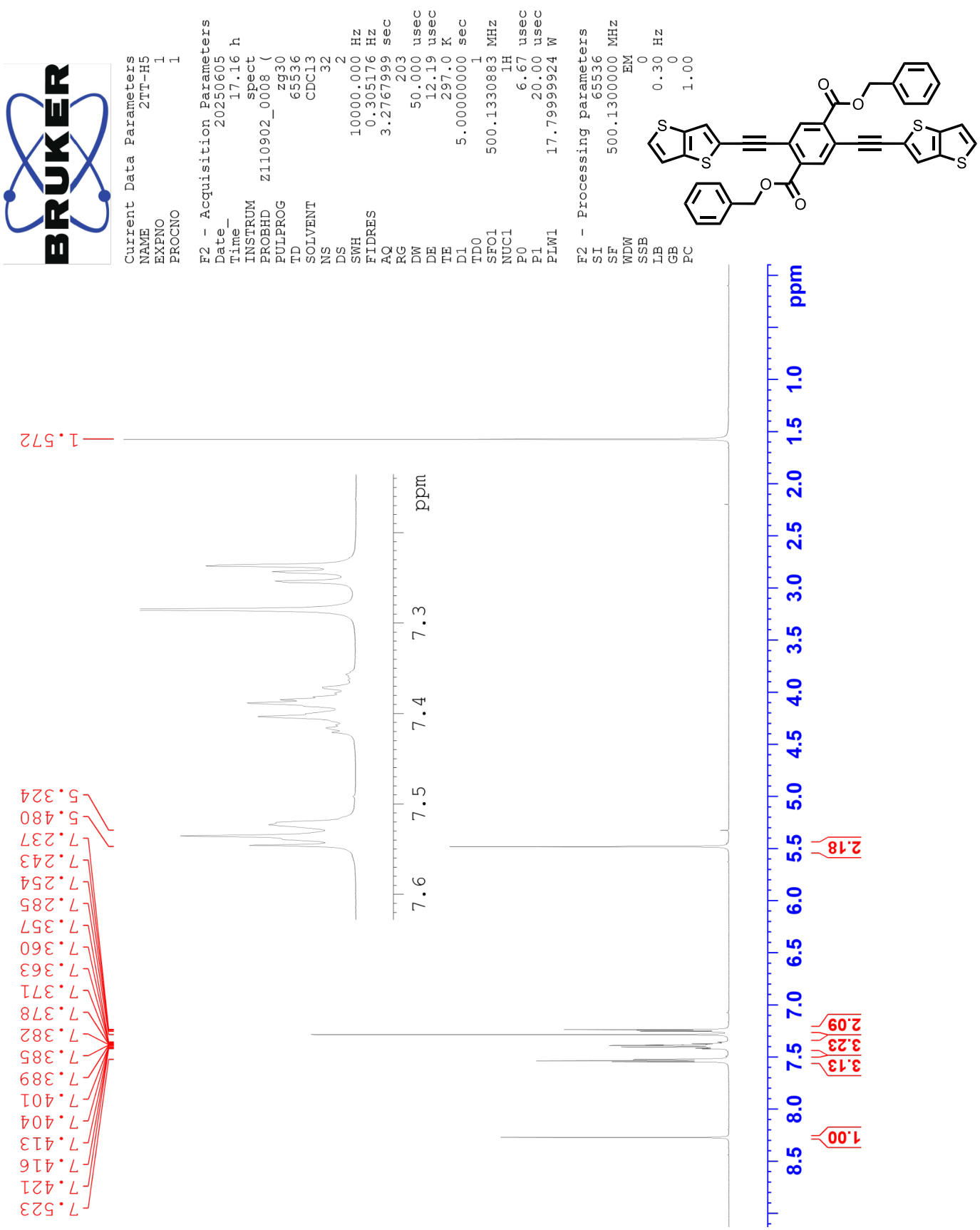

Figure S8: ^{13}C NMR spectrum of **2TT-H5**

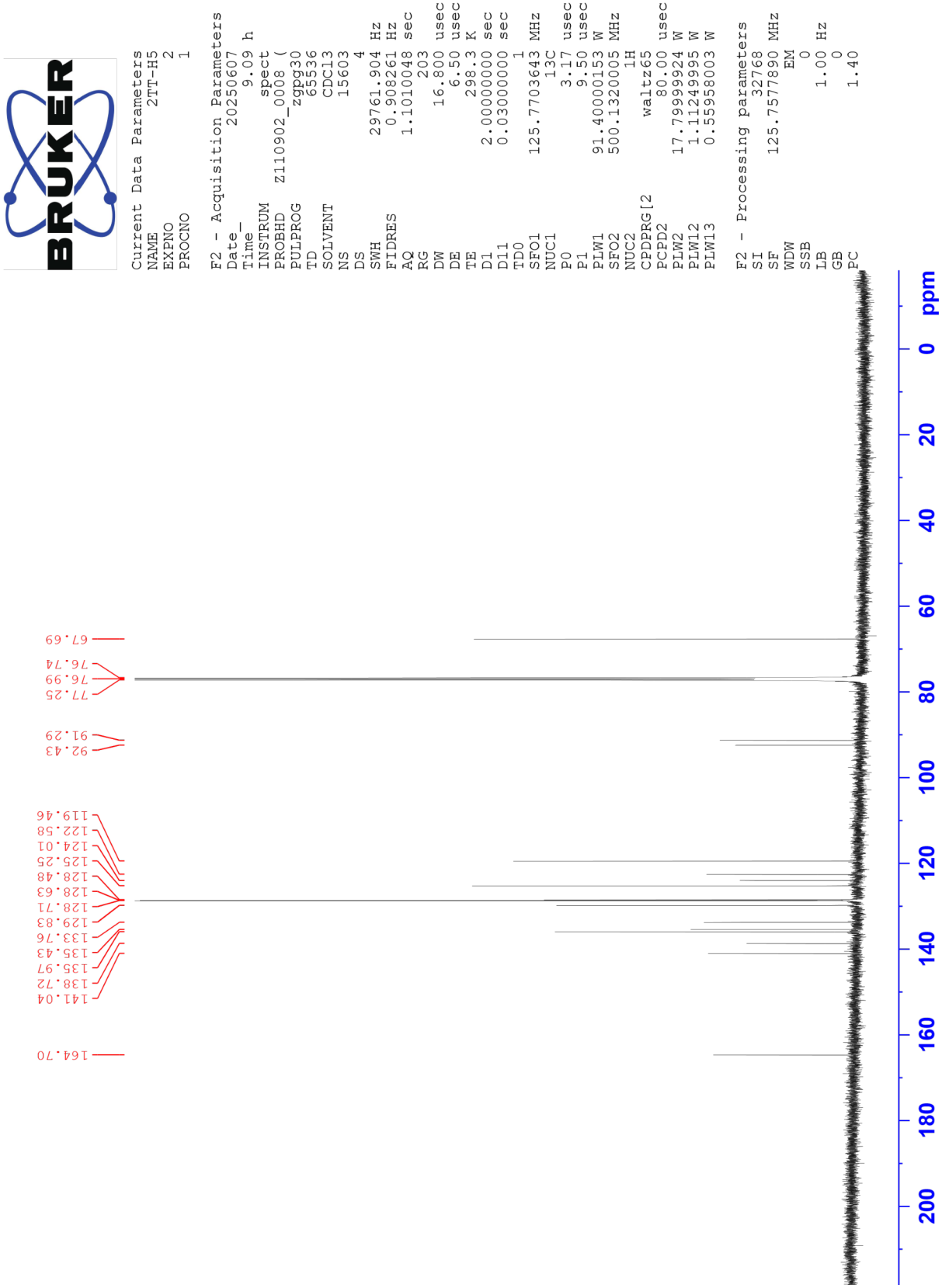

Figure S9: ^{1}H NMR spectrum of **5BT-F5**

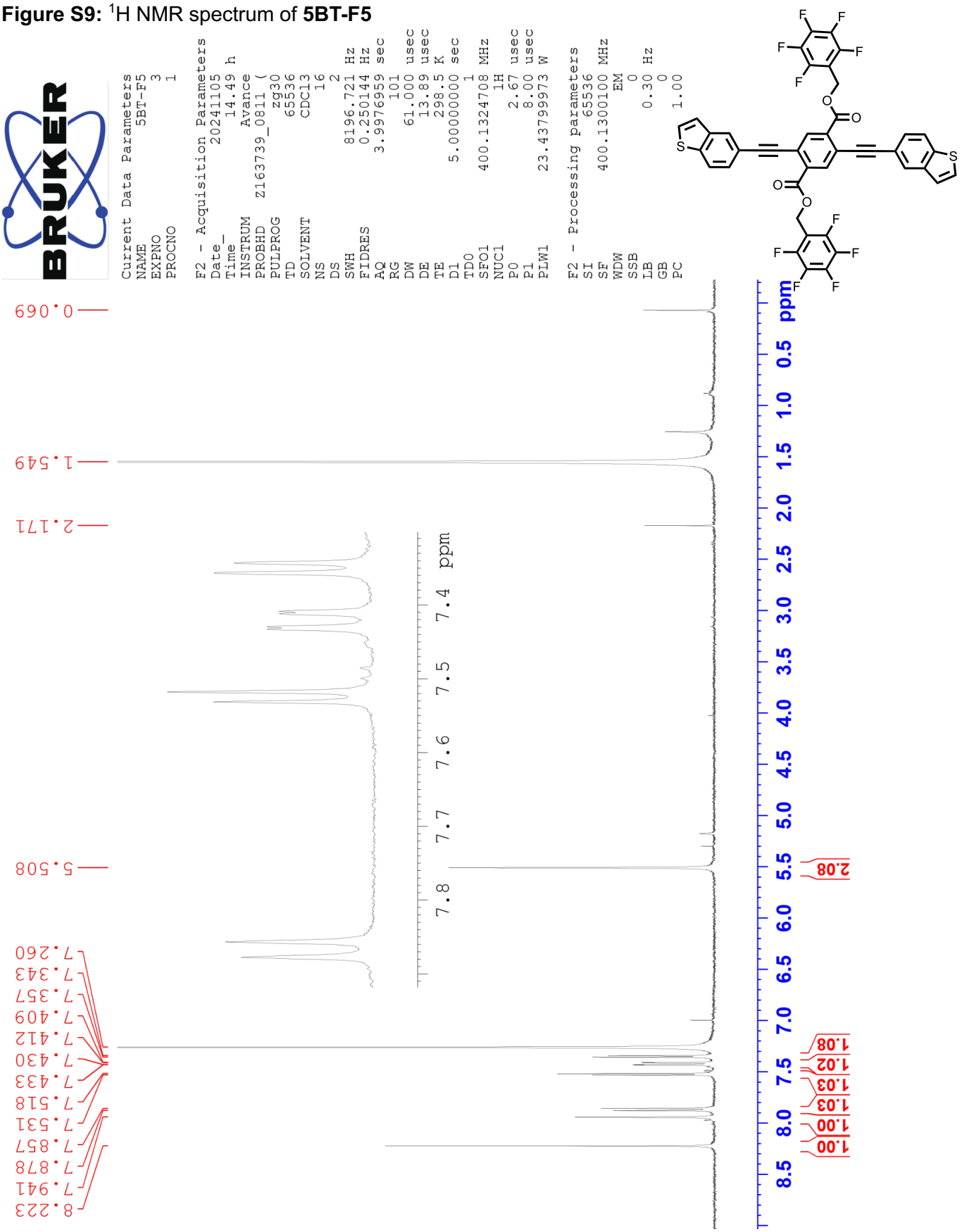

Figure S10: ^{1}H NMR spectrum of **5BT-F3**

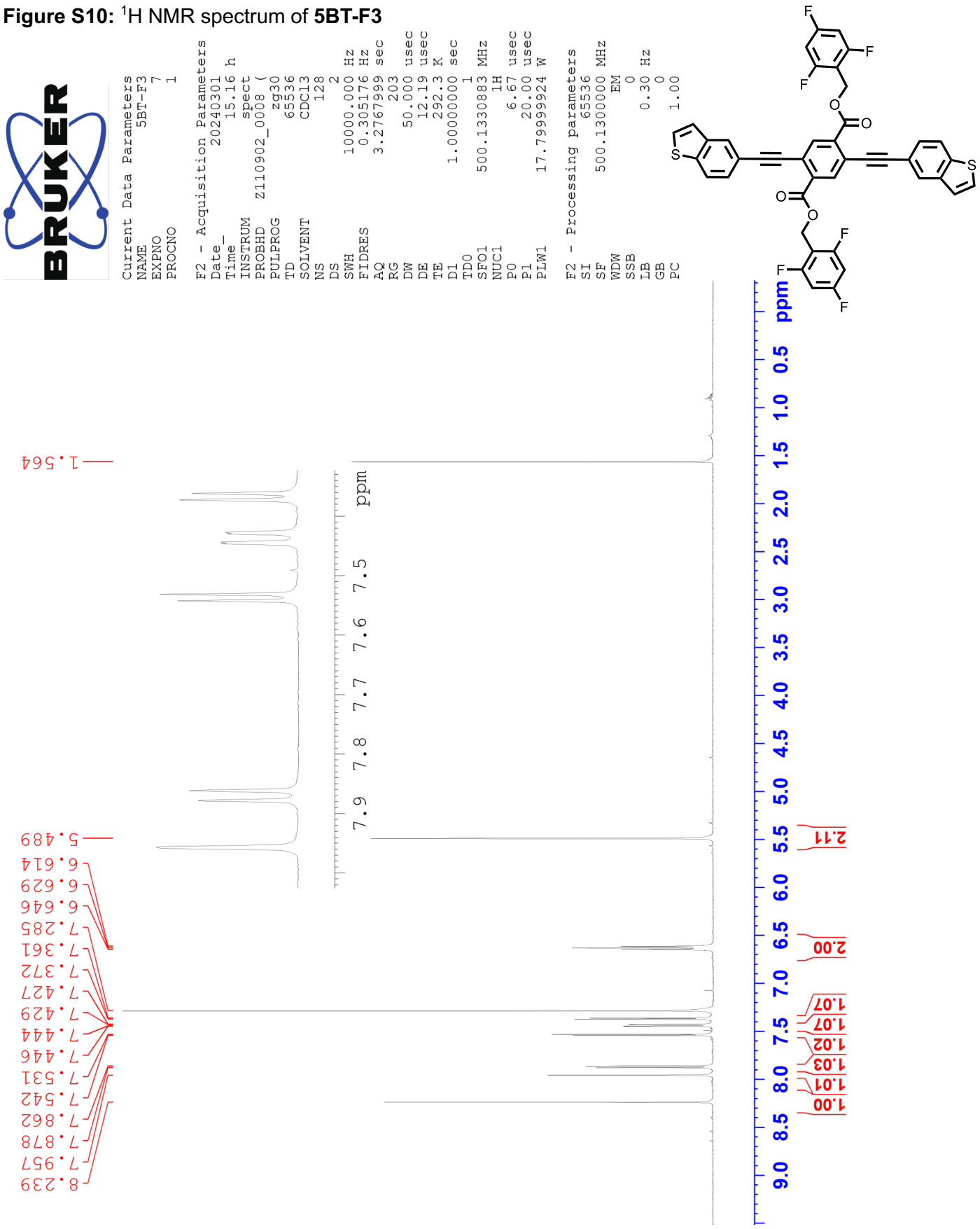

Figure S11: ^{13}C NMR spectrum of **5BT-F3**

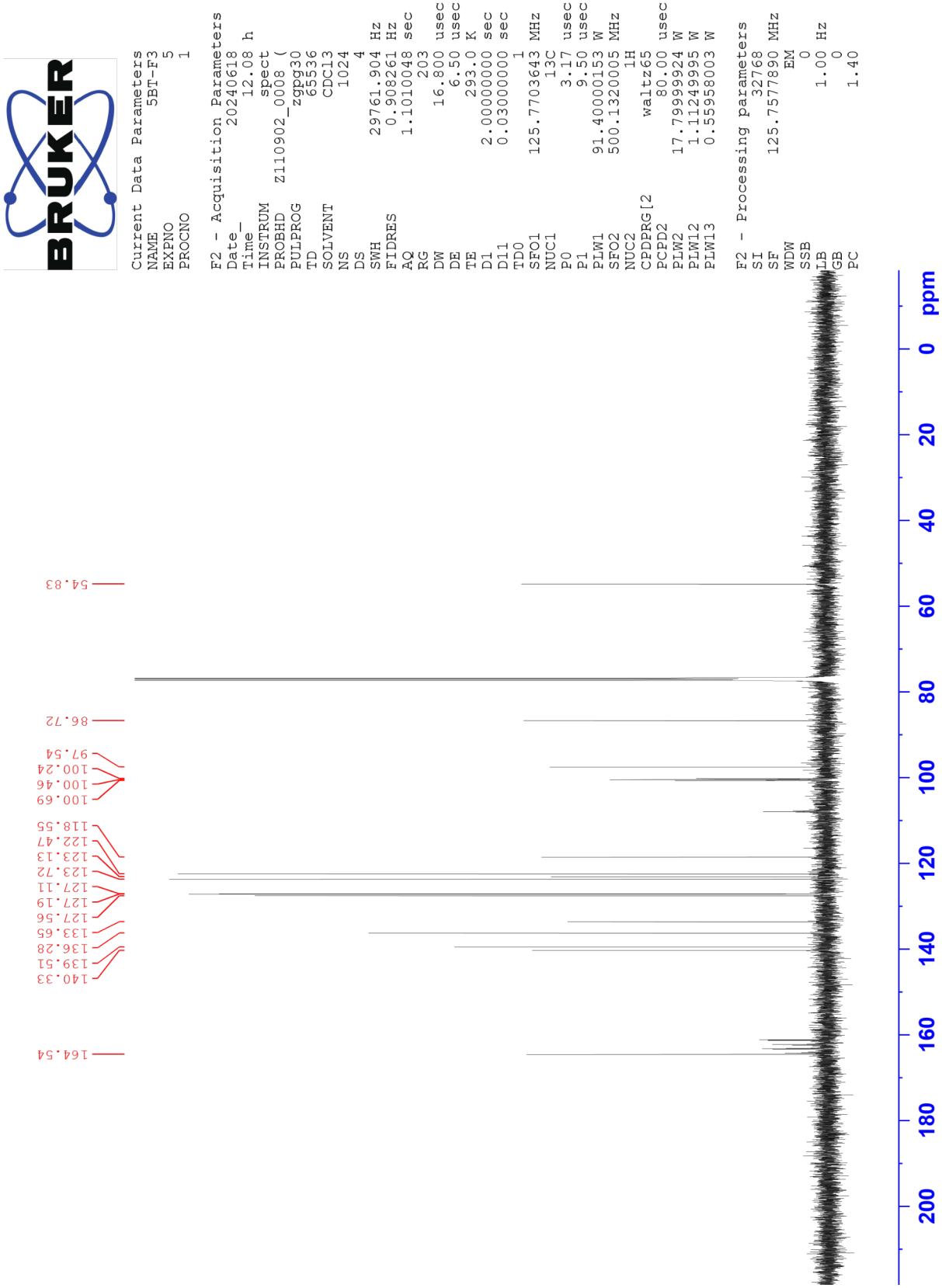

Figure S12: ^{1}H NMR spectrum of **5BT-H5**

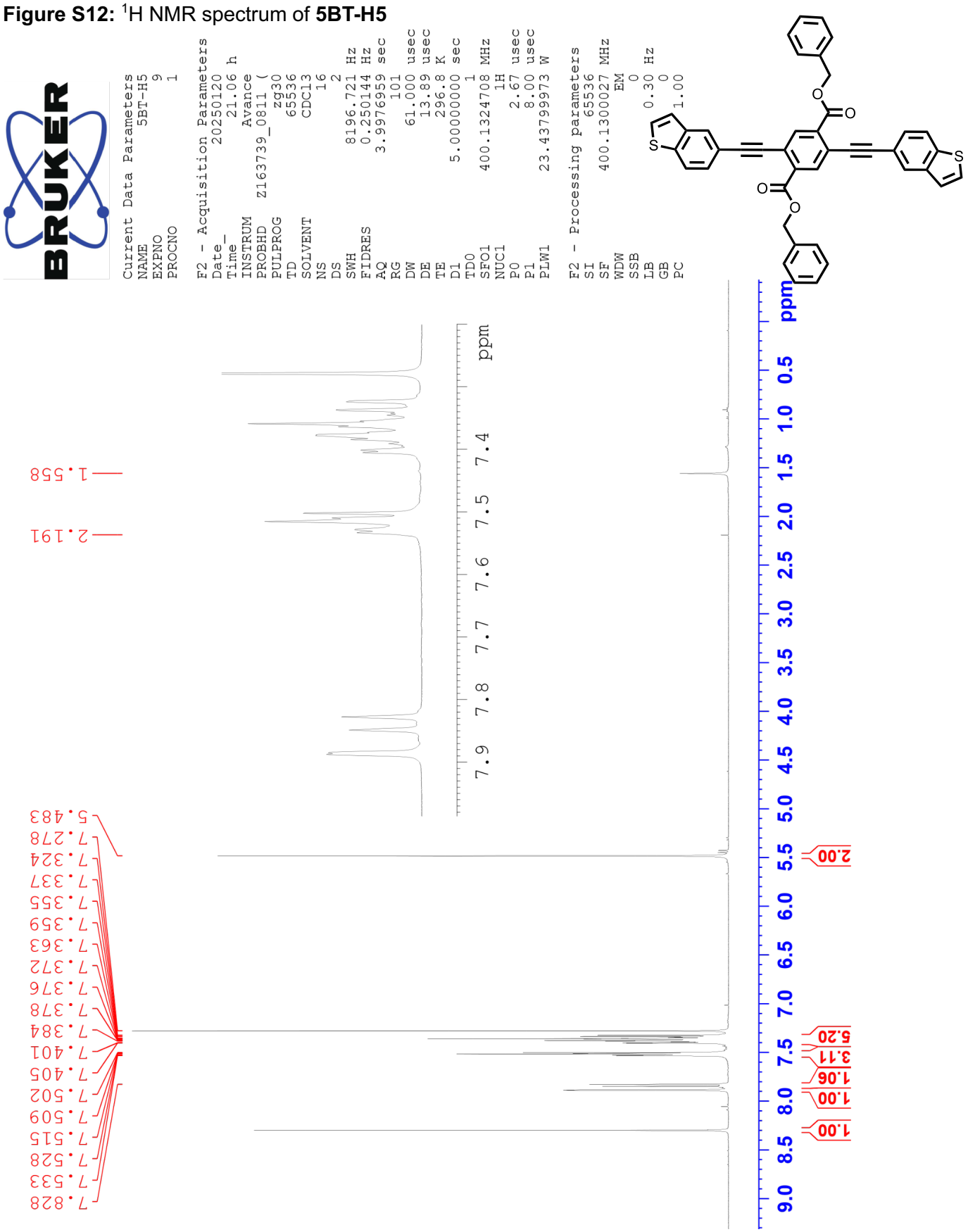

Figure S13: ^{13}C NMR spectra of **5BT-H5**

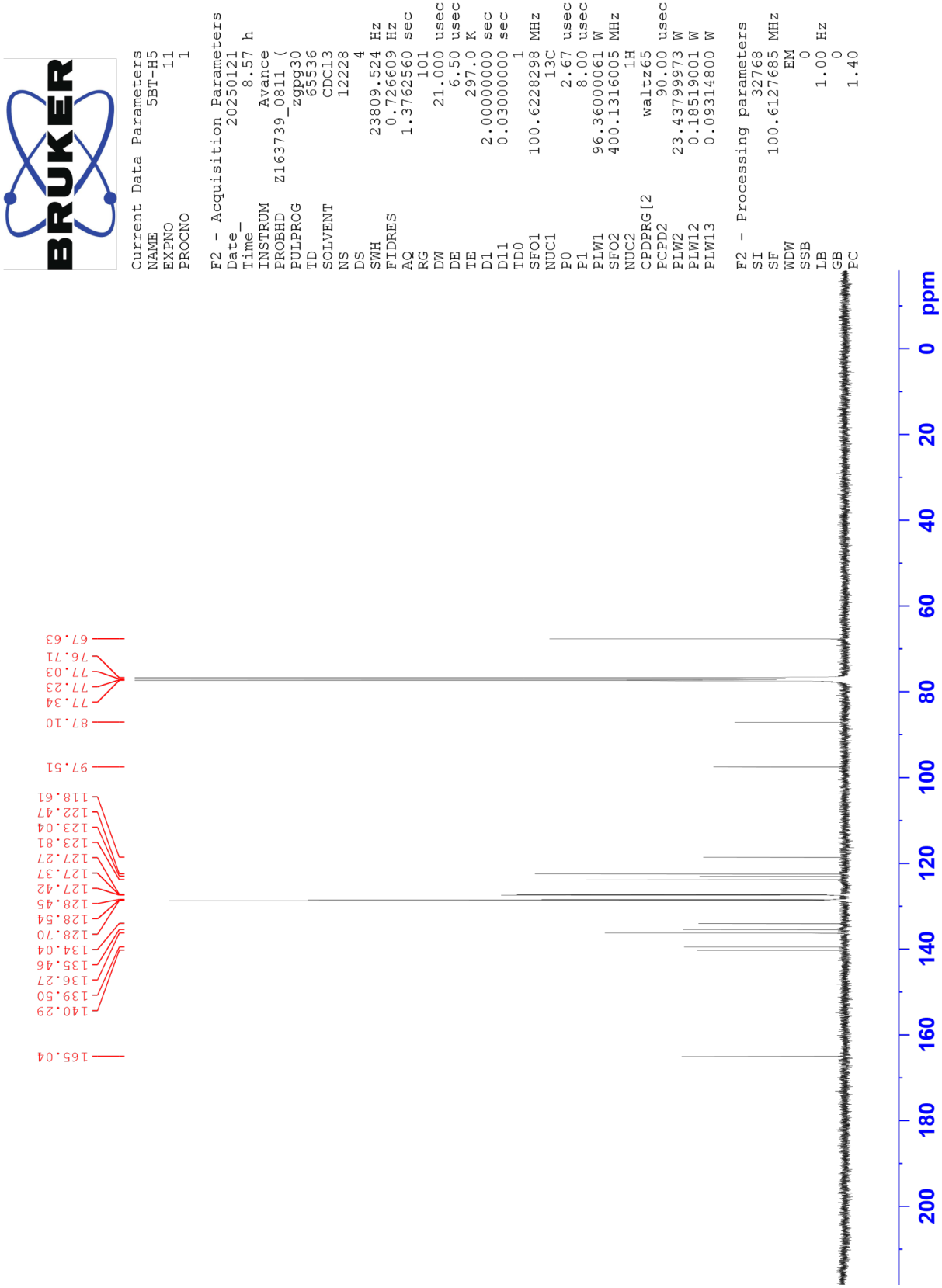

Figure S14: ^{1}H NMR spectrum of **6BT-F5**

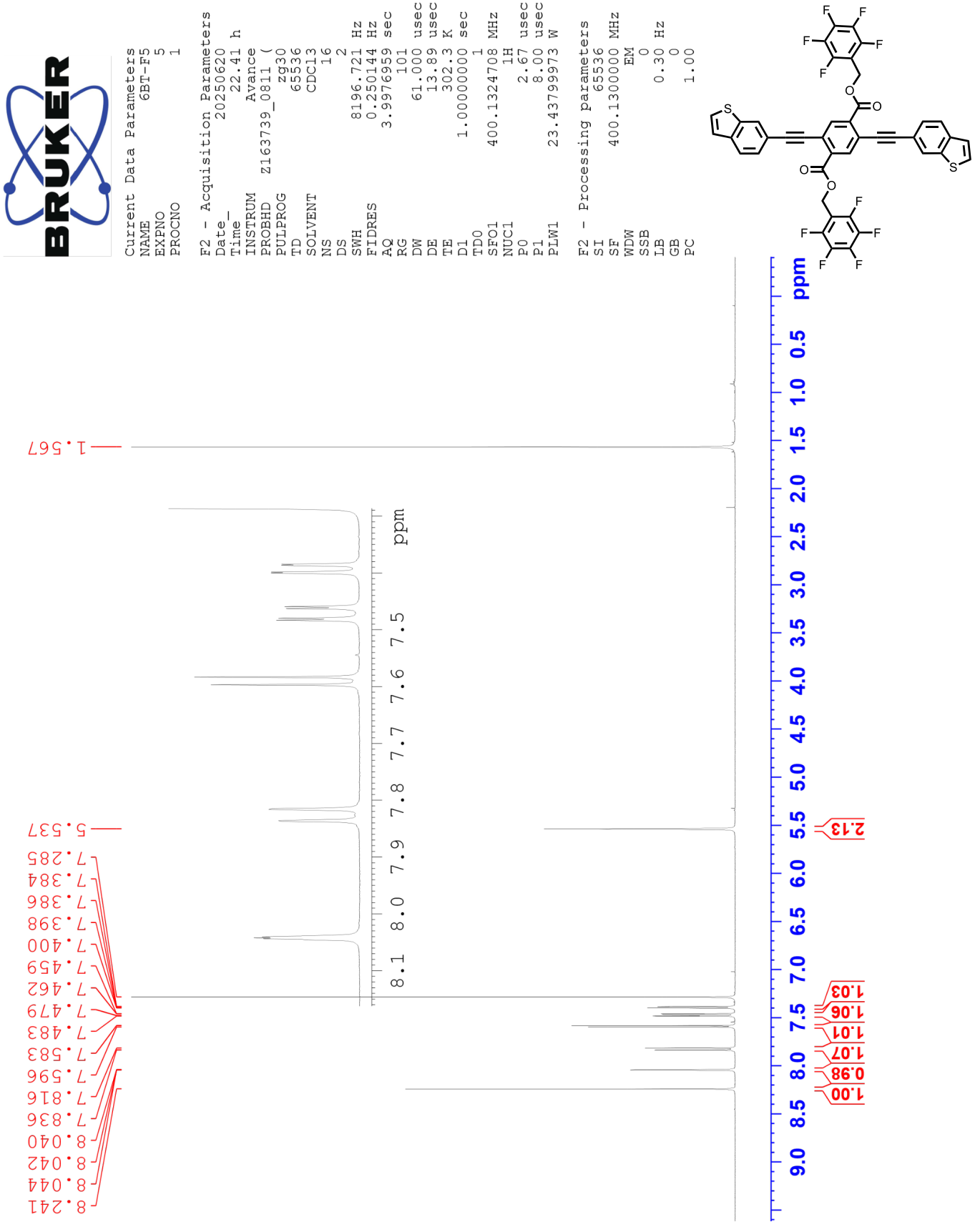

Figure S15: ^{13}C NMR spectrum of **6BT-F5**

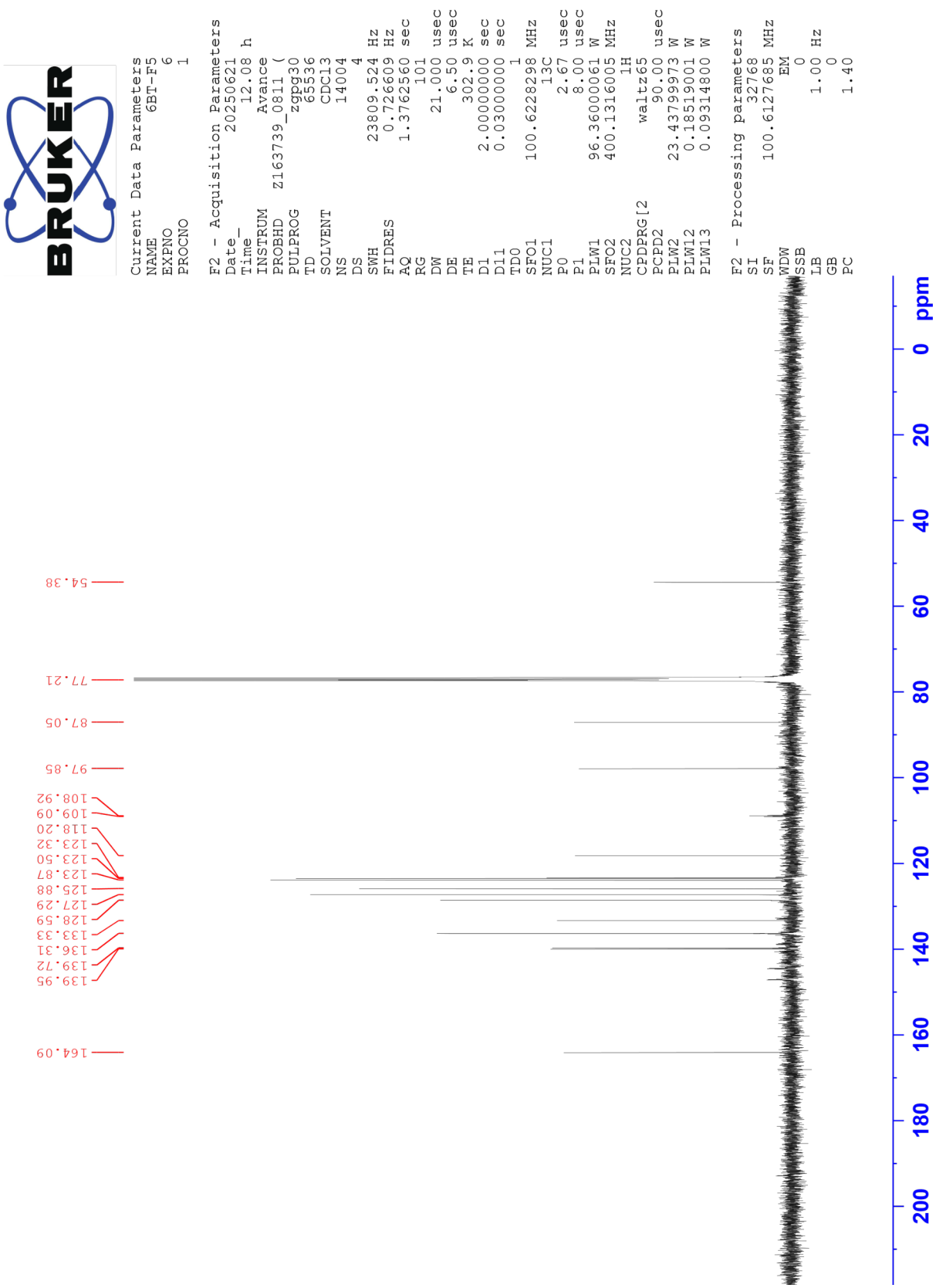

Figure S16: ^{1}H NMR spectrum of **6BT-F3**

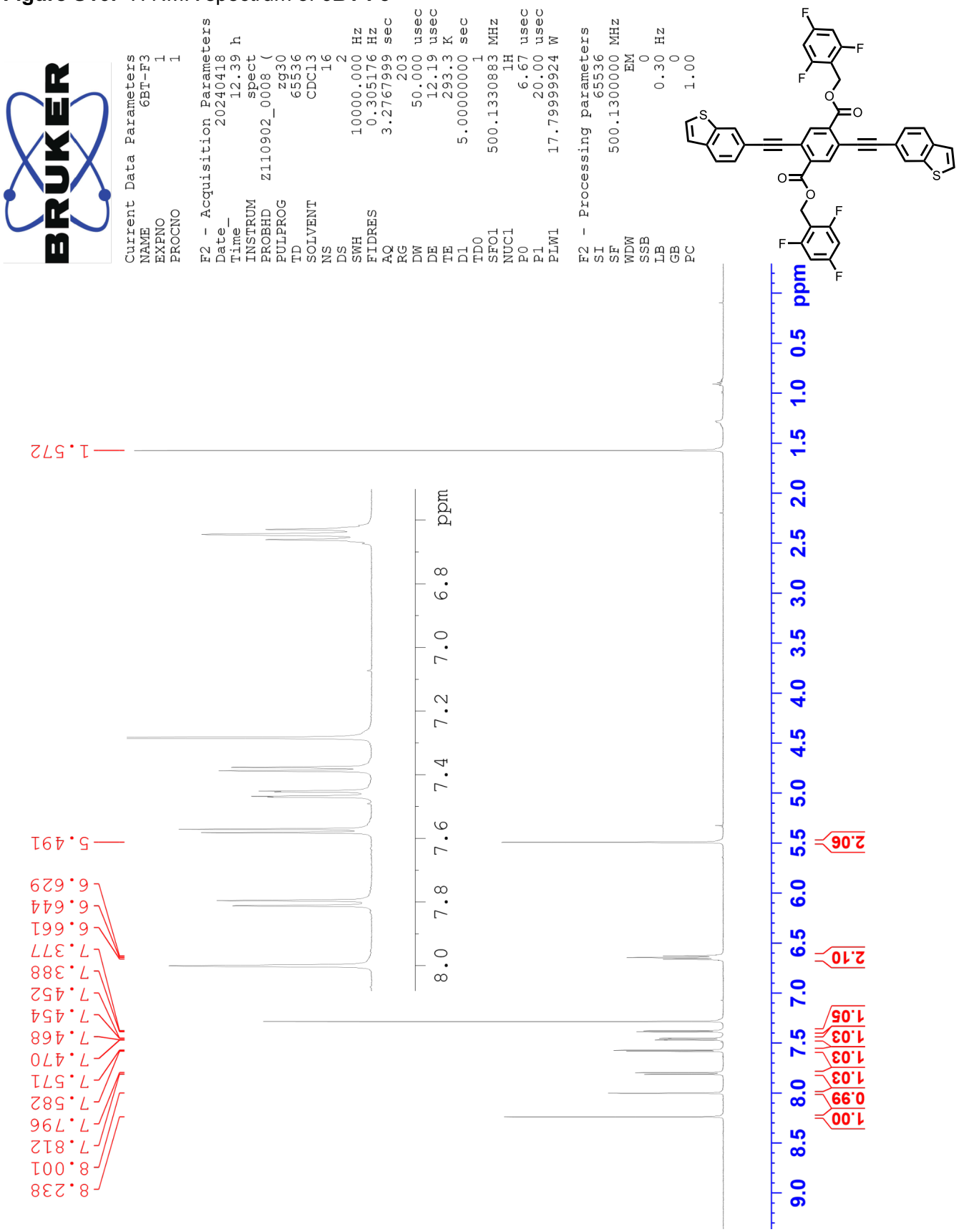

Figure S17: ^{13}C NMR spectrum of **6BT-F3**

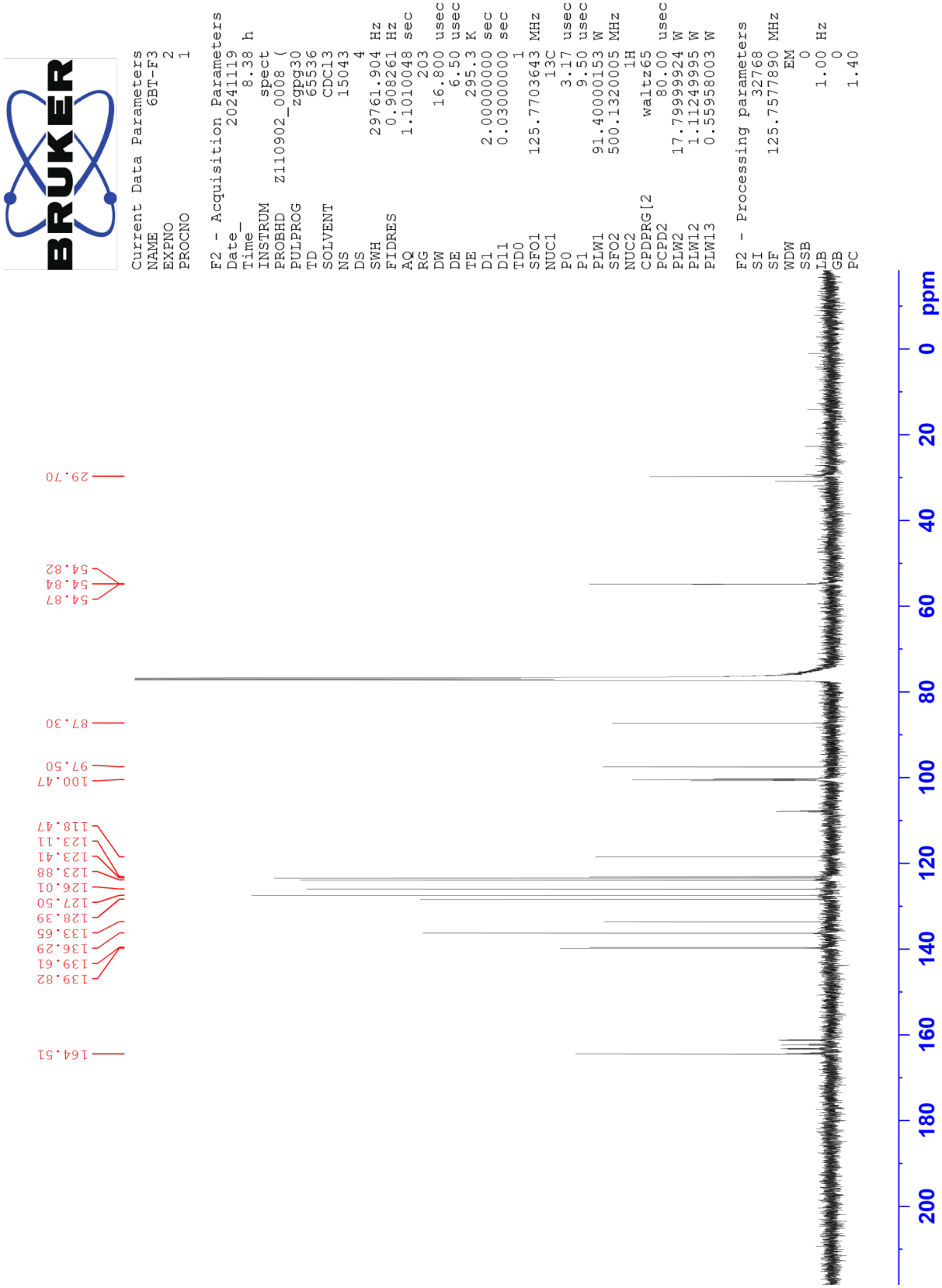

Figure S18: ^{1}H NMR spectrum of **6BT-H5**

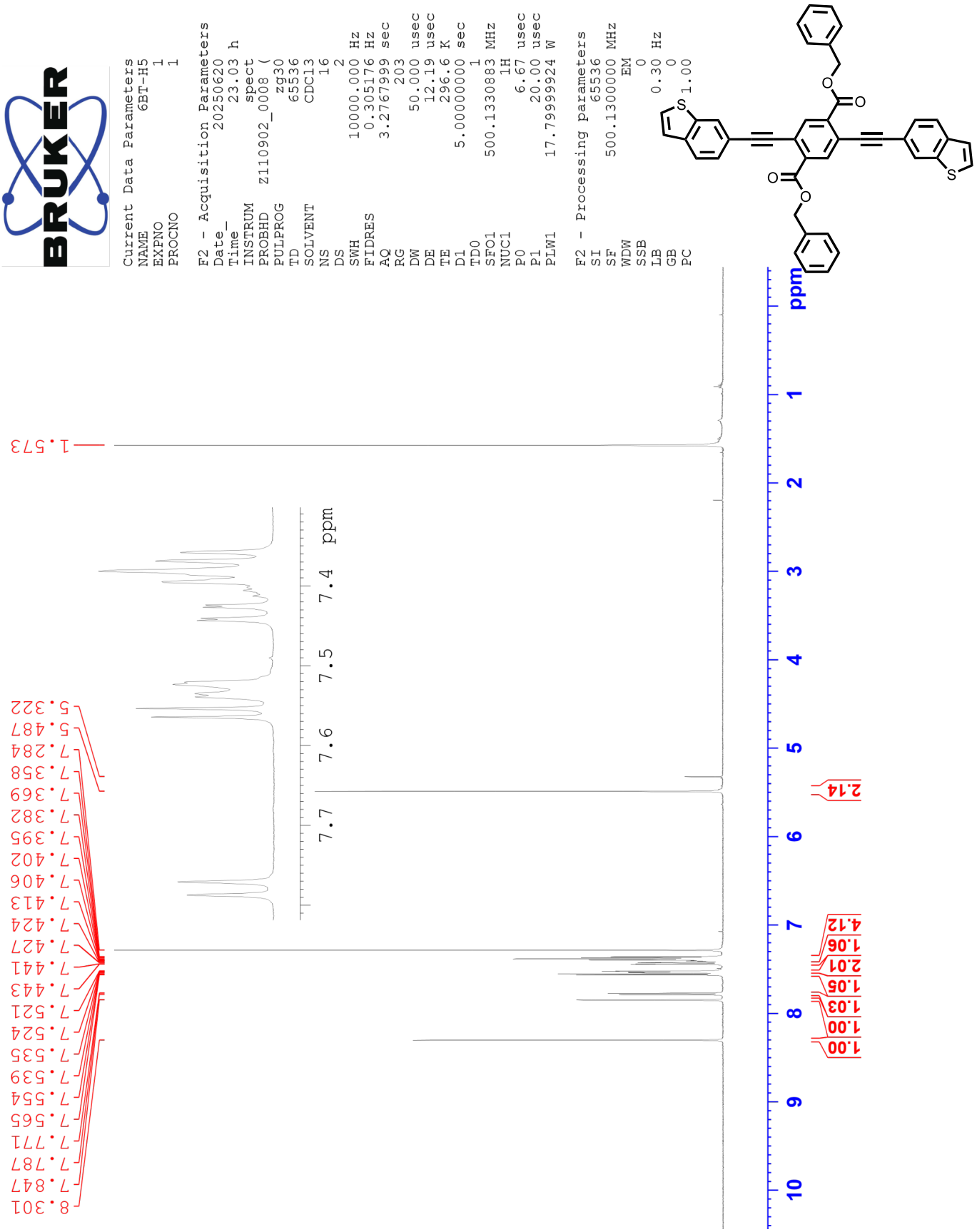

Figure S19: ^{13}C NMR spectrum of **6BT-H5**

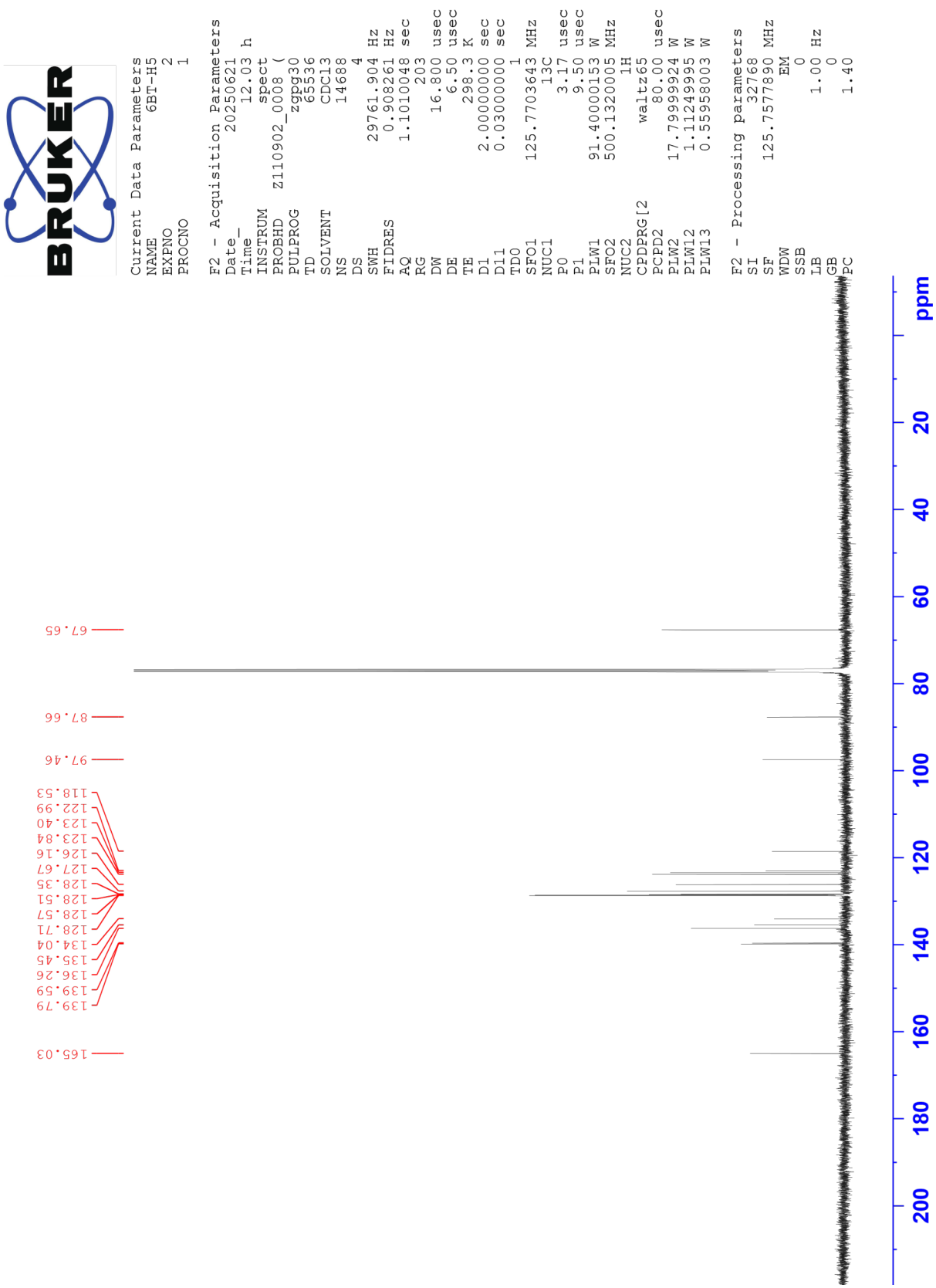

High Resolution Mass Spectroscopy

Figure S20: HRMS of **2TT-F5**

Elemental Composition Report Page 1

Single Mass Analysis
Tolerance = 5.0 PPM / DBE: min = -1.5, max = 100.0
Element prediction: Off
Number of isotope peaks used for i-FIT = 8

Monoisotopic Mass, Even Electron Ions
56 formula(e) evaluated with 1 results within limits (up to 50 best isotopic matches for each mass) Elements Used:
C: 0-80 H: 0-100 O: 0-8 F: 10-10 S: 4-4

Order# 37207 Elisa Guzman 2TT-F5 MSL, SCS, UIUC SYNAPTG2-Si#UGA354
Synapt2_49060a 43 (0.862) Cm (36:49-3:6x2.000) 1: TOF MS ES+
2.88e+004

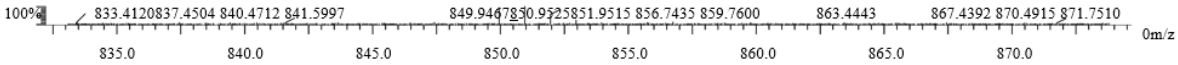

Minimum: -1.5
Maximum: 5.0 5.0 100.0

Mass	Calc. Mass	mDa	PPM	DBE	i-FIT	Norm	Conf(%)	Formula
850.9525	850.9537	-1.2	-1.4	27.5	1863.8	n/a	n/a	C38 H13 O4 F10 S4

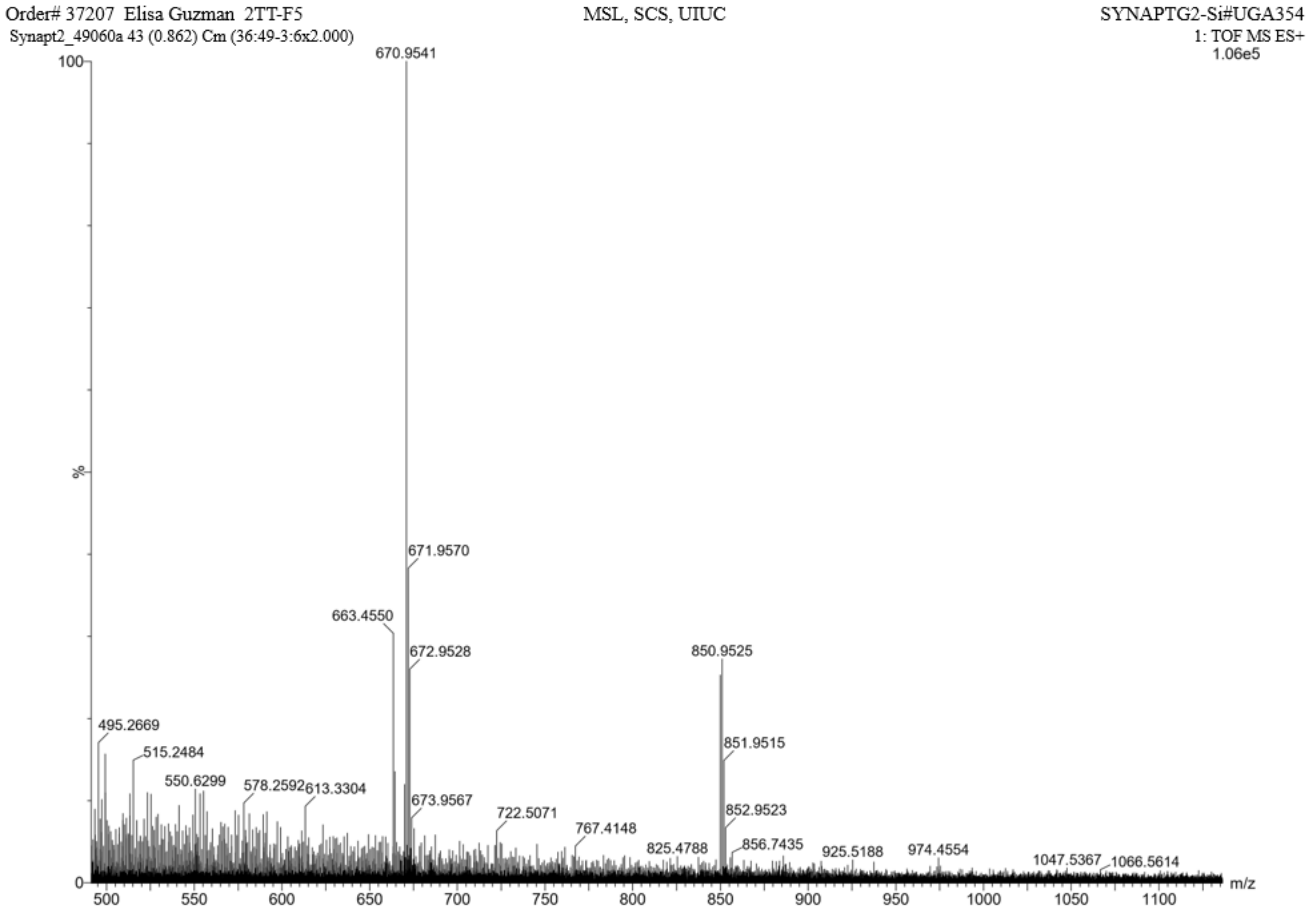

Figure S21: HRMS of **2TT-F3**

Elemental Composition Report Page 1

Single Mass Analysis
Tolerance = 5.0 PPM / DBE: min = -1.5, max = 100.0
Element prediction: Off
Number of isotope peaks used for i-FIT = 8

Monoisotopic Mass, Even Electron Ions
57 formula(e) evaluated with 1 results within limits (up to 50 best isotopic matches for each mass) Elements Used:
C: 0-80 H: 0-100 O: 0-8 S: 4-4 F: 6-6

Order# 37206 Elisa Guzman 2TT-F3 MSL, SCS, UIUC SYNAPTG2-Si#UGA354
Synapt2_49059a 33 (0.674) Cm (25:33-3:6x2.000) 1: TOF MS ES+

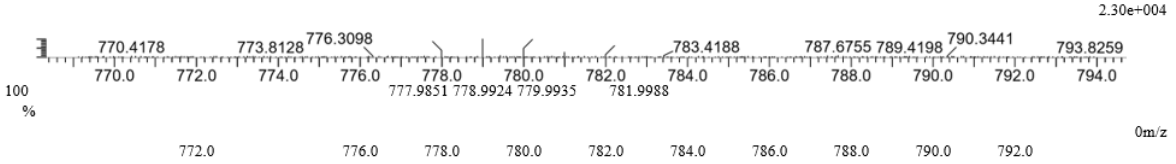

Minimum: -1.5
Maximum: 5.0 5.0 100.0

Mass	Calc. Mass	mDa	PPM	DBE	i-FIT	Norm	Conf(%)	Formula
778.9924	778.9914	1.0	1.3	27.5	1136.7	n/a	n/a	C38 H17 O4 S4 F6

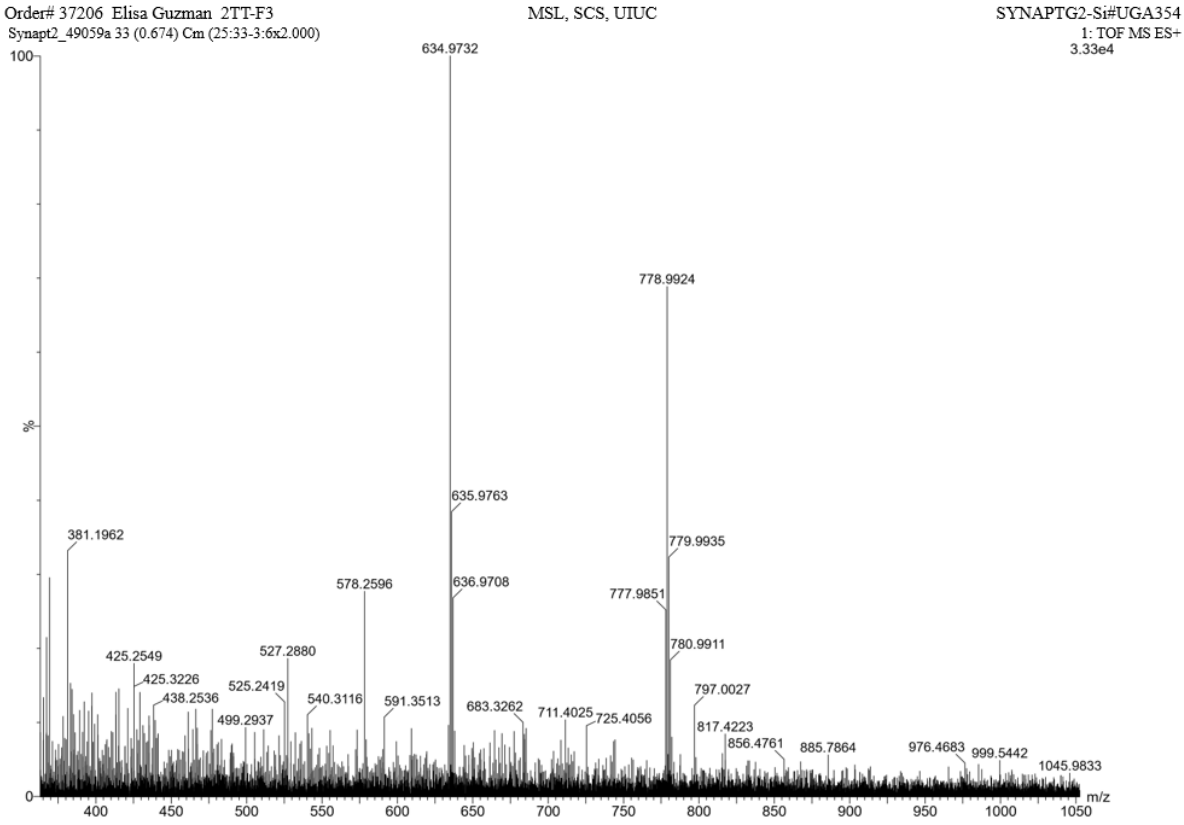

Figure S22: HRMS of **6BT-F5**

Elemental Composition Report Page 1

Single Mass Analysis
Tolerance = 5.0 PPM / DBE: min = -1.5, max = 100.0
Element prediction: Off
Number of isotope peaks used for i-FIT = 8

Monoisotopic Mass, Even Electron Ions
61 formula(e) evaluated with 1 results within limits (up to 50 best isotopic matches for each mass) Elements Used:
C: 0-80 H: 0-100 O: 0-8 F: 10-10 S: 2-2

Order# 37209 Elisa Guzman 6BT-F5 MSL, SCS, UIUC SYNAPTG2-Si#UGA354
Synapt2_49062 26 (0.535) Cm (26:40-2:7x2.000) 1: TOF MS ES+
3.54e+004

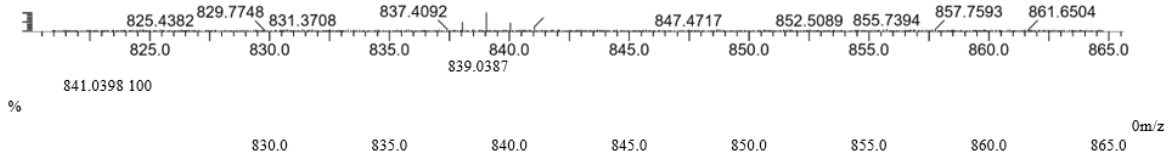

Minimum: -1.5
Maximum: 5.0 5.0 100.0

Mass	Calc. Mass	mDa	PPM	DBE	i-FIT	Norm	Conf(%)	Formula
839.0387	839.0409	-2.2	-2.6	29.5	1659.0	n/a	n/a	C42 H17 O4 F10 S2

Order# 37209 Elisa Guzman 6BT-F5 MSL, SCS, UIUC SYNAPTG2-Si#UGA354
Synapt2_49062 26 (0.535) Cm (26:40-2:7x2.000) 1: TOF MS ES+
1.02e5

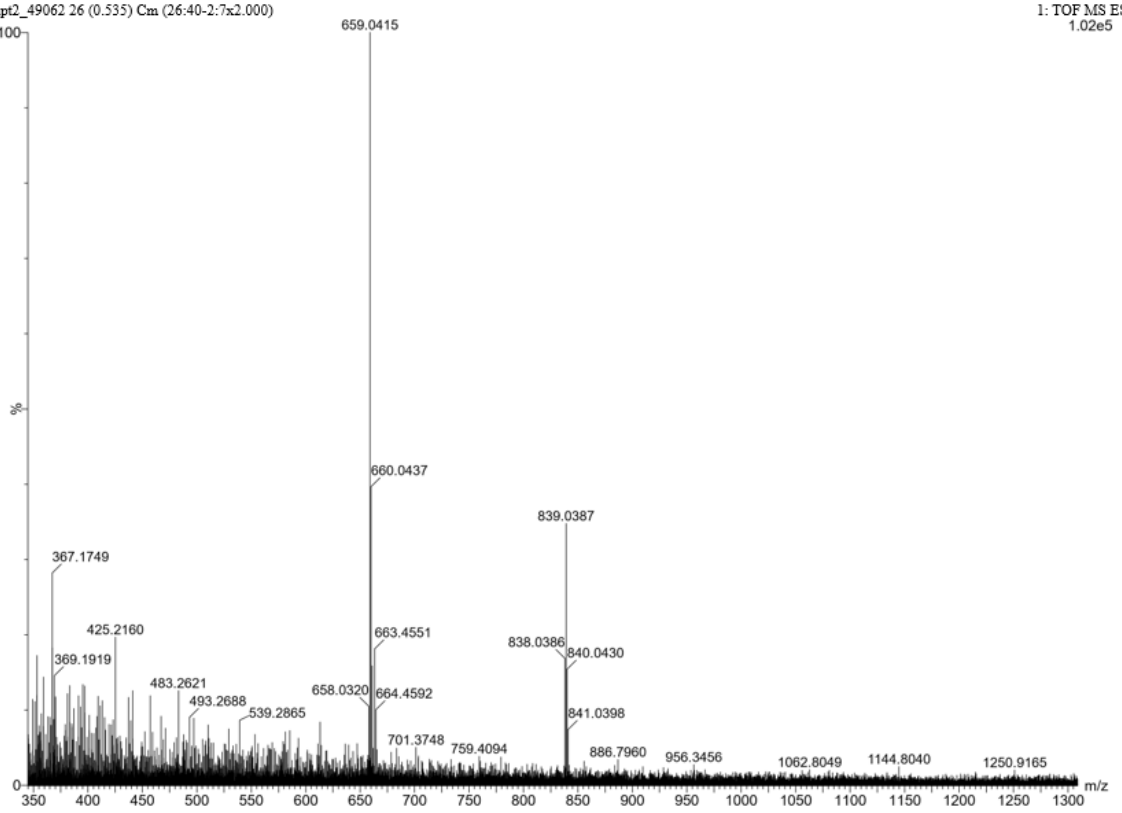

Figure S23: HRMS of **6BT-F3**

Elemental Composition Report Page 1

Single Mass Analysis
Tolerance = 5.0 PPM / DBE: min = -1.5, max = 100.0
Element prediction: Off
Number of isotope peaks used for i-FIT = 8

Monoisotopic Mass, Even Electron Ions
62 formula(e) evaluated with 1 results within limits (up to 50 best isotopic matches for each mass) Elements Used:
C: 0-80 H: 0-100 O: 0-8 S: 2-2 F: 6-6

Order# 37208 Elisa Guzman 6BT-F3 MSL, SCS, UIUC SYNAPTG2-Si#UGA354
Synapt2_49061 23 (0.465) Cm (23:29-2:5x2.000) 1: TOF MS ES+

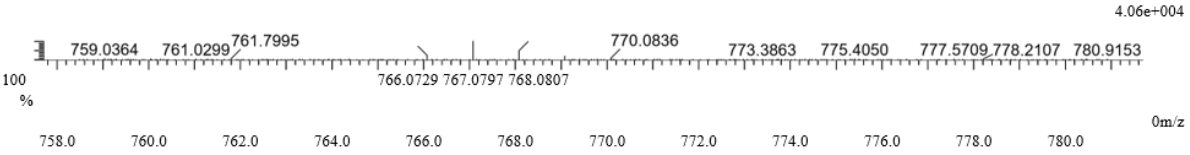

Minimum:			-1.5				
Maximum:		5.0	5.0	100.0			
Mass	Calc. Mass	mDa	PPM	DBE	i-FIT	Norm	Conf(%) Formula
767.0797	767.0785	1.2	1.6	29.5	937.7	n/a	n/a C42 H21 O4 S2 F6

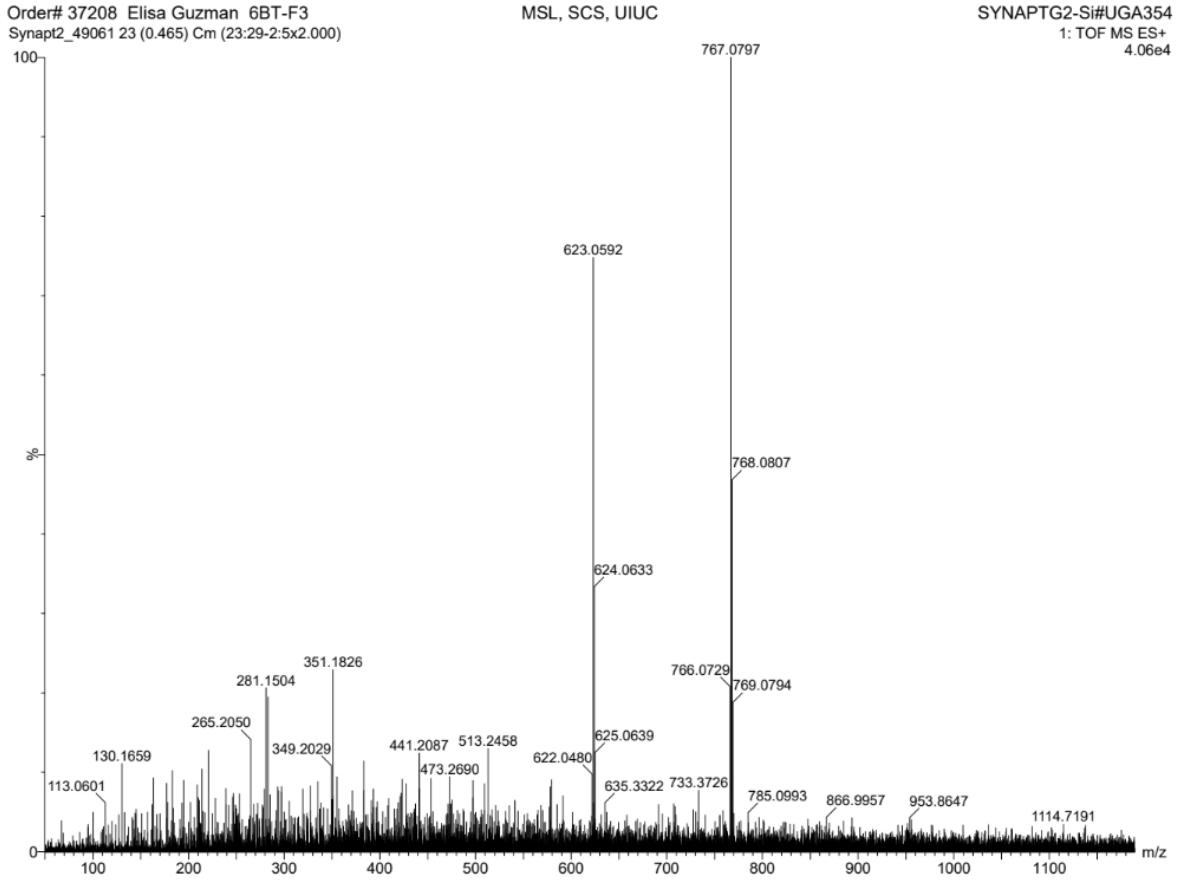

Figure S24: HRMS of **6BT-H5**

Elemental Composition Report Page 1

Single Mass Analysis
Tolerance = 5.0 PPM / DBE: min = -1.5, max = 100.0
Element prediction: Off
Number of isotope peaks used for i-FIT = 8

Monoisotopic Mass, Even Electron Ions
67 formula(e) evaluated with 1 results within limits (up to 50 best isotopic matches for each mass) Elements Used:
C: 0-80 H: 0-100 O: 0-8 S: 2-2

Order# 37210 Elisa Guzman 6BT-H5 MSL, SCS, UIUC SYNAPTG2-Si#UGA354
Synapt2_49063a 42 (0.846) Cm (33:44-3:5x2.000) 1: TOF MS ES+
1.12e+005

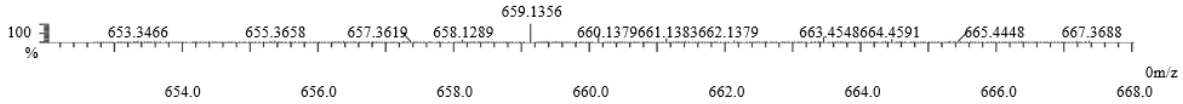

Minimum:			-1.5					
Maximum:		5.0	5.0	100.0				
Mass	Calc. Mass	mDa	PPM	DBE	i-FIT	Norm	Conf(%)	Formula
659.1356	659.1351	0.5	0.8	29.5	2119.0	n/a	n/a	C42 H27 O4 S2

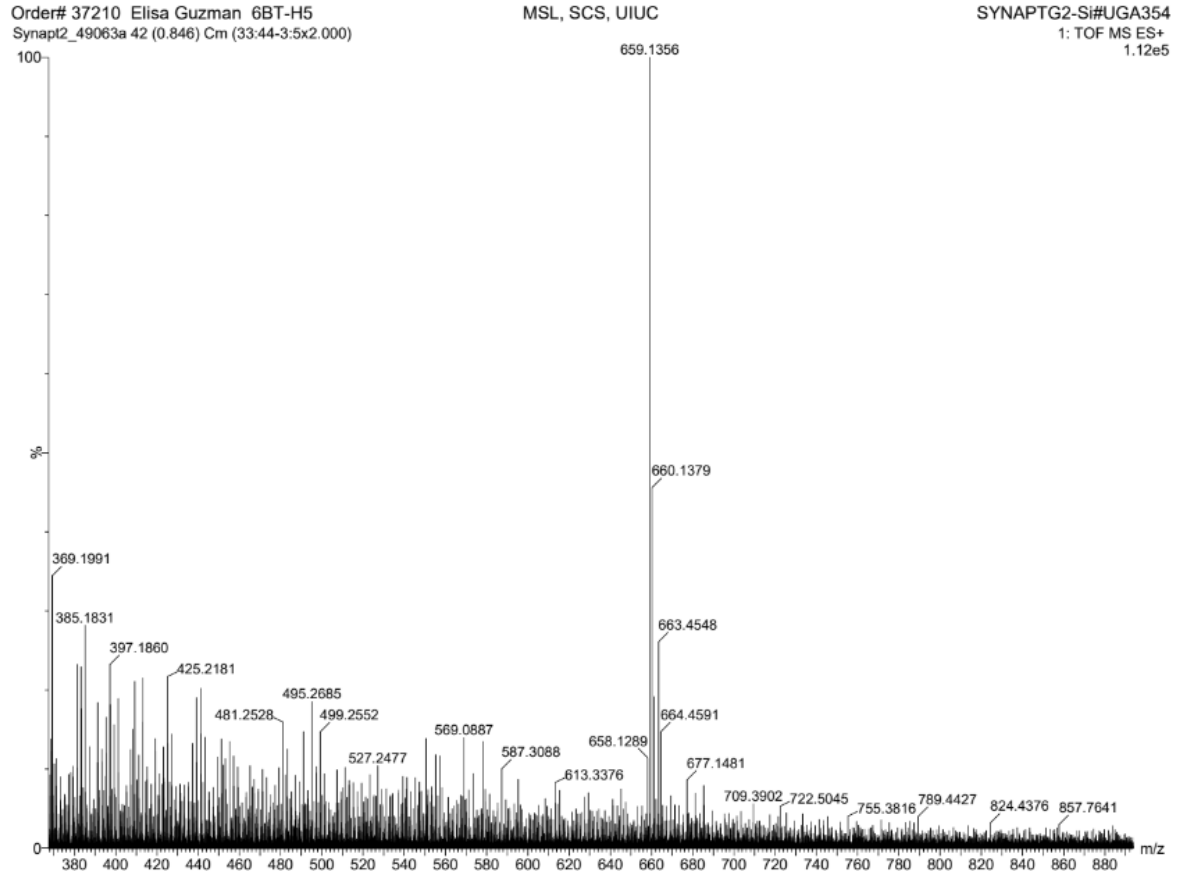

Optical Properties

Figure S25: 2-Benzothiophene with trifluoro substitution chloroform solution excitation (blue), chloroform solution emission (green), and thin film emission (orange).

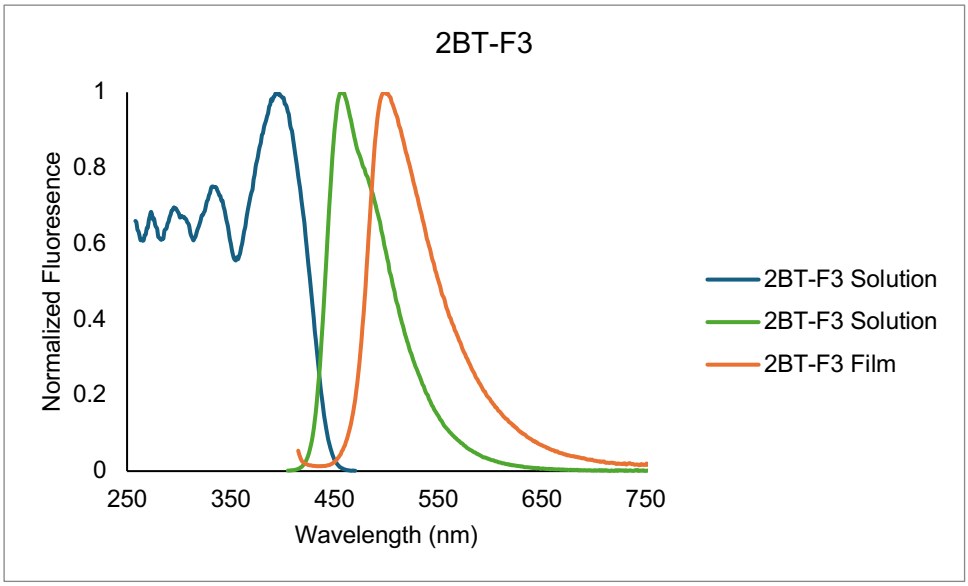

Figure S26: 2-Benzothiophene solution and thin film comparison with hydrogenated phenyl side chains (blue), trifluorophenyl (green), and perfluorinated phenyl side chains (orange).

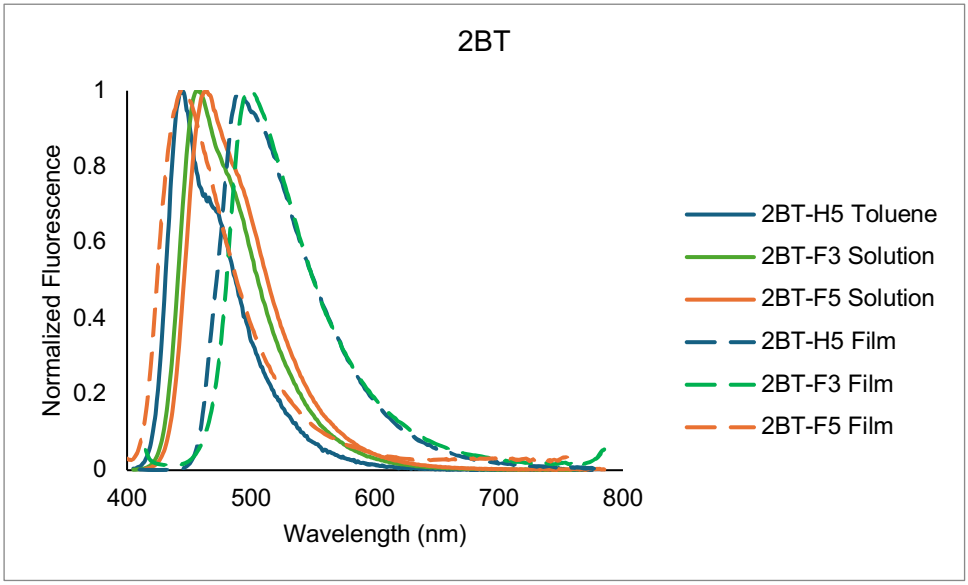

Figure S27: 2-Thienothiophene with perfluorinated benzyl side chains chloroform solution excitation (blue), chloroform solution emission (green), and thin film emission (orange).

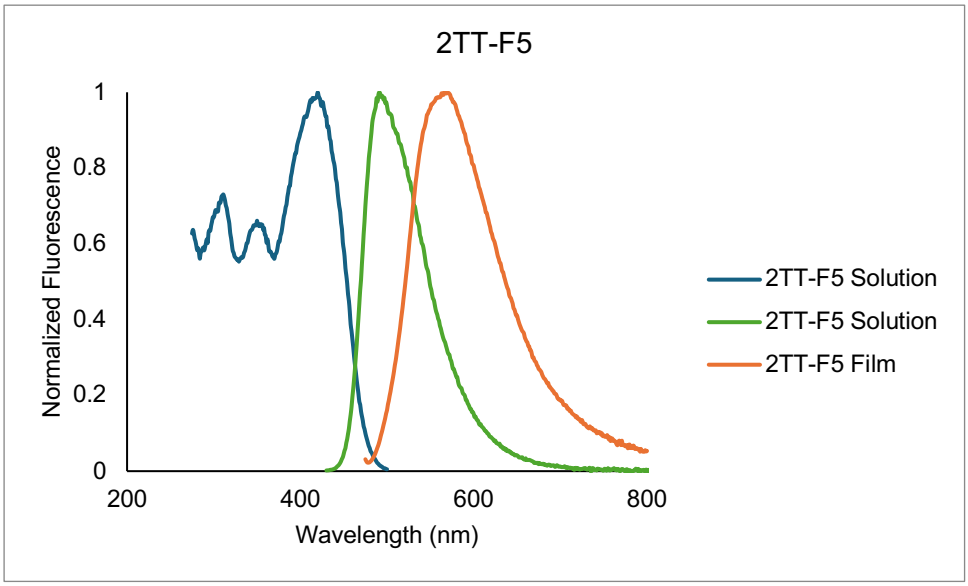

Figure S28: 2-Thienothiophene with trifluorinated benzyl side chains chloroform solution excitation (blue), chloroform solution emission (green), and thin film emission (orange).

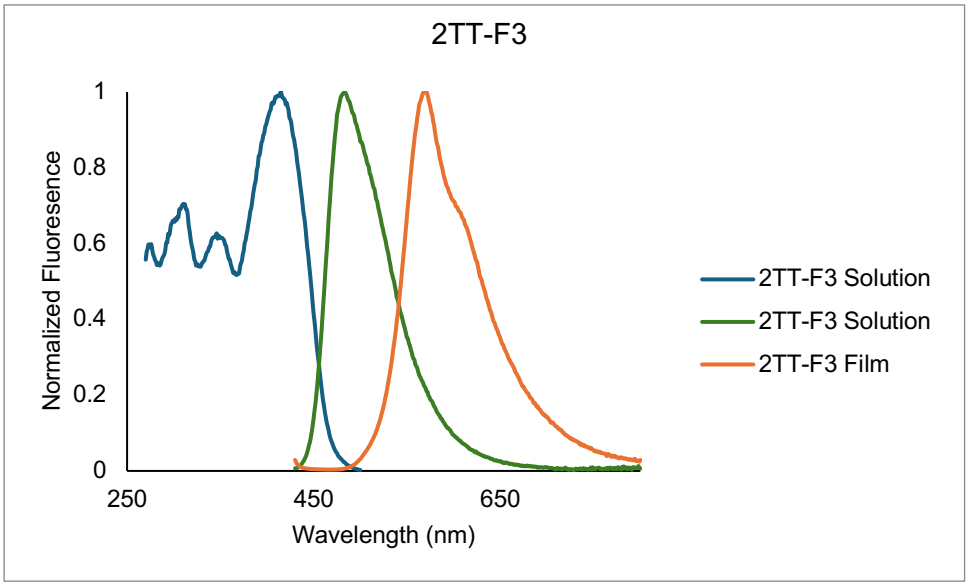

Figure S29: 2-Thienothiophene with hydrogenated benzyl side chains chloroform solution excitation (blue), chloroform solution emission (green), thin film emission for orange emitting solid (orange), and thin film emission for green emitting solid (black).

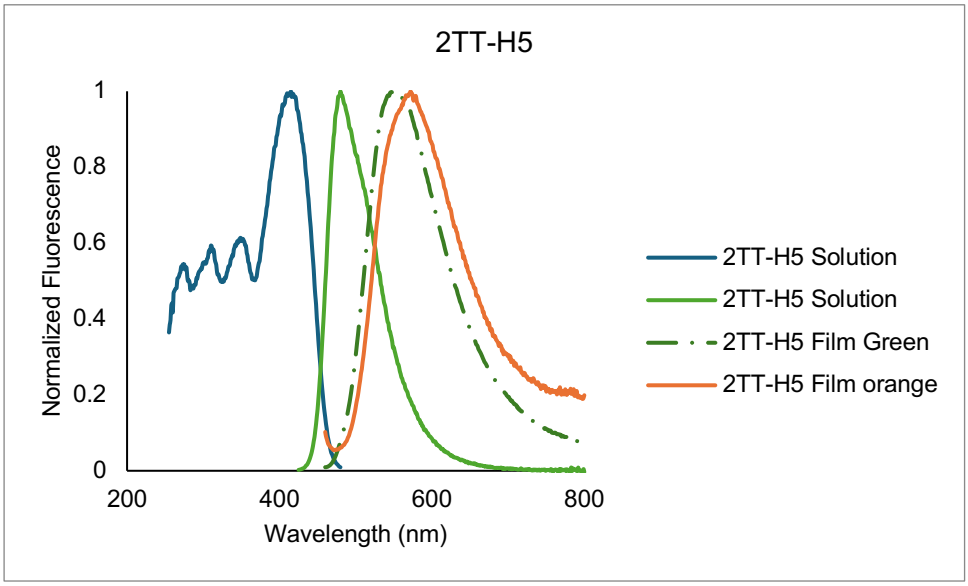

Figure S30: 2-Thienothiophene solution and thin films comparison with hydrogenated phenyl side chains (blue), trifluorophenyl (green), and perfluorinated phenyl side chains (orange). The additional green emitting solid is also presented (black).

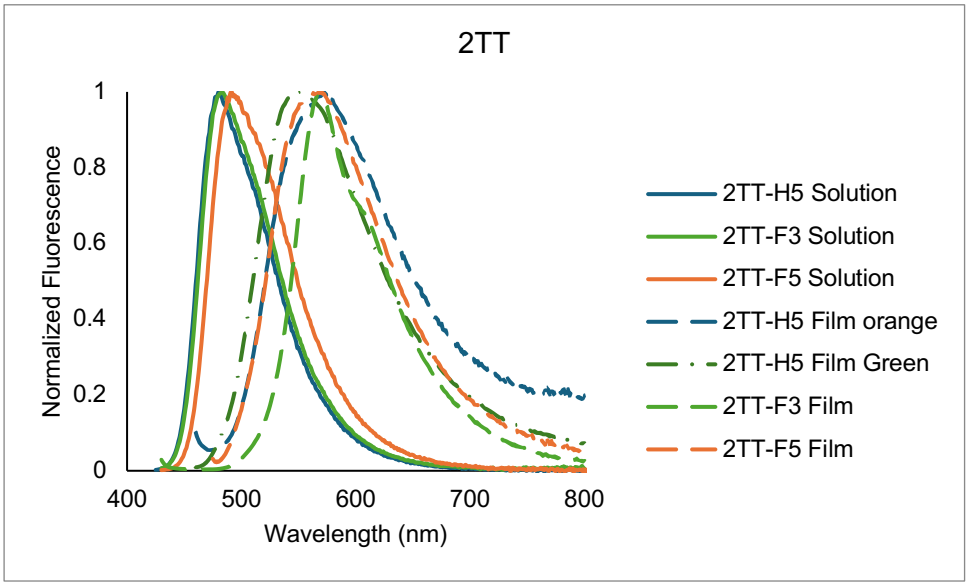

Figure S31: 5-Benzothiophene with perfluorinated benzyl side chains showing chloroform solution excitation (blue), chloroform solution emission (green), and thin film emission (orange).

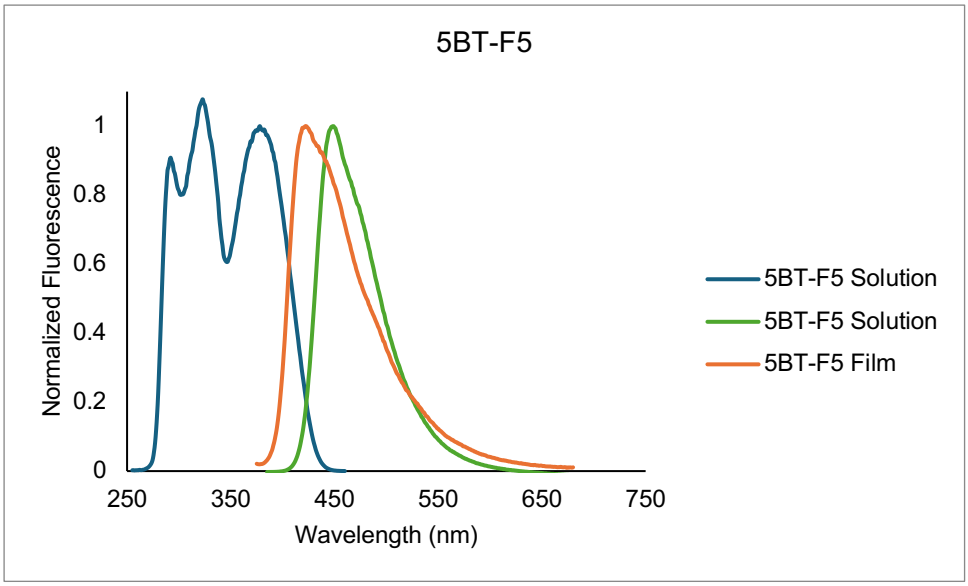

Figure S32: 5-Benzothiophene with trifluorinated benzyl side chains showing chloroform solution excitation (blue), chloroform solution emission (green), and thin film emission (orange).

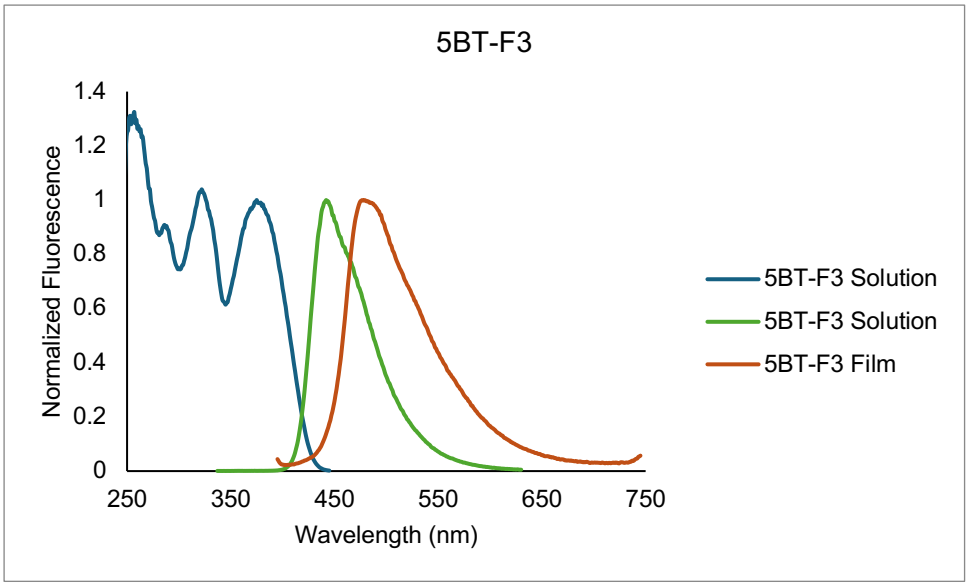

Figure S33: 5-Benzothiophene with hydrogenated benzyl side chains showing chloroform solution excitation (blue), chloroform solution emission (green), and thin film emission (orange).

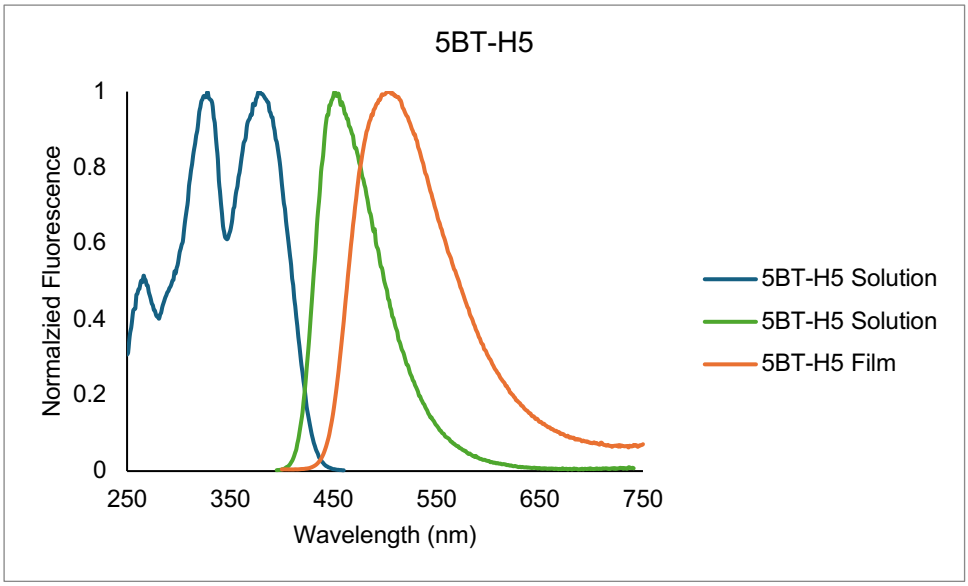

Figure S34: 5-Benzothiophene solution and thin films comparison with hydrogenated phenyl side chains (blue), trifluorophenyl (green), and perfluorinated phenyl side chains (orange).

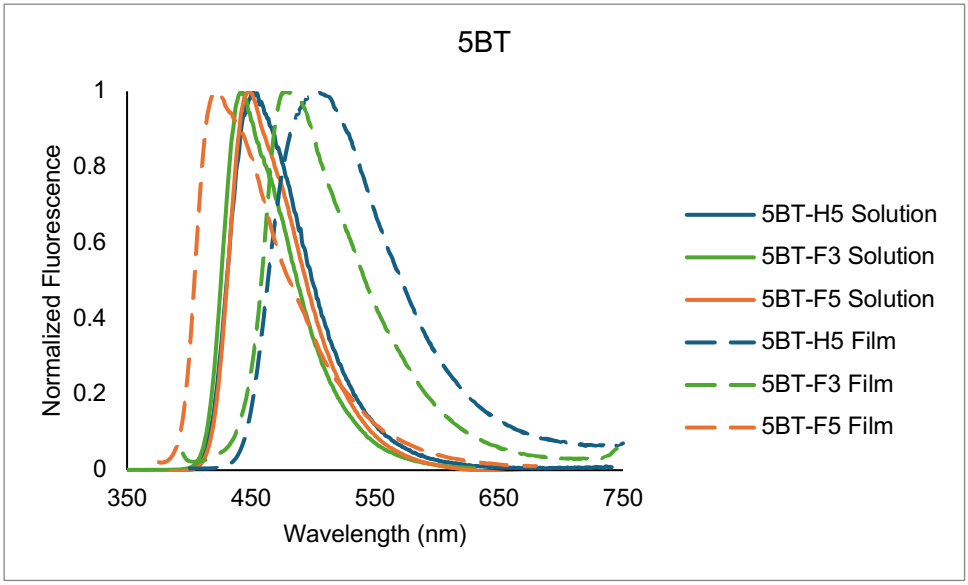

Figure S35: 6-Benzothiophene with perfluorinated benzyl side chains showing chloroform solution excitation (blue), chloroform solution emission (green), and thin film emission (orange).

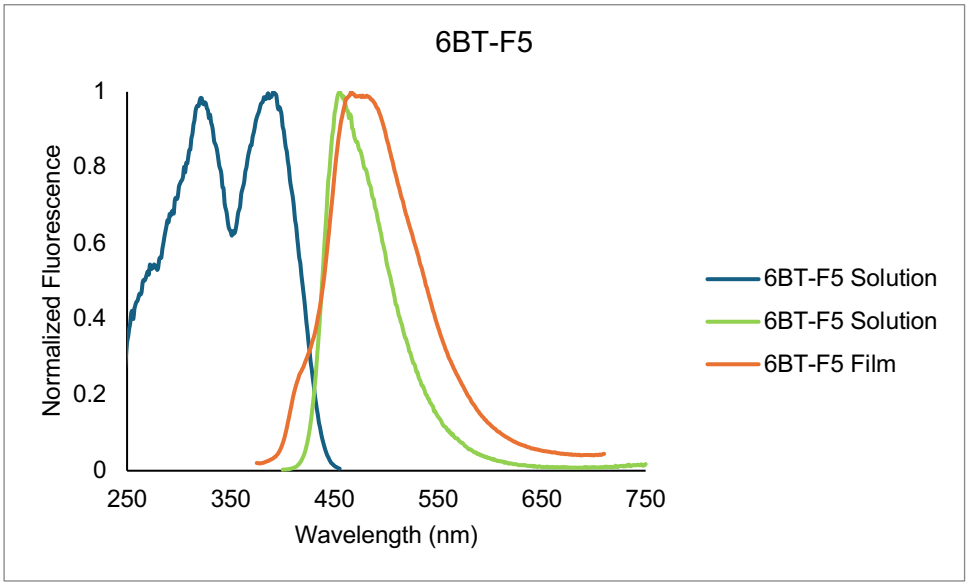

Figure S36: 6-Benzothiophene with trifluorinated benzyl side chains showing chloroform solution excitation (blue), chloroform solution emission (green), and thin film emission (orange).

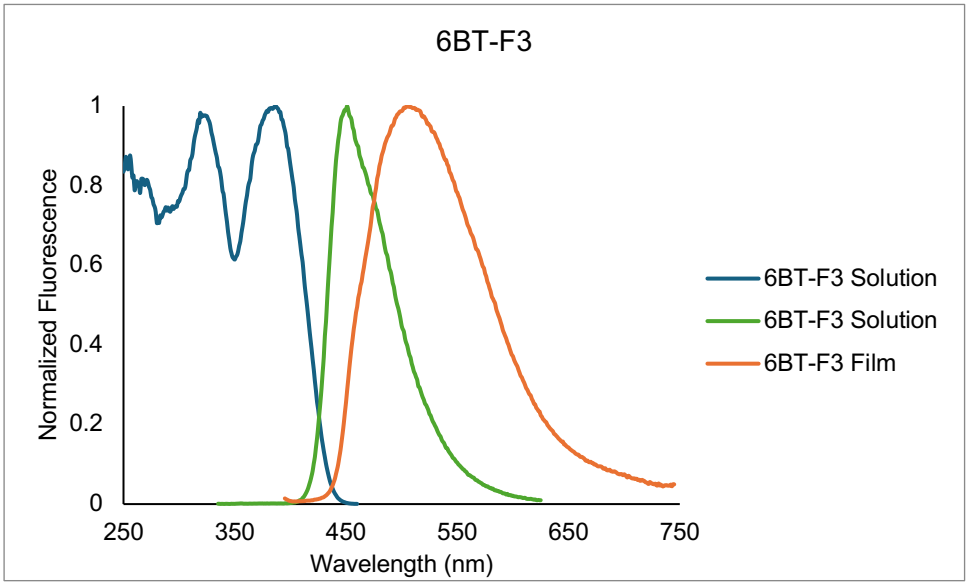

Figure S37: 6-Benzothiophene with hydrogenated benzyl side chains showing chloroform solution excitation (blue), chloroform solution emission (green), and thin film emission (orange).

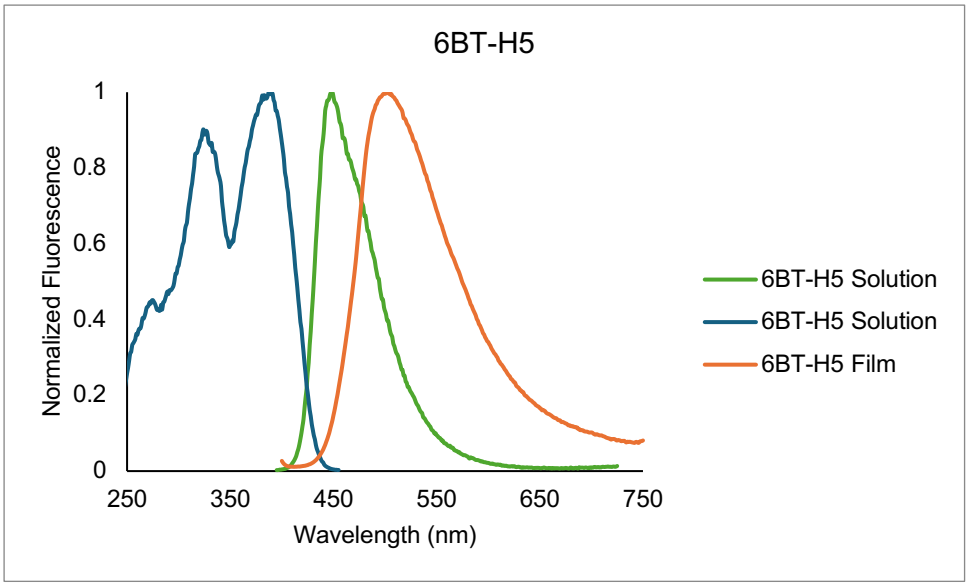

Figure S38: 6-Benzothiophene solution and thin films comparison with hydrogenated phenyl side chains (blue), trifluorophenyl (green), and perfluorinated phenyl side chains (orange).

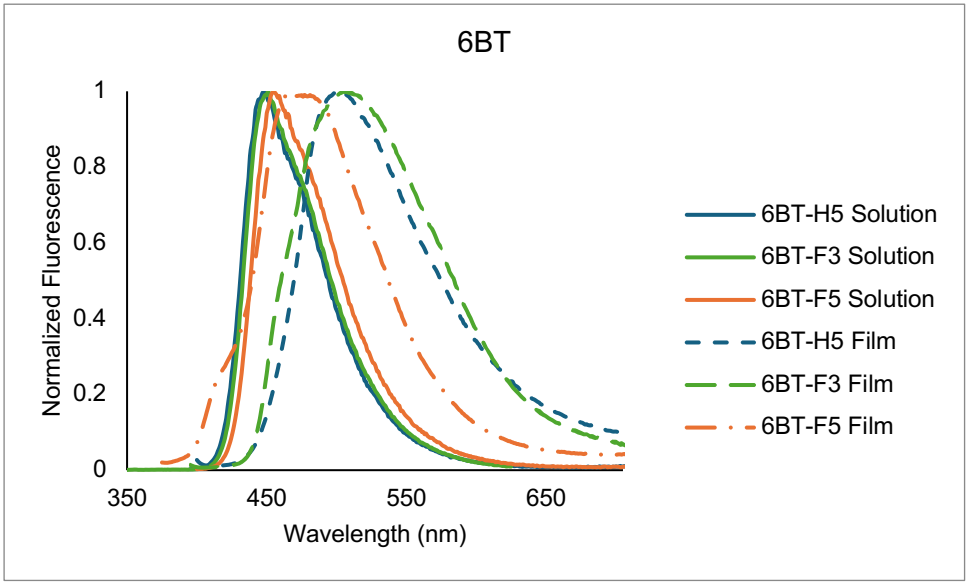

Differential Scanning Calorimetry

Figure S39: 2BT-F3 DSC analysis in heat-cool-heat cycles of orange (A) melting at 205°C and yellow (B) melting at 211°C solids. This shows that the polymorphic compound is thermally accessible. Repeating the heat-cool cycle once more for the orange (C) and yellow (D) shows a third polymorph, melting at 185°C.

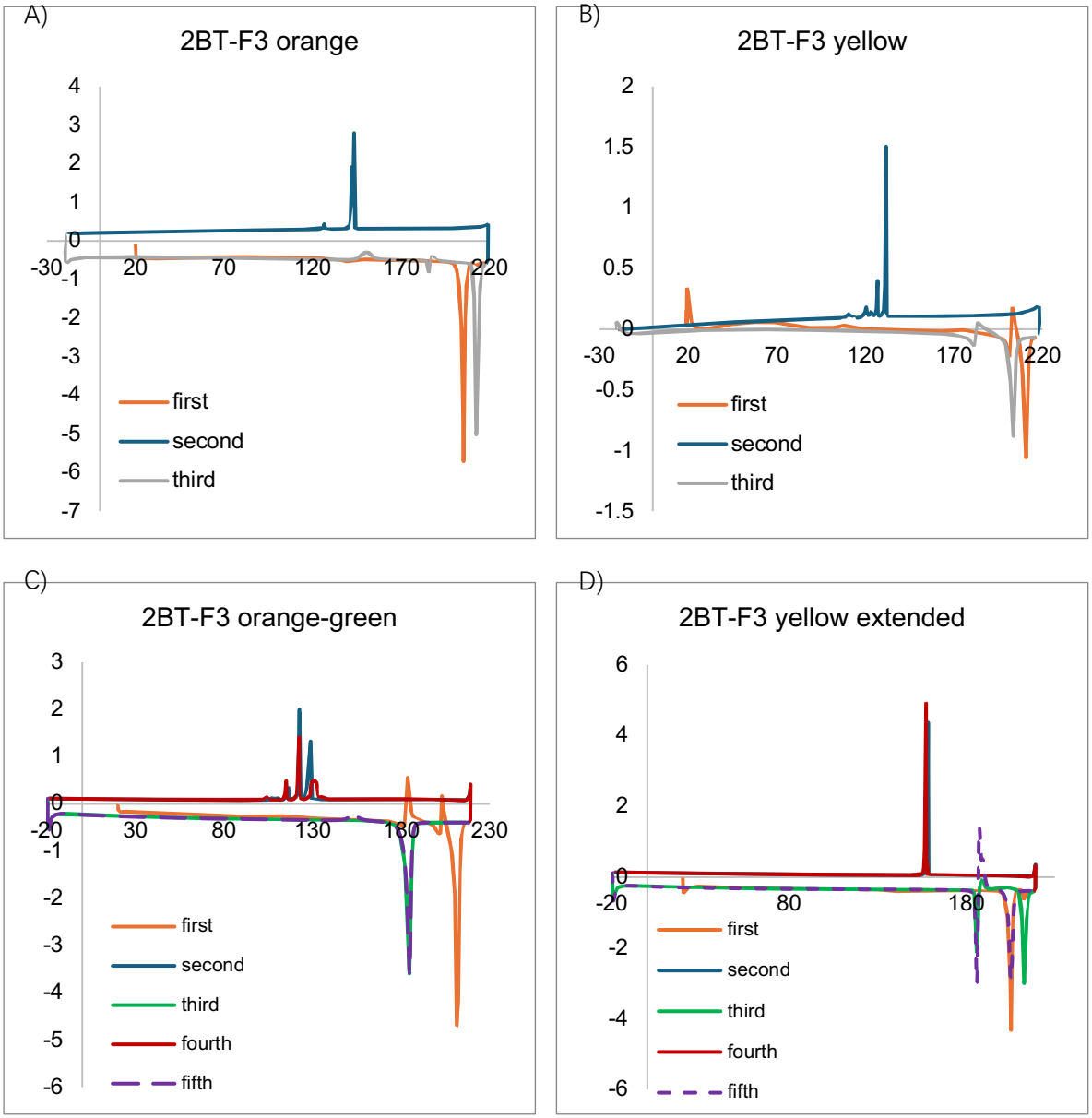

Figure S40: A final analysis of the stock sample of **2BT-F3** shows the thermal stability of the orange solid with a repeating MP of 205°C in the third and fifth controlled change in temperature run

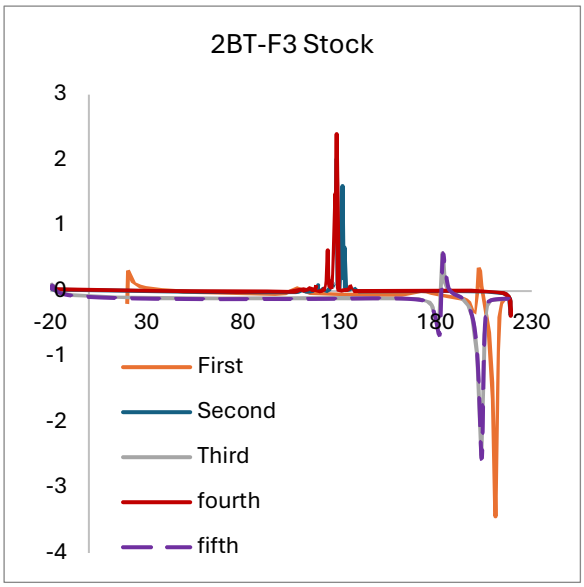

Figure S41: Analysis of **5BT-H5** shows thermal accessibility of a polymorph.

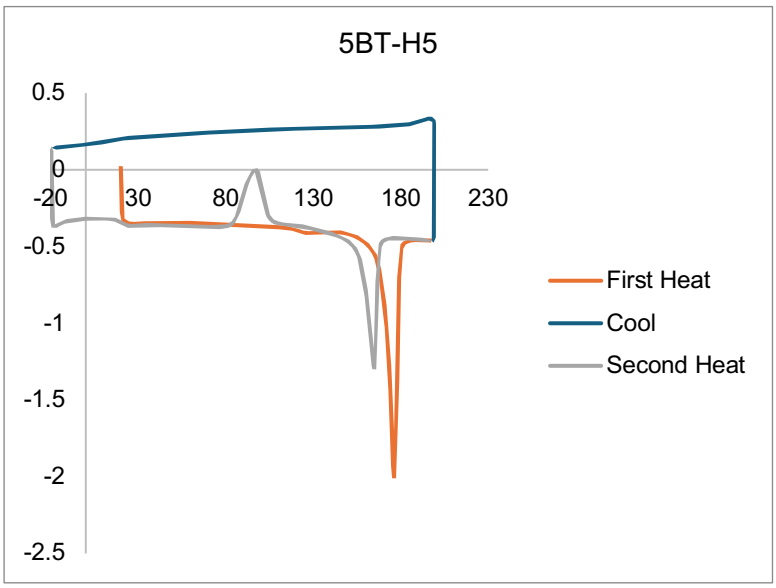

Figure S42. Mechanofluorochromism effects on a) **2TT-H5** b) 2BT-F3 showing a bathochromic shift to a green emitting solid and c) 5BT-F3 d) 5BT-H5 showing hypsochromic shift to a green emitting solid.

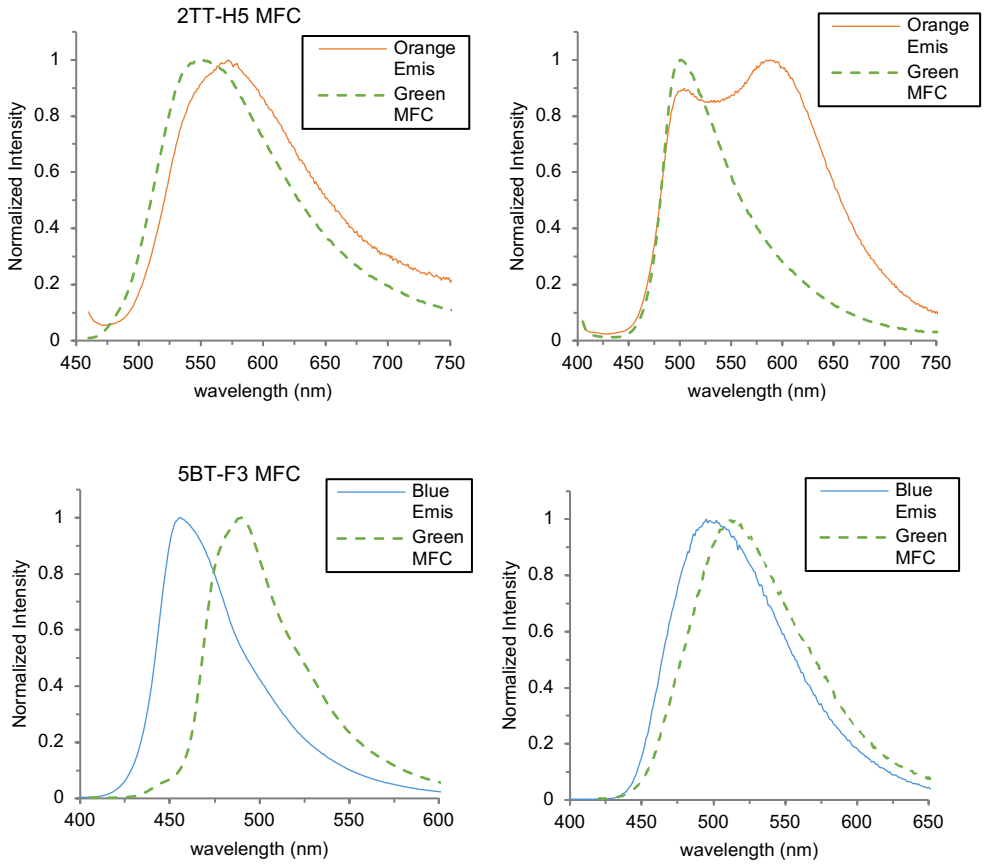

Figure S43: An analysis of **5BT-F3** shows the subtle differences between the melting points of the blue (A) and green (B) emission samples melting at 195°C and 194 °C respectively. Even with an extended run with an additional heat-cool cycle for each blue (C) and green (D) emissive sample, the melting point differences are subtle, with a slight preference for the lower melting point solid.

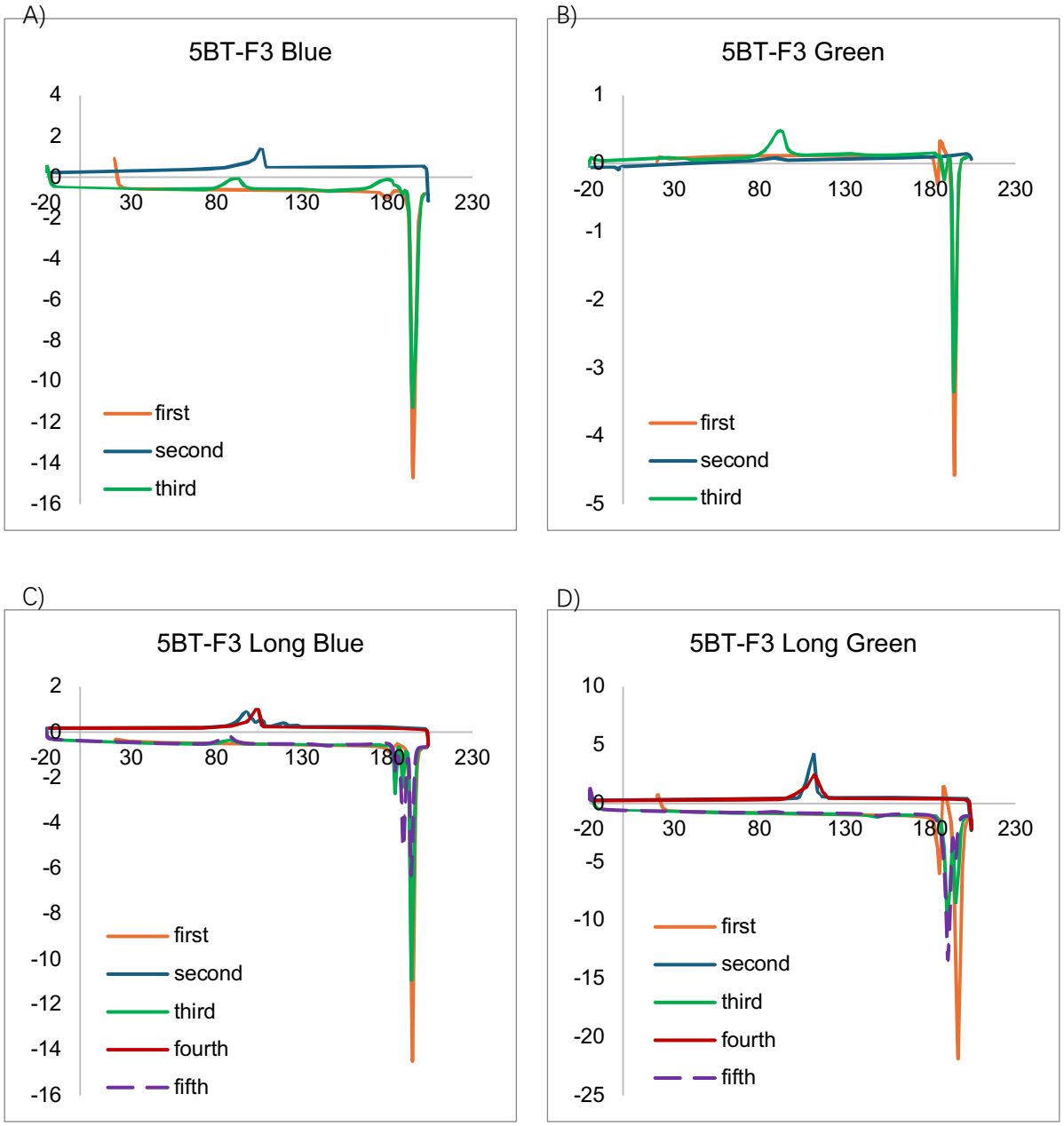

Figure S44: A final analysis of the stock sample of **5BT-F3** shows similar results to the extended runs with a lower melting point present.

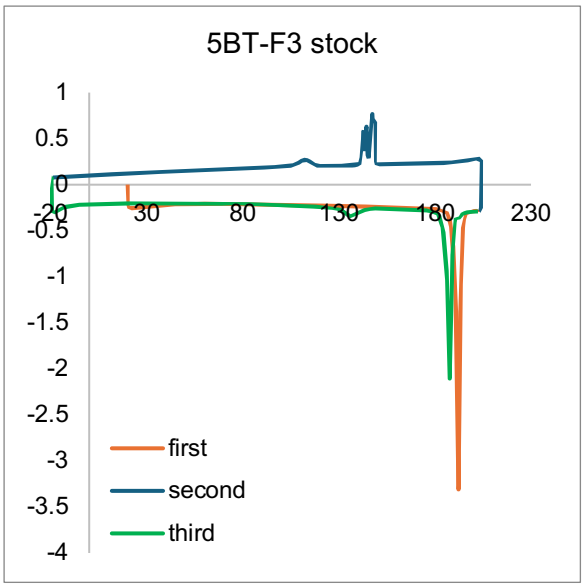

Single Crystal X-Ray Diffraction

Table S1: Crystal data and structure refinement for **5BT-H5**

Identification code	5BTH5	
Empirical formula	C42 H26 O4 S2	
Formula weight	658.75	
Temperature	150(2) K	
Wavelength	0.71073 Å	
Crystal system	Monoclinic	
Space group	$P2_1/c$	
Unit cell dimensions	a = 11.5509(18) Å	α= 90°.
	b = 15.346(3) Å	β= 96.009(7)°.
	c = 8.6788(13) Å	γ = 90°.
Volume	1529.9(4) $Å^3$	
Z	2	
Density (calculated)	1.430 Mg/m^3	
Absorption coefficient	0.221 mm^{-1}	
F(000)	684	
Crystal size	0.320 x 0.310 x 0.140 mm^3	
Theta range for data collection	2.655 to 28.277°.	
Index ranges	-15<=h<=15, -20<=k<=20, -11<=l<=11	
Reflections collected	68779	
Independent reflections	3804 [R(int) = 0.0708]	
Completeness to theta = 25.242°	99.7 %	
Absorption correction	Semi-empirical from equivalents	
Refinement method	Full-matrix least-squares on F^2	
Data / restraints / parameters	3804 / 550 / 297	
Goodness-of-fit on F^2	1.197	
Final R indices [I>2sigma(I)]	R1 = 0.0814, wR2 = 0.2133	
R indices (all data)	R1 = 0.1179, wR2 = 0.2655	
Extinction coefficient	0.032(9)	
Largest diff. peak and hole	0.685 and -0.492 $e.Å^{-3}$	

Table S2: Crystal data and structure refinement for **5BT-F3 blue**

Identification code	5btf3bl	
Empirical formula	C42 H20 F6 O4 S2	
Formula weight	766.70	
Temperature	150(2) K	
Wavelength	0.71073 Å	
Crystal system	Monoclinic	
Space group	$P2_1/c$	
Unit cell dimensions	a = 5.5255(3) Å	α= 90°.
	b = 14.5551(9) Å	β= 90.282(3)°.
	c = 20.8809(12) Å	γ = 90°.
Volume	1679.31(17) $Å^3$	
Z	2	
Density (calculated)	1.516 Mg/m^3	
Absorption coefficient	0.238 mm^{-1}	
F(000)	780	
Crystal size	0.345 x 0.190 x 0.095 mm^3	
Theta range for data collection	2.401 to 25.677°.	
Index ranges	-6<=h<=6, -17<=k<=17, -25<=l<=25	
Reflections collected	40254	
Independent reflections	3180 [R(int) = 0.0437]	
Completeness to theta = 25.242°	99.9 %	
Absorption correction	Semi-empirical from equivalents	
Refinement method	Full-matrix least-squares on F^2	
Data / restraints / parameters	3180 / 0 / 245	
Goodness-of-fit on F^2	1.092	
Final R indices [I>2sigma(I)]	R1 = 0.0566, wR2 = 0.1289	
R indices (all data)	R1 = 0.0829, wR2 = 0.1613	
Extinction coefficient	0.020(3)	
Largest diff. peak and hole	0.409 and -0.536 $e.Å^{-3}$	

Table S3: Crystal data and structure refinement for **5BT-F3 green**

Identification code	5btf3gr	
Empirical formula	C42 H20 F6 O4 S2	
Formula weight	766.70	
Temperature	150(2) K	
Wavelength	0.71073 Å	
Crystal system	Monoclinic	
Space group	C2/c	
Unit cell dimensions	a = 26.4994(17) Å	α= 90°.
	b = 9.1903(6) Å	β= 127.388(2)°.
	c = 17.2983(10) Å	γ = 90°.
Volume	3347.2(4) $Å^3$	
Z	4	
Density (calculated)	1.521 Mg/m^3	
Absorption coefficient	0.239 mm^{-1}	
F(000)	1560	
Crystal size	0.345 x 0.190 x 0.090 mm^3	
Theta range for data collection	2.418 to 30.531°.	
Index ranges	-37<=h<=37, -13<=k<=13, -24<=l<=24	
Reflections collected	92076	
Independent reflections	5050 [R(int) = 0.0239]	
Completeness to theta = 25.242°	98.5 %	
Absorption correction	Semi-empirical from equivalents	
Refinement method	Full-matrix least-squares on F^2	
Data / restraints / parameters	5050 / 0 / 244	
Goodness-of-fit on F^2	1.034	
Final R indices [I>2sigma(I)]	R1 = 0.0343, wR2 = 0.0887	
R indices (all data)	R1 = 0.0387, wR2 = 0.0934	
Extinction coefficient	n/a	
Largest diff. peak and hole	0.424 and -0.317 $e.Å^{-3}$	

Table S4: Crystal data and structure refinement for **5BT-F5-Br**

Identification code	5BTF5	
Empirical formula	C32 H11 Br F10 O4 S	
Formula weight	761.38	
Temperature	150(2) K	
Wavelength	0.71073 Å	
Crystal system	Monoclinic	
Space group	C2/c	
Unit cell dimensions	a = 29.7472(5) Å	α= 90°.
	b = 11.6861(2) Å	β= 118.1352(8)°.
	c = 18.5422(4) Å	γ = 90°.
Volume	5684.15(19) Å^3	
Z	8	
Density (calculated)	1.779 Mg/m^3	
Absorption coefficient	1.626 mm^{-1}	
F(000)	3008	
Crystal size	0.250 x 0.170 x 0.140 mm^3	
Theta range for data collection	2.471 to 25.361°.	
Index ranges	-35<=h<=35, -14<=k<=14, -22<=l<=22	
Reflections collected	69363	
Independent reflections	5198 [R(int) = 0.0525]	
Completeness to theta = 25.242°	99.8 %	
Absorption correction	Semi-empirical from equivalents	
Max. and min. transmission	0.5246 and 0.4646	
Refinement method	Full-matrix least-squares on F^2	
Data / restraints / parameters	5198 / 690 / 529	
Goodness-of-fit on F^2	1.029	
Final R indices [I>2sigma(I)]	R1 = 0.0325, wR2 = 0.0804	
R indices (all data)	R1 = 0.0449, wR2 = 0.0876	
Extinction coefficient	n/a	
Largest diff. peak and hole	0.506 and -0.482 e.Å^{-3}	

Table S5: Crystal data and structure refinement for **2BT-F3**

Identification code	2BT-F3	
Empirical formula	C42 H20 F6 O4 S2	
Formula weight	766.70	
Temperature	150(2) K	
Wavelength	0.71073 Å	
Crystal system	Triclinic	
Space group	P-1	
Unit cell dimensions	a = 11.8761(11) Å	α= 103.607(4)°.
	b = 13.6042(12) Å	β= 96.964(5)°.
	c = 21.7324(18) Å	γ = 100.154(5)°.
Volume	3310.2(5) $Å^3$	
Z	4	
Density (calculated)	1.538 Mg/m^3	
Absorption coefficient	0.241 mm^{-1}	
F(000)	1560	
Crystal size	0.441 x 0.176 x 0.170 mm^3	
Theta range for data collection	2.520 to 26.372°.	
Index ranges	-14<=h<=14, -16<=k<=16, -27<=l<=27	
Reflections collected	225658	
Independent reflections	13515 [R(int) = 0.0723]	
Completeness to theta = 25.242°	99.8 %	
Absorption correction	Semi-empirical from equivalents	
Refinement method	Full-matrix least-squares on F^2	
Data / restraints / parameters	13515 / 2334 / 1266	
Goodness-of-fit on F^2	1.154	
Final R indices [I>2sigma(I)]	R1 = 0.0561, wR2 = 0.1399	
R indices (all data)	R1 = 0.0986, wR2 = 0.1855	
Extinction coefficient	0.0024(7)	
Largest diff. peak and hole	0.381 and -0.396 $e.Å^{-3}$	

Table S6: Crystal data and structure refinement for **2TT-H5**

Identification code	2TT-H5	
Empirical formula	C38 H22 O4 S4	
Formula weight	670.79	
Temperature	150(2) K	
Wavelength	0.71073 Å	
Crystal system	Triclinic	
Space group	P-1	
Unit cell dimensions	a = 8.7036(2) Å	α= 103.6524(15)°.
	b = 9.4891(3) Å	β= 104.5605(14)°.
	c = 10.2069(3) Å	γ = 106.3588(14)°.
Volume	738.91(4) $Å^3$	
Z	1	
Density (calculated)	1.507 Mg/m^3	
Absorption coefficient	0.367 mm^{-1}	
F(000)	346	
Crystal size	0.200 x 0.180 x 0.150 mm^3	
Theta range for data collection	2.184 to 30.997°.	
Index ranges	-12<=h<=12, -13<=k<=13, -14<=l<=14	
Reflections collected	59434	
Independent reflections	4686 [R(int) = 0.0508]	
Completeness to theta = 25.242°	99.6 %	
Absorption correction	Semi-empirical from equivalents	
Max. and min. transmission	0.7469 and 0.7210	
Refinement method	Full-matrix least-squares on F^2	
Data / restraints / parameters	4686 / 392 / 230	
Goodness-of-fit on F^2	1.069	
Final R indices [I>2sigma(I)]	R1 = 0.0668, wR2 = 0.1157	
R indices (all data)	R1 = 0.1106, wR2 = 0.1488	
Extinction coefficient	n/a	
Largest diff. peak and hole	0.642 and -0.603 $e.Å^{-3}$	

Density Functional Theory and SAPT Calculation Results

Table S7. Energy difference between the closed and open conformers (ΔE=E_{Closed}-E_{Open}) of the 2BT ground states (S_0) as determined at the ωB97X-D/6-31G(d') level of theory.

Molecules	**ΔE (kcal/mol)**
2BT F3 closed	–9.95
2BT F3 open	
2BT F5 closed	–13.82
2BT F5 open	
2BT H5 closed	–10.06
2BT H5 open	

Table S8. Energy difference between the closed and open conformers (ΔE=E_{Closed}-E_{Open}) of the 5BT systems as determined at the ωB97X-D/6-31G(d') level of theory.

Molecules	**ΔE (kcal/mol)**
5BT F3 closed (yellow)	–11.67
5BT F3 open (no twist)	
5BT F5 closed	–15.00
5BT F5 open	
5BT H5 closed	–9.11
5BT H5 open	

Table S9. Energy difference between the closed and open conformers (ΔE=E_{Closed}-E_{Open}) of the 6BT systems as determined at the ωB97X-D/6-31G(d') level of theory.

Molecules	ΔE (kcal/mol)
6BT F3 closed	–11.56
6BT F3 open	
6BT F5 closed	–14.51
6BT F5 open	
6BT H5 closed	–9.47
6BT H5 open	

Table S10. Energy difference between the closed and open conformers (ΔE=E_{Closed}-E_{Open}) of the 2TT systems as determined at the ωB97X-D/6-31G(d') level of theory.

Molecules	ΔE (kcal/mol)
2TT F3 closed	–9.74
2TT F3 open	
2TT F5 closed	–9.92
2TT F5 open	
2TT H5 closed	–8.11
2TT H5 open	

Table S11. Noncovalent interaction energies for select intramolecular fragments in the closed conformer at the SAPT0/jun-cc-pVDZ level of theory. Images of the fragments are shown in Figure S45.

Fragment 1	Fragment 2	Electrostatics (kcal/mol)	Exchange (kcal/mol)	Induction (kcal/mol)	Dispersion (kcal/mol)	Total (kcal/mol)
2BT	F3	-6.081	22.560	-2.235	-15.520	-1.276
2BT	F5	-7.263	24.080	-2.455	-15.682	-1.320
2BT	H5	-6.896	24.963	-2.518	-15.834	-0.284
5BT	F3	-9.206	28.773	-2.548	-17.663	-0.603
5BT	F5	-7.355	24.482	-2.416	-17.018	-2.307
5BT	H5	-8.504	29.103	-2.698	-17.791	0.110
6BT	F3	-6.156	23.744	-2.247	-15.709	-0.369
6BT	F5	-6.372	23.506	-2.336	-15.733	-0.935
6BT	H5	-5.770	23.673	-2.367	-15.713	-0.177
2TT	F3	-5.497	21.934	-1.881	-14.936	-0.380
2TT	F5	-6.110	22.381	-2.284	-15.401	-1.415
2TT	H5	-5.277	21.786	-1.994	-14.916	-0.402

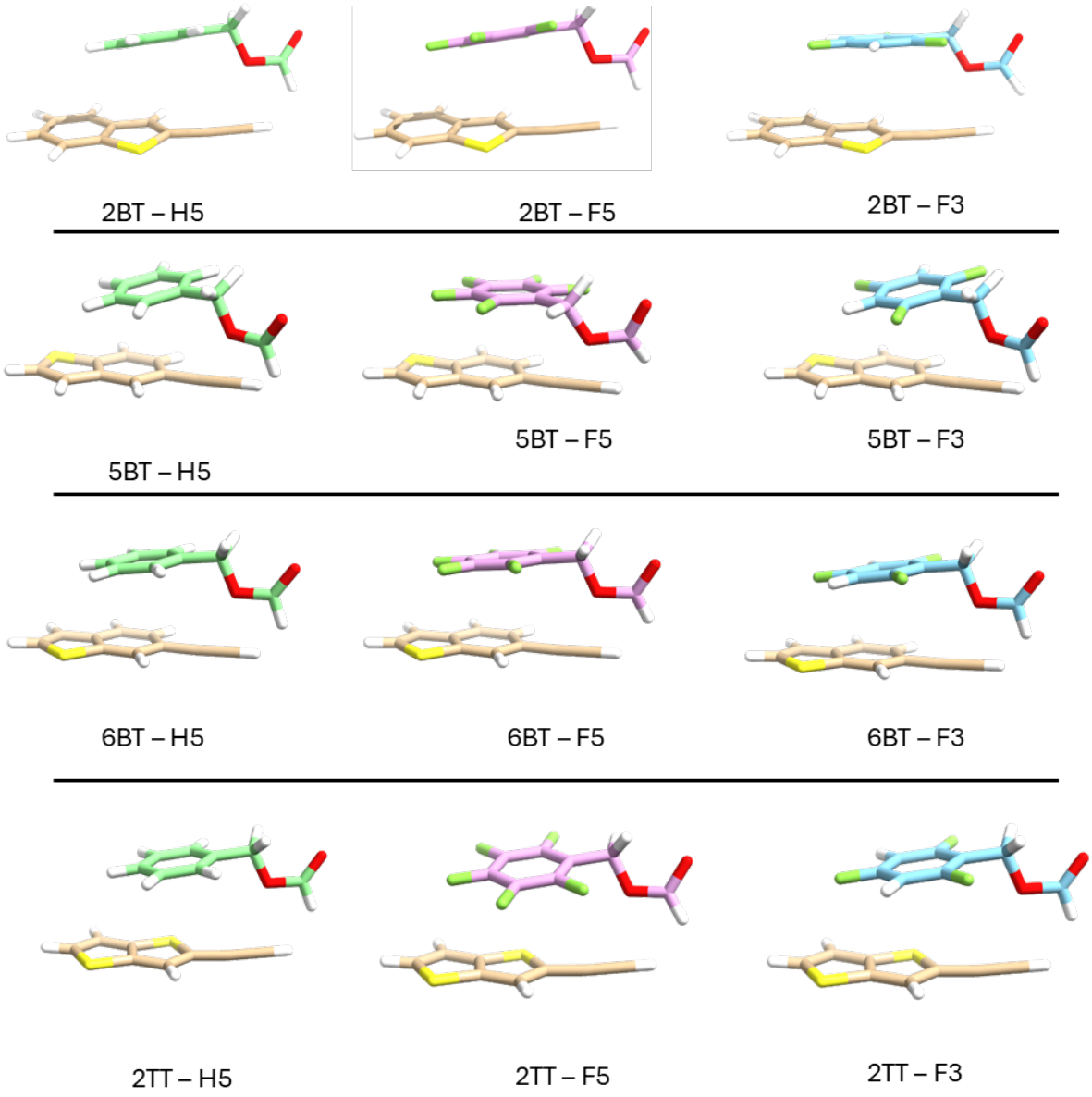

Figure S45. Pictorial representations of the intramolecular fragments used for the SAPT0/jun-cc-pVDZ calculations.

Table S12. Noncovalent interaction energies for modified intramolecular fragments in the closed conformer at the SAPT0/jun-cc-pVDZ level of theory. The formate group in Figure S1 was modified to a hydroxyl group. Images of the fragments are shown in Figure S46.

Fragment 1	Fragment 2	Electrostatics (kcal/mol)	Exchange (kcal/mol)	Induction (kcal/mol)	Dispersion (kcal/mol)	Total (kcal/mol)
2BT	F3	-5.405	17.350	-2.083	-13.749	-3.887
2BT	F5	-7.164	21.527	-2.473	-14.453	-2.563
2BT	H5	-6.765	22.112	-2.730	-14.565	-1.949
5BT	F3	-8.753	26.481	-2.789	-16.482	-1.544
5BT	F5	-7.203	20.193	-2.263	-15.400	-4.673
5BT	H5	-8.030	26.598	-3.002	-16.624	-1.059
6BT	F3	-5.464	19.746	-2.178	-14.194	-2.090
6BT	F5	-5.861	19.330	-2.160	-14.211	-2.902
6BT	H5	-5.063	19.671	-2.395	-14.201	-1.988
2TT	F3	-5.197	19.027	-2.956	-13.624	-1.750
2TT	F5	-6.049	18.061	-2.077	-13.837	-3.903
2TT	H5	-5.008	19.099	-2.362	-13.640	-1.912

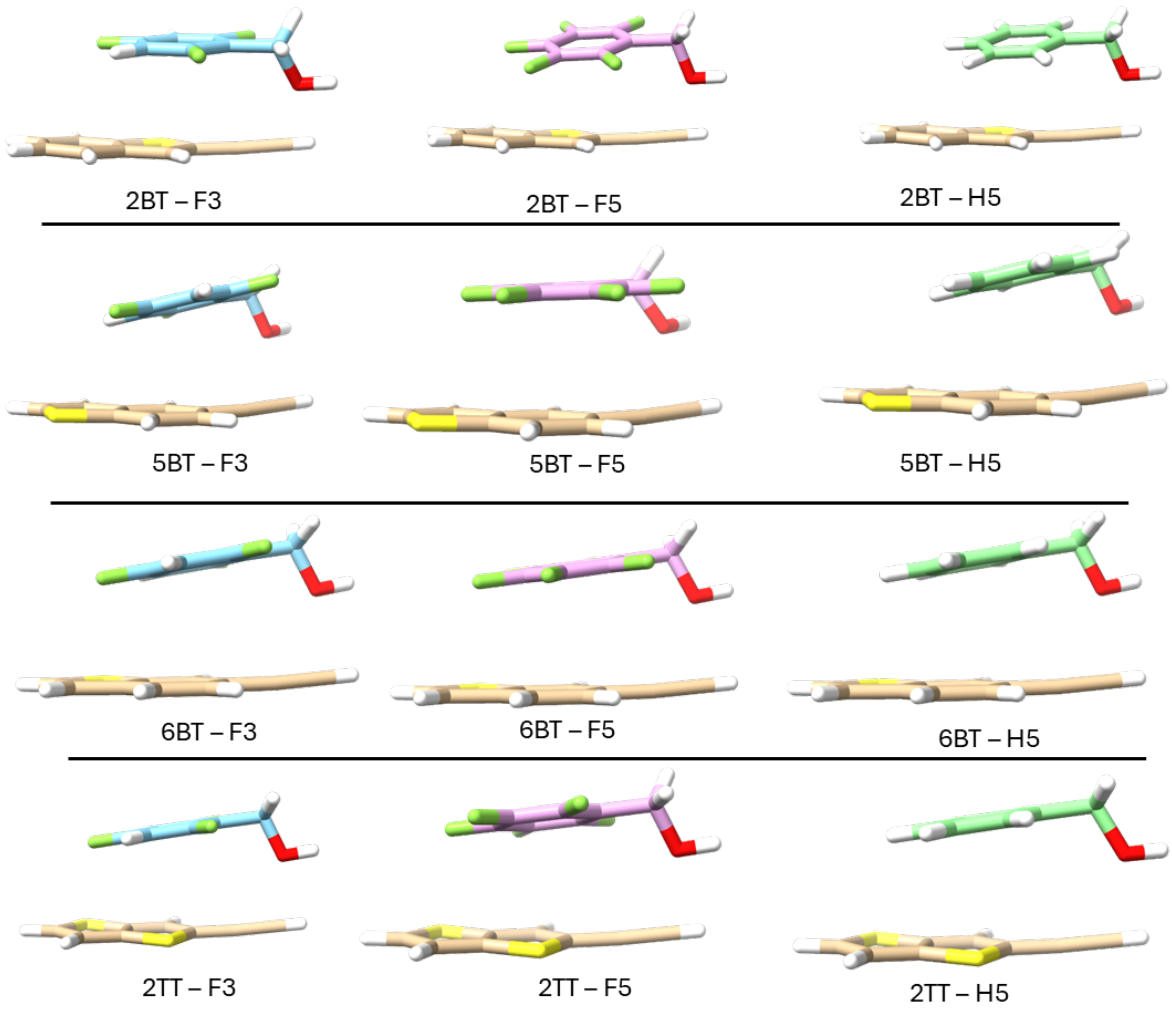

Figure S46. Pictorial representations of the intramolecular fragments used for the SAPT0/jun-cc-pVDZ calculations where the formate group is truncated to a hydroxyl group.

Table S13. Noncovalent interaction energies for idealized cofacial intramolecular fragments in the closed conformer at the SAPT0/jun-cc-pVDZ level of theory. Images of the fragments are shown in Figure S47.

Fragment 1	Fragment 2	Electrostatics (kcal/mol)	Exchange (kcal/mol)	Induction (kcal/mol)	Dispersion (kcal/mol)	Total (kcal/mol)
2BT	F3	-25.184	71.217	-5.504	-19.631	20.897
2BT	F5	-26.393	71.317	-5.654	-19.593	19.677
2BT	H5	-24.775	72.230	-5.732	-19.908	21.816
5BT	F3	-12.992	43.538	-3.143	-16.398	11.005
5BT	F5	-13.645	42.601	-3.080	-16.258	9.618
5BT	H5	-12.383	44.066	-3.189	-16.690	11.805
6BT	F3	-25.750	71.597	-5.686	-19.592	20.570
6BT	F5	-26.658	72.001	-5.811	-19.598	19.934
6BT	H5	-12.616	44.701	-3.261	-16.787	12.037
2TT	F3	-25.591	71.250	-5.581	-19.714	20.365
2TT	F5	-26.484	71.414	-5.715	-19.679	19.534
2TT	H5	-25.649	73.170	-5.948	-20.128	21.445

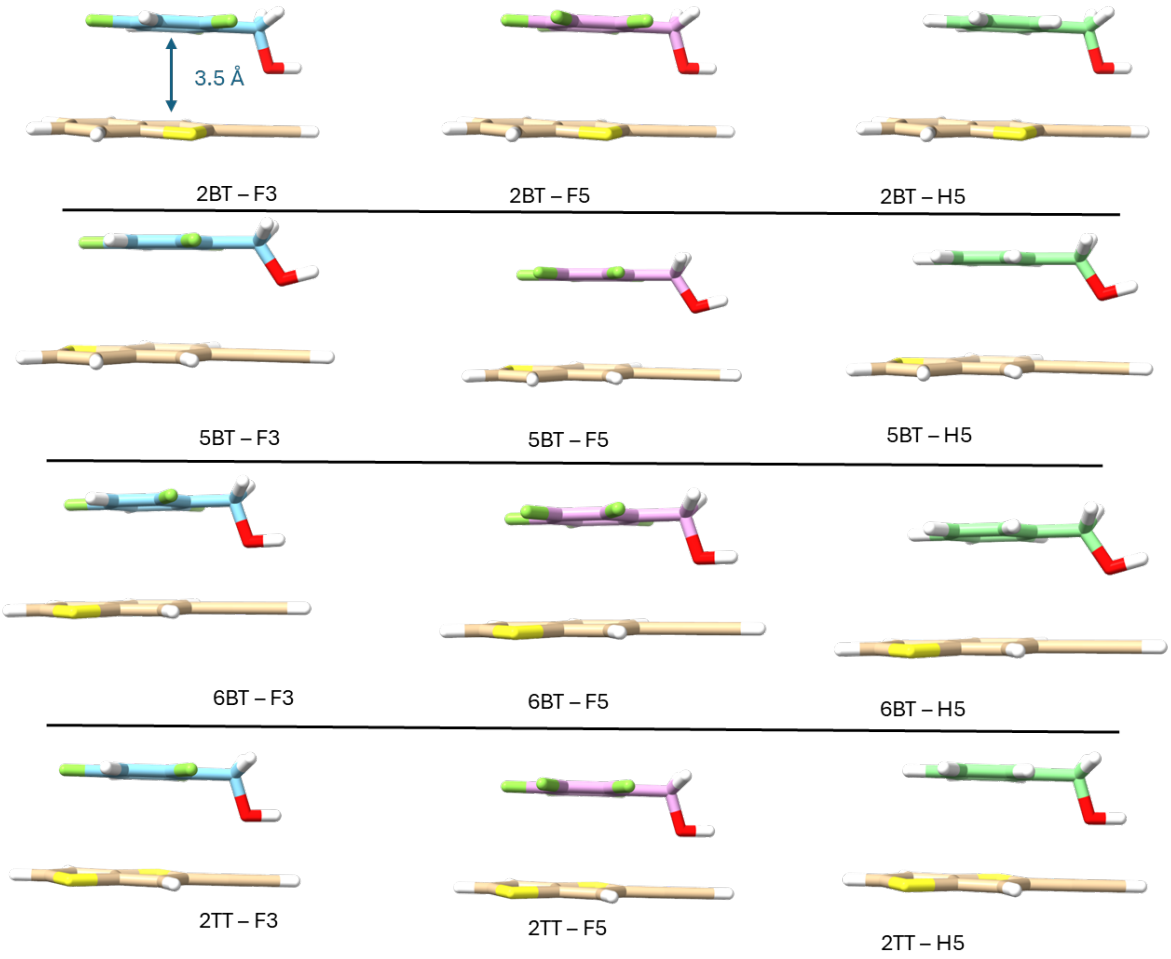

Figure S47. Pictorial representations of idealized cofacial intramolecular fragments used for the SAPT0/jun-cc-pVDZ calculations.

Table S14. Noncovalent interaction energies for idealized T-shaped intramolecular fragments in the closed conformer at the SAPT0/jun-cc-pVDZ level of theory. The thiophene group's S atom is positioned on top and oriented perpendicular to the benzyl group. Images of the fragments are shown in Figure S48

Fragment 1	Fragment 2	Electrostatics (kcal/mol)	Exchange (kcal/mol)	Induction (kcal/mol)	Dispersion (kcal/mol)	Total (kcal/mol)
2BT	F3	0.447	0.275	-0.125	-1.895	-1.297
2BT	F5	0.461	0.261	-0.091	-1.878	-1.247
2BT	H5	0.415	0.343	-0.248	-1.943	-1.437
5BT	F3	-0.218	0.233	-0.114	-1.571	-1.671
5BT	F5	0.248	0.200	-0.084	-1.550	-1.186
5BT	H5	-0.867	0.271	-0.196	-1.619	-2.411
6BT	F3	0.701	1.372	-0.299	-2.868	-1.095
6BT	F5	0.985	1.331	-0.240	-2.851	-0.775
6BT	H5	0.258	1.025	-0.344	-2.681	-1.742
2TT	F3	0.387	0.237	-0.127	-1.740	-1.242
2TT	F5	0.518	0.223	-0.089	-1.724	-1.071
2TT	H5	0.142	0.308	-0.247	-1.791	-1.588

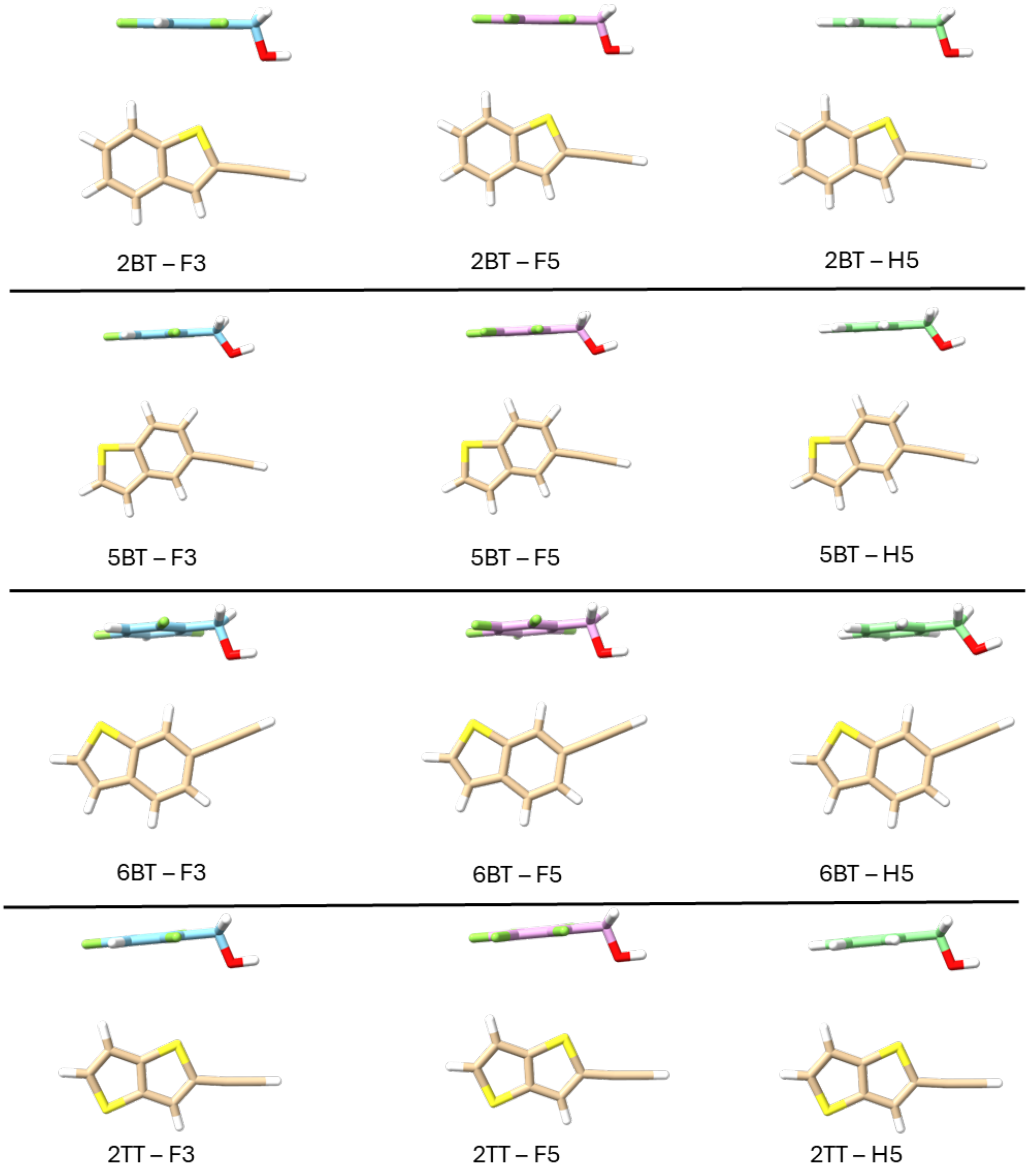

Figure S18. Pictorial representations of the idealized T-shaped intramolecular fragments used for the SAPT0/jun-cc-pVDZ calculations. The thiophene group's S atom is positioned on top and oriented perpendicular to the benzyl group.

Table S15. Noncovalent interaction energies for idealized T-shaped intramolecular fragments in the closed conformer at the SAPT0/jun-cc-pVDZ level of theory. The thiophene group's S atom is positioned on the bottom and oriented perpendicular to the benzyl group. Images of the fragments are shown in Figure S49

Fragment 1	Fragment 2	Electrostatics (kcal/mol)	Exchange (kcal/mol)	Induction (kcal/mol)	Dispersion (kcal/mol)	Total (kcal/mol)
2BT	F3	0.099	0.204	-0.117	-1.626	-1.439
2BT	F5	0.522	0.185	-0.085	-1.611	-0.988
2BT	H5	-0.527	0.268	-0.229	-1.672	-2.160
5BT	F3	0.299	0.137	-0.085	-1.272	-0.922
5BT	F5	0.627	0.108	-0.063	-1.257	-0.585
5BT	H5	-0.257	0.188	-0.153	-1.312	-1.534
6BT	F3	-0.570	0.236	-0.136	-1.547	-2.017
6BT	F5	-0.242	0.216	-0.099	-1.531	-1.656
6BT	H5	-0.862	0.210	-0.182	-1.494	-2.328
2TT	F3	0.435	0.414	-0.167	-2.031	-1.349
2TT	F5	0.844	0.407	-0.123	-2.016	-0.888
2TT	H5	-0.275	0.453	-0.293	-2.084	-2.200

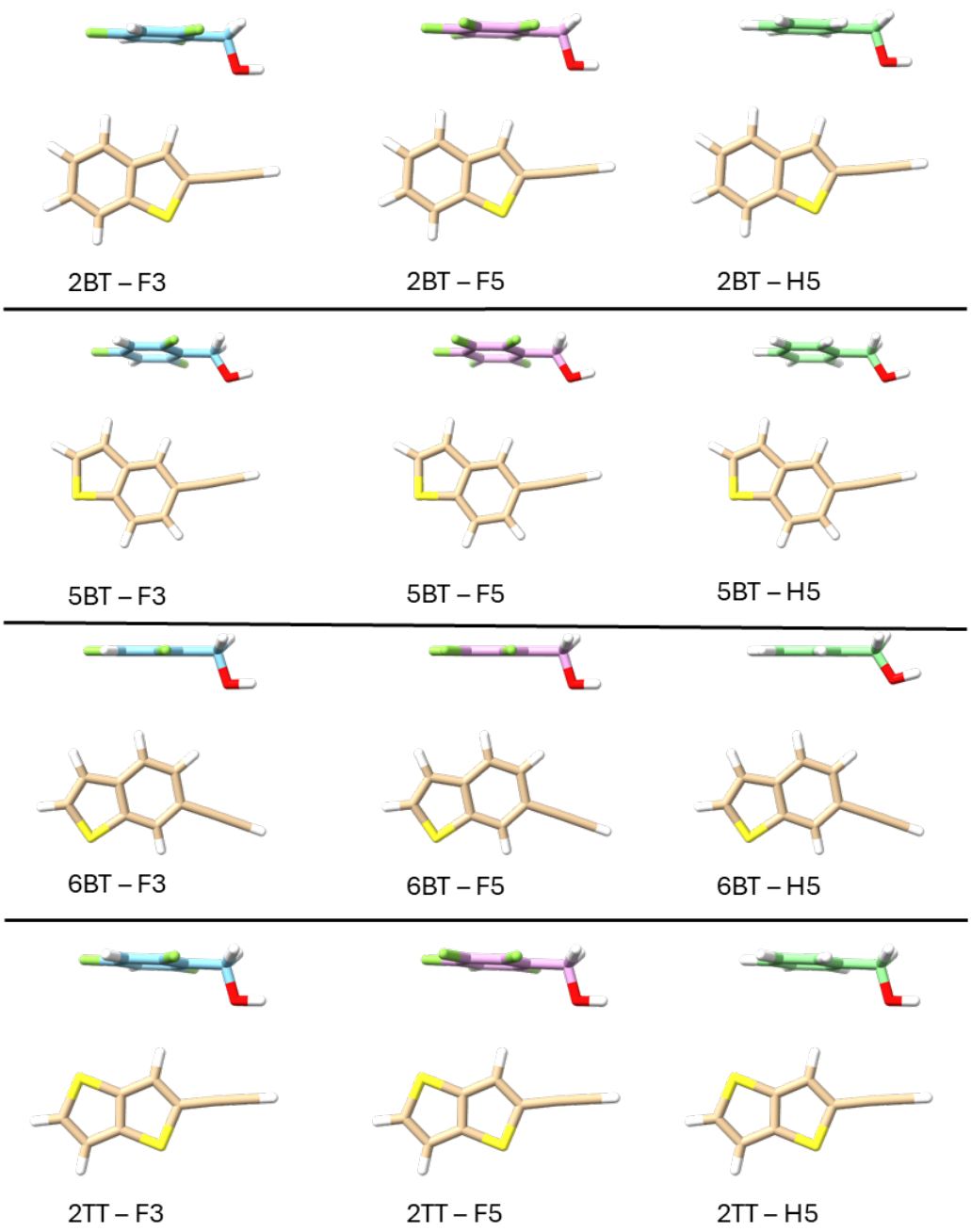

Figure S49. Pictorial representations of the idealized T-shaped intramolecular fragments used for the SAPT0/jun-cc-pVDZ calculations. The thiophene group's S atom is positioned on the bottom and oriented perpendicular to the benzyl group.

Table S16. Select vertical transition ($S_0 \rightarrow S_n$) energies (E, eV), wavelengths (λ, nm), oscillator strengths (osc. str.), and electronic configurations for the closed conformers as determined via TDDFT at the ωB97X-D/6-31G(d') level of theory. Transitions are reported for those transitions with oscillator strengths larger than 0.1.

Conformer (Closed)	$S_0 \rightarrow S_n$, where n =	E (eV)	λ (nm)	Osc. Str.
2BT_F3	1	3.77	329	1.24
	4	4.59	270	0.49
	8	4.78	259	0.36
	12	5.34	232	0.24
	13	5.37	231	0.33
2BT_F5	1	3.78	328	1.12
	4	4.59	270	0.58
	6	4.63	268	0.11
	8	4.77	260	0.38
	14	5.34	232	0.25
2BT_H5	1	3.49	356	1.48
	3	4.31	287	0.27
	5	4.60	270	0.12
	7	4.71	263	0.10
	8	4.85	256	0.11
	11	5.11	242	0.15
	12	5.30	234	0.35
2TT_F3	1	3.75	330	0.93
	3	4.28	290	0.12
	4	4.45	278	0.78
	5	4.56	272	0.23
	14	5.30	234	0.20
2TT_F5	1	3.73	333	0.92
	4	4.47	277	0.91
	5	4.55	272	0.16
2TT_H5	1	3.38	367	1.50
	3	4.24	292	0.29
	4	4.58	271	0.21
	12	5.22	237	0.29
5BT_F3_yellow	1	3.94	315	0.88
	4	4.67	265	0.36
	8	5.04	246	0.15
	10	5.09	244	0.17
	12	5.36	231	1.41
5BT_F5	1	3.98	311	0.80
	4	4.70	264	0.26
	6	4.71	263	0.12
	10	5.12	242	0.33
	12	5.31	234	0.10
	14	5.37	231	1.20
5BT_H5	1	3.73	333	1.05
	3	4.42	281	0.15

	4	4.64	267	0.31
	8	4.99	248	0.15
	12	5.31	233	1.32
6BT_F3	1	3.96	313	0.86
	4	4.67	266	0.52
	6	4.73	262	0.20
	7	4.84	256	0.30
	13	5.44	228	0.69
6BT_F5	1	3.99	311	0.73
	4	4.66	266	0.41
	6	4.76	260	0.37
	7	4.84	256	0.36
	15	5.41	229	0.41
6BT_H5	1	3.73	332	1.20
	3	4.36	284	0.10
	4	4.60	270	0.42
	8	4.91	252	0.31
	12	5.35	232	0.69

Table S17. Select vertical transition ($S_0 \rightarrow S_n$) energies, wavelengths, oscillator strengths (osc. str.) and electronic configurations for the open conformers as determined via TDDFT at the ωB97X-D/6-31G(d') level of theory. Transitions are reported for those transitions with oscillator strengths larger than 0.1.

Conformer (Open)	$S_0 \rightarrow S_n$, where n =	E (eV)	λ (nm)	Osc. Str.
2BT_F3_cif	1	3.36	369	1.78
	3	4.23	293	0.32
	11	5.10	243	0.35
	12	5.30	234	0.28
2BT_F5	1	3.29	376	1.69
	3	4.15	299	0.52
	11	5.12	242	0.47
	12	5.28	235	0.13
	14	5.54	224	0.14
2BT_H5	1	3.23	384	1.87
	3	4.12	301	0.36
	11	5.03	246	0.31
	12	5.24	237	0.28
2TT_F3	1	3.28	378	1.76
	3	4.14	299	0.39
	6	4.71	263	0.17
	9	5.02	247	0.25
	14	5.35	232	0.19
2TT_F5	1	3.29	377	1.65
	3	4.14	300	0.40
	6	4.67	265	0.21
	9	5.01	247	0.32
	14	5.39	230	0.23
2TT_H5	1	3.27	380	1.73
	3	4.13	300	0.41
	6	4.72	263	0.18
	9	5.05	246	0.19
	11	5.07	245	0.22
	14	5.33	233	0.24
5BT_3F_no_twist	1	3.46	358	1.39
	3	4.28	290	0.61
	12	5.26	236	1.08
	14	5.48	226	0.33
5BT_F5	1	3.46	358	1.34
	2	4.27	290	0.62
	10	5.14	241	0.25
	12	5.28	235	0.61
5BT_H5	1	3.47	358	1.35
	3	4.28	290	0.60
	10	5.14	241	0.24
	12	5.25	236	0.83
	14	5.50	225	0.60

6BT_F3	1	3.41	364	1.57
	2	4.22	294	0.55
	11	5.11	243	0.16
	12	5.34	232	0.66
6BT_F5	1	3.45	360	1.61
	2	4.23	293	0.50
	8	5.04	246	0.13
	12	5.37	231	0.59
6BT_H5	1	3.42	362	1.59
	2	4.23	293	0.52
	11	5.11	243	0.14
	12	5.34	232	0.67

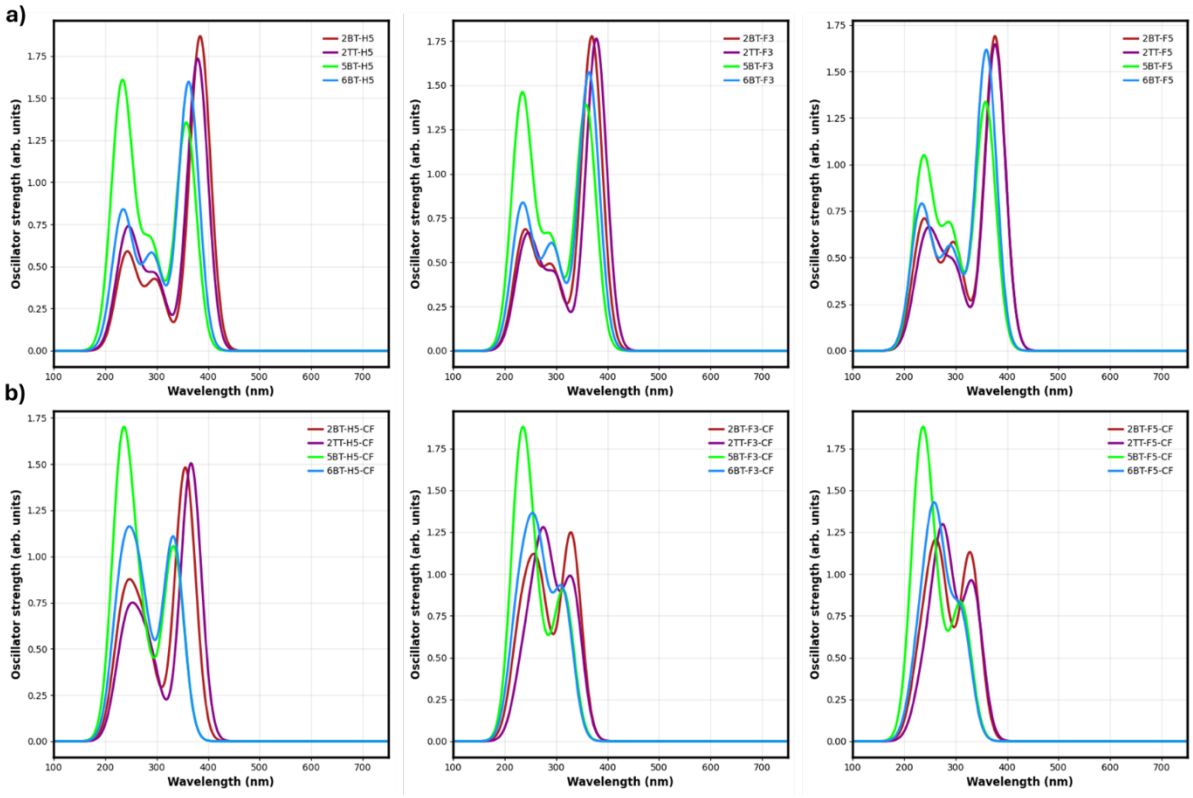

Figure S46. Simulated absorption spectra for the a) open conformers and b) closed conformers as determined via TDDFT at the ωB97X-D/6-31G(d') level of theory.

Table S18. Energy difference between the closed and open *conformers* ($\Delta E = E_{Closed} - E_{Open}$) of the 2BT S_1 state as determined at the ωB97X-D/6-31G(d') level of theory.

Molecules	ΔE (kcal/mol)
2BT F3 closed	–7.06
2BT F3 open	
2BT F5 closed	–10.11
2BT F5 open	
2BT H5 closed	–9.93
2BT H5 open	

Table S19. Energy difference between the closed and open *conformers* ($\Delta E = E_{Closed} - E_{Open}$) of the 5BT S_1 state as determined at the ωB97X-D/6-31G(d') level of theory.

Molecules	ΔE (kcal/mol)
5BT F3 closed (yellow)	–8.18
5BT F3 open (no twist)	
5BT F5 closed	–11.67
5BT F5 open	
5BT H5 closed	–8.84
5BT H5 open	

Table S20. Energy difference between the closed and open *conformers* ($\Delta E = E_{Closed} - E_{Open}$) of the 6BT S_1 state as determined at the ωB97X-D/6-31G(d') level of theory.

Molecules	ΔE (kcal/mol)
6BT F3 closed	–7.54
6BT F3 open	
6BT F5 closed	–10.29
6BT F5 open	
6BT H5 closed	–9.40
6BT H5 open	

Table S21. Energy difference between the closed and open *conformers* ($\Delta E = E_{Closed} - E_{Open}$) of the 2TT S_1 state as determined at the ωB97X-D/6-31G(d') level of theory.

Molecules	**ΔE (kcal/mol)**
2TT F3 closed	–6.97
2TT F3 open	
2TT F5 closed	–7.77
2TT F5 open	
2TT H5 closed	–8.31
2TT H5 open	

Table S22. Summary of electronic transition transitions and Stokes shifts for the open conformers as determined via TDDFT at the ωB97X-D/6-31G(d') level of theory.

Molecules (Open)	Absorption		Emission		Stokes Shift (eV)
	E (eV)	λ (nm)	E (eV)	λ (nm)	
2BT F3	3.36	369	2.92	424	0.43
2BT F5	3.29	376	2.86	433	0.43
2BT H5	3.23	384	2.93	424	0.30
5BT F3	3.46	358	3.03	409	0.43
5BT F5	3.46	358	2.97	418	0.49
5BT H5	3.47	358	3.01	412	0.46
6BT F3	3.41	364	2.99	415	0.42
6BT F5	3.45	360	2.95	420	0.49
6BT H5	3.42	362	3.00	414	0.43
2TT F3*	3.28	378	2.81	442	0.47
2TT F5*	3.29	377	2.75	451	0.54
2TT H5*	3.27	380	2.84	436	0.43

* Represents systems were TDDFT optimization of the S_1 resulted in geometries in which negative normal modes are present. The data for these structures is provided here for completeness.

Table S23. Summary of electronic transition transitions and Stokes shifts for the closed conformers as determined via TDDFT at the ωB97X-D/6-31G(d') level of theory.

Molecules (Closed)	Absorption		Emission		Stokes Shift (eV)
	E (eV)	λ (nm)	E (eV)	λ (nm)	
2BT F3	3.77	329	2.92	425	0.85
2BT F5	3.78	328	3.31	374	0.47
2BT H5	3.49	356	2.90	427	0.58
5BT F3	3.94	315	3.55	349	0.39
5BT F5	3.98	311	3.15	394	0.84
5BT H5	3.73	333	3.07	404	0.66
6BT F3	3.96	313	3.02	410	0.94
6BT F5	3.99	311	3.05	406	0.94
6BT H5	3.73	332	3.00	413	0.73
2TT F3*	3.75	330	2.84	436	0.91
2TT F5*	3.73	333	2.91	426	0.81
2TT H5*	3.38	367	2.83	439	0.55

* Represents systems were TDDFT optimization of the S_1 resulted in geometries in which negative normal modes are present. The data for these structures is provided here for completeness.

References

(1) Frisch, M. J.; Trucks, G. W.; Schlegel, H. B.; Scuseria, G. E.; Robb, M. A.; Cheeseman, J. R.; Scalmani, G.; Barone, V.; Petersson, G. A.; Nakatsuji, H.; et al. Gaussian 16 Rev. A.03. **2016**. (acccessed 07/28/2025).

(2) Grimme, S. Semiempirical GGA-type density functional constructed with a long-range dispersion correction. *J Comput Chem* **2006**, *27* (15), 1787-1799. DOI: 10.1002/jcc.20495 From NLM PubMed-not-MEDLINE.

(3) Hariharan, P. C.; Pople, J. A. The influence of polarization functions on molecular orbital hydrogenation energies. *Theoretica Chimica Acta* **1973**, *28* (3), 213-222. DOI: 10.1007/bf00533485.

(4) Jeziorski, B.; Moszynski, R.; Szalewicz, K. Perturbation Theory Approach to Intermolecular Potential Energy Surfaces of van der Waals Complexes. *Chemical Reviews* **1994**, *94* (7), 1887-1930. DOI: 10.1021/cr00031a008.

(5) Hohenstein, E. G.; Sherrill, C. D. Efficient evaluation of triple excitations in symmetry-adapted perturbation theory via second-order Møller–Plesset perturbation theory natural orbitals. *The Journal of Chemical Physics* **2010**, *133* (10), 104107. DOI: 10.1063/1.3479400.

(6) Hohenstein, E. G.; Sherrill, C. D. Density fitting of intramonomer correlation effects in symmetry-adapted perturbation theory. *The Journal of Chemical Physics* **2010**, *133* (1), 014101. DOI:

10.1063/1.3451077.
(7) Hohenstein, E. G.; Duan, J.; Sherrill, C. D. Origin of the surprising enhancement of electrostatic energies by electron-donating substituents in substituted sandwich benzene dimers. *J Am Chem Soc* **2011**, *133* (34), 13244-13247. DOI: 10.1021/ja204294q From NLM Medline.
(8) Smith, D. G. A.; Burns, L. A.; Simmonett, A. C.; Parrish, R. M.; Schieber, M. C.; Galvelis, R.; Kraus, P.; Kruse, H.; Di Remigio, R.; Alenaizan, A.; et al. Psi4 1.4: Open-source software for high-throughput quantum chemistry. *J Chem Phys* **2020**, *152* (18), 184108. DOI: 10.1063/5.0006002 From NLM PubMed-not-MEDLINE.
(9) Kendall, R. A.; Dunning, T. H.; Harrison, R. J. Electron affinities of the first-row atoms revisited. Systematic basis sets and wave functions. *The Journal of Chemical Physics* **1992**, *96* (9), 6796-6806. DOI: 10.1063/1.462569.
(10) Papajak, E.; Zheng, J.; Xu, X.; Leverentz, H. R.; Truhlar, D. G. Perspectives on Basis Sets Beautiful: Seasonal Plantings of Diffuse Basis Functions. *J Chem Theory Comput* **2011**, *7* (10), 3027-3034. DOI: 10.1021/ct200106a From NLM PubMed-not-MEDLINE.
(11) Parker, T. M.; Burns, L. A.; Parrish, R. M.; Ryno, A. G.; Sherrill, C. D. Levels of symmetry adapted perturbation theory (SAPT). I. Efficiency and performance for interaction energies. *The Journal of Chemical Physics* **2014**, *140* (9). DOI: 10.1063/1.4867135.
(12) Chen, X.-K.; Bakr, B. W.; Auffray, M.; Tsuchiya, Y.; Sherrill, C. D.; Adachi, C.; Bredas, J.-L. Intramolecular Noncovalent Interactions Facilitate Thermally Activated Delayed Fluorescence (TADF). *The Journal of Physical Chemistry Letters* **2019**, *10* (12), 3260-3268. DOI: 10.1021/acs.jpclett.9b01220.
(13) Trani, F.; Scalmani, G.; Zheng, G.; Carnimeo, I.; Frisch, M. J.; Barone, V. Time-Dependent Density Functional Tight Binding: New Formulation and Benchmark of Excited States. *J Chem Theory Comput* **2011**, *7* (10), 3304-3313. DOI: 10.1021/ct200461y From NLM PubMed-not-MEDLINE.
(14) Hédouin, M.; Luppi, E.; Ward, O.; Harrowven, D.; Fressigné, C.; Chataigner, I. Predictive TDDFT Methodology for Aromatic Molecules UV-Vis properties: from Benchmark to Applications. *ChemistrySelect* **2023**, *8* (29). DOI: 10.1002/slct.202301943.
(15) Zhu, Q.; Guo, X.; Zhang, J. Theoretical study on photophysical properties of a series of functional pyrimidine-based organic light-emitting diodes emitters presenting thermally activated delayed fluorescence. *J Comput Chem* **2019**, *40* (16), 1578-1585. DOI: 10.1002/jcc.25808 From NLM PubMed-not-MEDLINE.